THE CONSTRUCTION OF A SWEPT-FREQUENCY POLARIMETER FOR OBSERVING DECAMETRIC RADIATION FROM JUPITER

BY

D. E. BAKER

THE CONSTRUCTION OF A SWEPT-FREQUENCY POLARIMETER FOR OBSERVING DECAMETRIC RADIATION FROM JUPITER

by

DIRK E. BAKER

A thesis submitted in fulfillment of the requirements for the degree of Master of Science of Rhodes University.

January 1970.

Except where it is clear from the text that I am describing the work of others, or where it is obvious that I am making a survey of existing knowledge on the subject of the present study, the work described in this thesis is my own.

TO

MY MOTHER AND FATHER

and

CLAIRE

ABSTRACT

This thesis describes the design and construction of a swept-frequency polarimeter for observing Jupiter's decametric radiation in the frequency range from 15 to 45 MHz. The frequency band is tuned in two parts using two receivers for observing the left- and right-circular components of the radiation in the 15 to 26 MHz range and two receivers for observing the circular components in the 30 to 45 MHz range. The receivers are tuned electronically by means of varactor diodes and are of novel design in that they do not have any intermediate-frequency stages. The frequency band can be swept 10 times per second or 100 times per second. The antennas used for the polarimeter are helical beam antennas, two for each of the circular components in the 15 to 26 MHz range and two for the 30 to 45 MHz range. Model studies of the antennas were conducted to establish whether they have suitable characteristics for observing the polarization of Jupiter's decametric radiation over a wide frequency range. Many spectral records of Jupiter's decametric radiation were obtained using a preliminary version of the swept-frequency receiver and a log-periodic dipole antenna. Some of the records are presented and one record which shows an interesting case of Faraday rotation is analysed.

ACKNOWLEDGEMENTS

I would like to thank Professor E.E. Baart, my research director, for his constant encouragement and unfailing interest in this project. The many discussions, which I had with him, and his vast fund of ideas never failed to stimulate me when certain phases of the project presented seemingly insurmountable obstacles.

My grateful thanks are due to the Council for Scientific and Industrial Research and the Council of Rhodes University for Research Scholarships throughout the duration of this project.

I am indebted to Professor J.A. Gledhill who suggested a method for calibrating the intensities of an oscilloscope trace on photographic film. I would also like to thank Dr. L.M.G. Poole for the discussions regarding the orientation of Jupiter's rotation axis as seen from Earth and Mr. J. Greener who assisted in processing the Faraday rotation data.

Further thanks are due to Professor E.E. Baart and Mr. J.H. Grobbelaar for their assistance in the design and construction of some of the electronic apparatus. I would like to thank Mr. R. Arnott and Mr. A. Barnard for constructing the various antennas used throughout this project and their

assistance in other mechanical problems encountered.

My grateful thanks are also due to Miss. J. Williams and Mrs. J. Eley who converted my notes into a presentable thesis and to Mr. R. Williams who did the bulk of the photographic work. I would also like to thank all those people who wittingly or unwittingly assisted me throughout this project.

Lastly, I wish to thank my parents for their constant encouragement and their unfailing optimism.

TABLE OF CONTENTS

CHAPTER II

THEORIES OF JUPITER'S DECAMETRIC RADIATION

CHAPTER III

SWEPT-FREQUENCY POLARIMETERS

CHAPTER IV

ANTENNAS

CHAPTER V

ELECTRONIC CIRCUITRY OF THE SWEPT-FREQUENCY POLARIMETER

CHAPTER VI

RESULTS AND FURTHER PROPOSALS

LIST OF FIGURES

LIST OF PLATES

LIST OF TABLES

CHAPTER I

PROPERTIES OF JUPITER'S DECAMETRIC RADIATION

1.1 INTRODUCTION

In the fifteen years since the chance discovery of Jupiter's decametric radiation in 1954 (Burke and Franklin, 1955; Franklin, 1959) a large store of knowledge of this phenomenon has been acquired. Some aspects of the radiation which have been subject to intensive study are : probability-of-occurrence as a function of frequency and central meridian longitude, intensity, period of rotation of the radio sources, polarization, dynamic spectrum, effect of ionospheric scintillations and possible effects of Jupiter's satellites. Any attempt to review the present state of knowledge of all the above, even if only superficially, would be well beyond the scope of this dissertation.

As this thesis is primarily concerned with the polarization and dynamic spectra of Jupiter's decametric radiation, we shall review these two important aspects in some detail. A study of the polarization and dynamic spectra cannot be made completely independent of the other aspects of the radiation and consideration of these aspects will be introduced in appropriate sections.

A brief survey of some of the theories of the origin of the Jovian decametric radiation will be made in Chapter II. The main purpose of the survey will be to

indicate what the theories predict for the polarization and dynamic spectra and to show how these predictions compare with the experimental results. These comparisons reveal the need for more experimental observations and additional work on the theory.

1.2 POLARIZATION OF JUPITER'S DECAMETRIC RADIATION

Briefly, we can make the following comments about the polarization of Jupiter's decametric radiation.

The first observations of the polarization showed that the radiation was either right-handed circularly polarized or right-handed elliptically polarized, according to the radio convention of looking along the direction of propagation. The same sense of polarization was observed in both the northern and southern hemispheres, thereby ruling out the possibility that the polarization was produced by the Earth's ionosphere. This strongly implied the presence of a magnetic field on Jupiter. Subsequent observations showed that left-handed polarization occurs more and more frequently at longer wavelengths. The polarization depends on the observing frequency as well as Jupiter's System III (1957.0) central meridian longitude (See Appendix I).

Subsequent measurements determined the polarization of the radiation by measuring the polarization fraction and the axial ratio. The polarization fraction is simply the ratio of the polarized intensity to the total intensity,

the total intensity being the sum of the polarized and unpolarized intensities. The axial ratio is the ratio of the minor axis of the polarization ellipse to the major axis. The sign of the axial ratio indicates the sense of polarization - a negative value indicating right-handed polarization. The polarization fraction is usually rather high and is of the order of 0.7 for 80% of the bursts.

Measurements at fixed frequencies and swept-frequency observations indicate that the sense of polarization can vary very rapidly from right to left and back again.

Before we review the above experimental results in detail, we shall describe the various types of polarization that are possible for electromagnetic radiation and show how these types may be distinguished from each other with suitable apparatus.

1.21 Types of polarization and their indentification

Types of polarization:

There are seven basic types of polarization; these are: elliptical polarization, circular polarization, linear polarization, random polarization (unpolarized), elliptical plus random polarization, circular plus random polarization and linear plus random polarization. Our present discussion will not include linear polarization as it is unlikely that a natural source, such as Jupiter, will produce linearly polarized radiation.

Radiation is said to be elliptically polarized if

the tip of the electric field vector traces out an ellipse, of constant axial ratio and orientation, in a plane perpendicular to the direction of propagation. The tip of the electric field vector of a circularly polarized wave traces a circle in a plane perpendicular to the direction of propagation. We shall call radiation "mixed" polarized radiation when circularly or elliptically polarized radiation is mixed with randomly polarized radiation. If the polarization of the radiation alternates between left-handed circular and right-handed circular polarization, the radiation is of "varied" polarization. Sophisticated experimental techniques are required to determine the state of polarization of the radiation.

Identification of the type of polarization:

There are a number of ways of identifying the state of polarization of electromagnetic radiation. The method most frequently used by Jupiter observers requires the use of either two linearly polarized antennas set at right angles which, with suitable circuitry, yield the oppositely polarized circular components of the wave, or two circularly polarized antennas which yield the oppositely polarized components directly. These oppositely polarized components are usually referred to as the left- and right-circular components. After amplification and detection these left- and right- circular components are recorded on pen recorder charts or on photographic film. Measurement

of the cross-correlation product of the left- and right-circular components in addition to their intensities permits the determination of the polarization fraction as well.

Another factor which influences the analysis of the polarization records is the speed of recording. The detection time constants of the receivers limit the fastest changes of polarization from left-handed to right-handed sense which can be resolved. The chart speed imposes a further limitation. The chart speed must be large enough to enable the time difference between the successive left- and right-handed polarizations to be apparent.

If circularly polarized radiation is incident on the antennas, there will be an output on either the left-hand or the right-hand channel depending on the polarization of the incident radiation. Elliptically and mixed polarized radiation will give an output on both channels, the sense of the polarization being given by the component of larger amplitude. It is impossible to distinguish between complete elliptical and mixed polarization without the use of a correlation channel. Radiation of varied polarization will give outputs on both channels.

Slow recordings (i.e. large time constants and slow chart speeds), without a correlation channel, cannot distinguish between elliptical, mixed and varied polarization. Fast recordings, without a correlation channel, cannot distinguish between elliptical and mixed polarizations but they will be able to resolve the varied polarization into

alternate left- and right-handed circular polarizations. Fast recordings, with a correlation channel, can distinguish between all the different types of polarization.

The experimental results will now be reviewed.

1.22 Early fixed-frequency observations

The decametric radiation from Jupiter has a very irregular nature with time structure on a number of different scales. The shortest component of the radiation is usually referred to as a "burst"; these bursts last from a fraction of a millisecond to a few seconds. A number of consecutive bursts constitutes what is known as a "storm". Storms can last from about five minutes to a few hours but durations of about an hour are more usual. Early measurements of the polarization of the radiation were made on the assumption that the radiation was completely polarized (i.e. no correlation channel was needed) and thus a mixture of polarized and unpolarized radiation was classed as elliptically polarized. The sense of the polarization was however, correctly deduced.

Not long after the discovery of Jupiter's decametric radiation, it was realised that in addition to determinations of occurrence probability and the intensity of the radiation, more refined measurements would have to be made. In 1956 Gallet (1961) proposed the study of the polarization of the radiation as a means of investigating the possible existence of a magnetic field on Jupiter. Franklin and

Burke (1958) and Gardner and Shain (1958) reported observing predominantly right-handed circular or right-handed elliptical polarization. The former group made a few observations at 22 MHz and the latter a single observation at 19.6 MHz. It thus appeared that the radiation was predominantly right-handed polarized.

Predominance of right-handed polarization:

The initial investigations had indicated a predominance of right-handed polarization near 20 MHz and this was confirmed by many workers. Smith and Carr (1959) reported that the radiation is entirely right-handed polarized at 22.2MHz and concluded that the polarization was a property of the source. Smith et al. (1960) and Carr et al. (1961) reported making simultaneous polarization observations in Florida and Chile. Right-handed polarization was observed at both stations at 22.2 MHz. This indicated that the terrestrial ionosphere does not exert any great influence on the polarization of the Jupiter radiation since similar polarizations are observed simultaneously in magnetically opposite hemispheres. The axial ratios measured at 22.2 MHz did not show conclusive dependence on Jupiter's central meridian longitude.

Observations of left-handed polarization:

Up till the end of 1961 all the observations indicated that Jupiter's decametric radiation was polarized

exclusively in the right-handed sense. Barrow (1962) gave the first indication that, at frequencies below 22 MHz, the radiation is not entirely right-handed polarized. His observations at 24 MHz indicated that the radiation was predominantly right-handed circularly or right-handed elliptically polarized at this frequency. His apparatus did not have a correlation channel and thus could not distinguish between complete elliptical polarization and a mixture of circularly polarized and randomly polarized radiation. Most of the radiation at 18.3 MHz was randomly polarized. He reports that 86% of all the bursts analysed at 18.3 MHz were randomly polarized while 12% of the bursts were right-handed elliptically or circularly polarized. The remaining 2% of the bursts were left-handed elliptically or circularly polarized.

Barrow's observations of left-handed polarization were confirmed by Sherrill and Castles (1963) who reported observations made on a two-helix polarimeter operating at eight discrete frequencies between 15.2 and 24.2 MHz. They assumed that the radiation was completely polarized and they could thus determine the apparent axial ratio of the polarization ellipse from the amplitudes of the left- and right-circular components received on the helices. The polarization survey showed a significant number of left-handed circularly polarized bursts and bursts having both circular components at frequencies below 20 MHz. In view

of the slowness of their recorder and the absence of a correlation channel, these latter bursts could have been of elliptical, mixed or varied polarizations. These bursts showed changes in the sense of polarization on a time scale of a few seconds.

Baart, Barrow and Lee (1966) reported the existence of very short bursts (less than 50 milliseconds duration). These very short bursts exhibited both senses of polarization at 22 MHz while normal bursts (0.2 - 2 seconds duration) were present at 14, 16 and 18 MHz. In most cases the very short bursts were preceded or succeeded by normal bursts at the same frequency. The records showed that a large proportion of the very short bursts were completely circularly polarized.

Relation of polarization to central meridian longitude:

No conclusive evidence was available to support any definite relation between the sense of polarization and Jupiter's central meridian longitude until the extensive observations of Sherrill and Castles (1963).

Their observations indicated that the sense of polarization might be related to Jupiter's central meridian longitude, the left-handed polarization being associated with storms from the subsidiary "sources" B and C rather than with storms from the main source A (See Appendix II). Further interesting features were observed below 20 MHz.

Certain storms showed a systematic change from left- to right-handed sense at a given frequency over periods of an hour. Others showed as many as four changes of polarization sense at a given frequency over periods of a minute.

Dowden (1963) took polarization measurements at 10.1 MHz and found that bursts having both senses of polarization were often observed. The algebraic mean axial ratio was a function of Jupiter's central meridian longitude. This is almost entirely due to the variation with longitude of the relative proportion of bursts of opposite sense of polarization. If bursts of the two senses (left-handed and right-handed) are analysed separately the two mean axial ratios show little or no variation with longitude and are approximately equal in magnitude.

Barrow (1964a) reported observing left-handed polarized bursts at 16 MHz. In another paper, Barrow (1964b) described how the polarization at 16,18,22 and 26 MHz was studied during 1963. He found that in general, for the period of the observations, most of the radiation at the two higher frequencies was right-handed polarized, whereas at the two lower frequencies appreciable proportions of the bursts were left-handed polarized. He found that most of the left-handed activity was emitted by source C.

Carr et al. (1965) gave a detailed report of the work done at the University of Florida. Using the observations made at their stations in Florida and Chile, they showed

that the lower the observing frequency the more sinusoidal the variation in mean axial ratio with central meridian longitude becomes.

The observations thus indicate that the radiation is almost entirely right-handed polarized above 20 MHz while increasing numbers of left-handed bursts are present at frequencies below 20 MHz. Left-handed emission is observed chiefly from sources B and C and the mean axial ratio is a function of Jupiter's central meridian longitude at frequencies below 20 MHz.

A number of workers (Dowden, 1963; Sherrill and Castles, 1963; Barrow, 1964b and Sherrill, 1965a) reported storms where the sense of polarization varied rapidly during periods when the emission showed complex burstiness on a time scale of seconds. Their intruments could not resolve the complex burst structure and no explanation of the rapid variations of the polarization was forthcoming. Warwick and Gordon (1965) reported a rapid "flipping" of the sense of polarization on a time scale of about 40 milliseconds. We will return to this phenomenon later.

1.23 Determination of polarization fraction

All the axial ratio determinations reported above were made assuming completely polarized waves. An improved estimate of the axial ratio can be made by determining the polarization fraction as well.

Early determination of polarization fraction:

Sherrill (1965a) reported observations made during 1963 on an improved two-helix polarimeter at five discrete frequencies between 15.5 and 24.2 MHz. The use of a correlation channel permitted the determination of the polarization fraction and hence an improved estimate of the axial ratio and a more complete specification of the state of polarization of the radiation. Right-handed polarization was found to predominate at all observed frequencies, with the majority of bursts above 15.5 MHz indicating axial ratios more circular than 0.7 and with a polarization fraction greater than 0.8. However, an increasing incidence of left-handed and mixed polarized bursts was observed with decreasing frequency. Activity was also observed where bursts of both right-handed and left-handed polarization appeared at the same frequency within a period of seconds.

Polarization fraction at 18 MHz:

Barrow and Morrow (1968) reported the results of an extensive polarization study at 18 MHz. They used crossed Yagi antennas and could measure the left-handed and right-handed components of the radiation as well as the correlation between the amplitudes of these components. They reported that the distribution of axial ratio and polarization fraction indicated that some 45% of the bursts are

circularly polarized and that the polarization fraction is generally rather high, some 80% of the bursts having polarization fractions greater than 0.7. They found that a number of circularly polarized bursts are superimposed on a randomly polarized background and thus appear to be elliptically polarized if only the left-handed and right-handed components are used to calculate the axial ratio. The correlator channel in their studies indicated that many of the low axial ratio bursts are almost linearly polarized. They pointed out that Dowden (1963) had suggested that any observed linear polarization might be due to simultaneous observation of circularly polarized bursts of opposite sense.

To sum up, the axial ratio computed for the observing frequencies between 15.5 and 24.2 MHz indicate that right-handed bursts predominate at all frequencies, with axial ratios generally greater than 0.7. The very short bursts all show a definite sense of polarization and a large proportion of them are completely circularly polarized. In general the sense of polarization at 18 MHz is predominantly right-handed with almost half the bursts circularly polarized and frequently superimposed on a randomly polarized background. The polarization fraction is usually greater than 0.7 for some 80% of the bursts, thereby partially justifying the usual assumption of completely polarized waves for the Jupiter activity in the 16 to 24 MHz range. The effect of assuming complete polarization (as is often the case when

only left-handed and right-handed components are measured) is to obscure the amount of circular polarization present and hence to reduce the average axial ratio.

Swept-frequency polarization measurements:

Up till the end of 1963 all polarization measurements had been made at fixed frequencies. The frequency dependence had been studied by making simultaneous observations at adjacent fixed frequencies (usually 1 or 2 MHz apart). There are obvious limitations to this method of observation as little can be said about continuous variations in polarization with frequency. A swept-frequency polarimeter enables the frequency and time dependence of the polarization to be studied.

During the latter part of 1964, Warwick and Gordon (1965) operated a swept-frequency polarimeter at Arecibo in Puerto Rico. We shall not present the results of their observations here but rather defer the discussion of their swept-frequency polarimetry experiment until after we have reviewed the spectral characteristics of Jupiter's decametric radiation in section 1.3.

1.3 THE SPECTRAL CHARACTERISTICS OF JUPITER'S DECAMETRIC RADIATION

The first observations of the spectra of Jupiter's decametric radiation showed that storms had complicated structure in both frequency and time. Bursts lasting for

more than five seconds and having fairly narrow bandwidths (less than 1 MHz) were common. Storms extending over many MHz and lasting for periods up to an hour were also observed. Frequently storms drifted slowly from one frequency to another; a frequency drift is considered positive if frequency increases with time. Positive frequency drifts occurred at central meridian longitudes earlier than 190°, while negative frequency drifts occurred at later longitudes.

The spectra of individual storms exhibited certain characteristic features which tended to reappear near the same central meridian longitudes on different observing days. These observations indicated that Jupiter has a permanent radio spectrum. This permanent radio spectrum was subsequently shown to be Io-related.

Fast spectral measurements showed extremely short bursts which had large drift rates from high to low frequencies of the order of 20 MHz/sec and showed rapid "flipping" of the sense of polarization.

Before we describe the above experimental results in detail, we will indicate briefly how a swept-frequency receiver operates and how observations with such a receiver are presented.

1.31 Swept-frequency receivers

Almost all the early observations of Jupiter's radio spectrum were made using fixed-frequency receivers - i.e.

receivers which are tuned to a particular frequency for the duration of the observations. Many fixed-frequency receivers are needed to determine the spectral characteristics of Jupiter's decametric radiation. Since some of Jupiter's radio bursts are known to have bandwidths of the order of 50 kHz, receivers would have to be tuned to frequencies separated by this amount if the spectral characteristics of these narrow-band bursts are to be studied. This would require many receivers to cover even a 1 MHz frequency band; and this is only a small part of Jupiter's radio spectrum.

Swept-frequency receivers :

The above problem can be resolved by using a single receiver which tunes continuously to successive frequencies in a given frequency band and repeats the tuning cycle within a prescribed period. The process of tuning continuously across the frequency band is often referred to as "sweeping" and such a receiver is called a "swept-frequency" receiver.

Swept-frequency receivers are usually of the super-heterodyne type employing a sweeping local oscillator stage and one or more intermediate-frequency stages. The tuning across the frequency band (sweeping) can be done in one of several ways. The two most popular methods use motor-driven variable capacitors or voltage-variable capacitance diodes (varactor diodes) to change the frequency of the local oscillator. The output of the local oscillator is mixed with the incoming signals to give the intermediate frequency

which then contains all the required information. The output of the final intermediate-frequency stage is detected and amplified.

The frequency and time resolution of the receiver depend on the intermediate-frequency bandwidth, the post-detection time constant and the sweep rate of the receiver. The intermediate-frequency bandwidth sets the lower limit on the frequency resolution of the receiver while the time constant and the sweep rate limit the time resolution. A swept-frequency receiver which has a small sweep rate, large bandwidth and large time constant cannot detect very fast variations in frequency and time. This is a "slow" swept-frequency receiver. A "fast" or "high-resolution" swept-frequency receiver can detect fast variations such as Jupiter's short bursts.

Presentation of spectra:

The output of a fast swept-frequency receiver is complex and usually has to be monitored on an oscilloscope. The oscilloscope screen is photographed on a continuously moving film. The successive frequency sweeps will then appear as individual traces across the film and the sweeps will be separated in time along the length of the film. The amplitudes of the signals at any particular part of the frequency sweep can be shown by the deflections at the corresponding parts of the trace. The speed of the film past the oscilloscope screen must be large enough to separate the individual traces. This usually requires large film transport

speeds and long lengths of film are needed for a few minutes of recording.

It is far more convenient and economical to intensity-modulate the oscilloscope trace with the receiver output signal. A frequency sweep appears as a single straight trace across the screen and the film is blackened during those portions of the sweep where there are output signals from the receiver. Successive frequency sweeps appear as a series of closely spaced parallel traces across the width of the film. The receiver output is thus displayed as a three-dimensional frequency-time-intensity plot. The frequency axis is across the width of the film and the time axis is along the length of the film. The blackening of the film at any point of a particular trace gives the amplitude of the signal at the corresponding point in the frequency sweep.

The system of observation outlined above give dynamic (or continuous) recordings of the spectrum of Jupiter's decametric radiation.

We shall now review the experimental results.

1.32 Initial work at fixed-frequencies

Some of the earliest observations to determine the spectral characteristics of Jupiter's decametric radiation were carried out during the 1955/1956 apparition. These fixed-frequency observations were to determine the band-width of the radiation as well as the frequency range in which the radiation could be observed.

Observations reported by Gardner and Shain (1958)

showed a large decrease in activity with an increase in frequency. Initial indications of sharp spectral characteristics were confirmed when it was found that activity at any particular frequency was not necessarily accompanied by activity on frequencies 2 MHz higher or lower. Good correlation over a 0.1 MHz band was observed, establishing the radiation as relatively narrow-band, with a bandwidth somewhere between 0.1 and 0.2 MHz (Franklin and Burke, 1958). Storms having frequencies between 14 and 27 MHz were detected by Gardner and Shain, and Kraus (1958) reported an observation at 43 MHz.

Fixed-frequency observations determined the frequency band over which the radiation could be observed but gave little indication of the continuous variations of the radiation with frequency. A swept-frequency receiver enables the frequency and time dependence of the bursts and storms to be studied.

1.33 Results of the Boulder High Altitude Observatory Spectrograph

During 1960 a swept-frequency spectrograph went into operation at the High Altitude Observatory at Boulder in Colorado. The spectrograph was a modified version of a swept-frequency interferometer which had been used to study solar radiation. The spectral records of broad-band radiation all showed characteristic interferometer fringes which appeared as alternate light and dark diagonal bands

across the records.

Early spectral observations:

Warwick (1961) reported the first dynamic, that is continuous, recordings of the spectrum of Jupiter's decametric radiation in the frequency range from 15 to 34 MHz. The swept-frequency receiver was of the superheterodyne type using mechanical tuning. The records were presented as an intensity-modulated display on sensitised paper. The receiver had a sweep rate of 27 MHz/sec, repeated at 1.3 second intervals, a bandwidth of 1 MHz and an integration time constant of about three seconds. Fine structure in frequency, on a scale smaller than 1 MHz, could therefore not be observed. Individual bursts less than several seconds apart did not show as distinct entities on the records.

Burst structures lasting for 5 or more seconds and having bandwidths narrower than 2 MHz were frequent, thus confirming the earlier fixed-frequency observations. Several striking features not previously reported were apparent. On numerous occasions broadband storms covering 5 or more MHz and lasting for periods greater than one hour appeared on the records. These broadband storms often drifted slowly from one frequency to another, positive drifts occurred at central meridian longitudes earlier than 190° while negative drifts occurred at later longitudes. One storm drifted up to the 34 MHz high-frequency limit of the receiver and this was the highest recorded frequency since that reported by Kraus in

1958. Warwick states that these slowly drifting phenomena could not be attributed to effects in the terrestrial ionosphere as one negatively drifting storm was observed simultaneously at Yale University where very limited spectral observations were made.

During 1961 the Boulder spectrograph was extended in frequency range to cover the band between 7.6 and 41 MHz (Warwick, 1963a). The receiver bandwidth was decreased to 0.6 MHz and the receiver sensitivity was increased. The longitude and drift correlations as well as the other features of the earlier spectra were immediately confirmed by the improved instrument. However, several new features were also apparent. One storm remained constant in frequency for an hour and had a bandwidth of about 0.6 MHz, the frequency resolution of the receiver. Some storms showed isolated patches of emission made up of bursts which probably lasted for less than a second. Warwick suggested that these short bursts were probably not a property of the source but were caused by scintillations in the terrestrial ionosphere.

Repeatability of Jupiter's decametric radio emission:

Warwick (1963a,b) reported the results of an extensive study of the spectra obtained during 1961 and 1962. A number of characteristic features in Jupiter's radio spectrum are reproduced repeatedly when Jupiter presents certain narrow ranges of longitude toward the Earth. Furthermore the

frequency drifts in the spectrum also repeat, with virtually identical slopes in the time-frequency domain. By analogy with the optical features of the planet Warwick calls the characteristic radio features landmarks, and suggests that Jupiter possesses a more or less permanent set of radio landmarks. i.e. a permanent dynamic spectrum.

Io-control of the early source dynamic spectra:

The great importance of the Boulder spectrographic data was emphasised in 1964 by the discovery by Bigg (1964) that Io, Jupiter's first Galilean satellite, strongly modulates Jupiter's decametric radiation.

Bigg, using all the Boulder spectrographic data available at the time, found that the probability of a Jupiter storm being observed on Earth depended strongly on the position of Io. Three-dimensional plots of probability-of-occurrence against central meridian longitude and Io departure from superior geocentric conjunction, at the times of the storms, were made. Superior geocentric conjunction occurs when Io is directly behind Jupiter as seen from the Earth. These three-dimensional plots showed that for Io positions between 70° and 110° from superior geocentric conjunction and central meridian longitudes between 90° and 185° there is a high-probability peak. There is a second broader and lower-probability peak for longitudes in the range 200° to 280° and Io positions in the range 220° to

260^{o}. The Io-control of the decametric radiation is more complete at frequencies above 30 MHz (Duncan, 1966; Gruber, 1967). The Boulder spectrograph can record emission up to 41 MHz which is about 10 MHz higher than the frequencies of prior observations. It is in this 10 MHz range that the radiation responds most sensitively to Io; this probably explains why it took so long to discover the Io-effect.

One of the striking initial results of the Boulder spectrographic observations was that the central meridian longitude defined Jupiter's radio spectrum. Dulk (1965a,b) first recognised Io's control of these earlier spectra and showed that there is a strong ordering of early source dynamic spectral types according to the exact position of Io at the time of emission. The maximum frequency reached by the emission during an early-source storm also depends on Io's orbital position. The Io-control of the main source and the third source spectra is not nearly as complete as the Io-control of the early source spectra.

The discovery of the Io-effect on the dynamic spectrum of Jupiter's decametric radiation caused some modifications to the theories of the origin of Jupiter's radio noise and also stimulated much theoretical work.

1.34 High-resolution dynamic spectra

Up till the end of the 1963 apparition the only continuous swept-frequency spectrograph in operation was that at Boulder. This instrument was useful for studies of the

coarse frequency-time structure of Jupiter's dynamic spectrum. However the spectrograph, with its sweep period of 1.3 seconds and long integration time constant, cannot resolve very rapid variations of intensity. The frequency resolution is also limited by the relatively wide bandwidth, but the spectral records nevertheless showed a considerable amount of fine structure in frequency.

Fixed-frequency observations of fine structure in Jupiter's decametric bursts were reported by Gardner and Shain (1958), Kraus (1958), Gallet (1961), Carr et al. (1961), and other workers. Rapid variations in intensity as a function of time were found, and most workers agreed on the existence of short bursts with durations of a fraction of a second. High-resolution spectrum analysers were needed to study the frequency and time dependence of these short bursts (roughly 0.1 seconds duration). The high-resolution spectral observations that have been carried out to date can be divided into two classes: observations carried out over a wide range of frequencies and observations carried out over a narrow range of frequencies. The only high-resolution observations that have been made over a frequency band greater than 2 MHz are those of Warwick and Gordon (1965) at Arecibo in Puerto Rico. Their swept-frequency polarimeter operated over the frequency range from 24 to 36 MHz. The only other high-resolution observations that have been made are those made by Riihimaa (1964a,b; 1966a,b,c) over

a frequency band of 2 MHz or less.

We shall first present the observations made by Riihimaa and then describe the observations of Warwick and Gordon. It is fitting that the review of the experimental observations of the polarization and spectral characteristics of Jupiter's decametric radiation should conclude with a discussion of the only swept-frequency polarimetry experiment which has been carried out.

High-resolution studies by Riihimaa:

Riihimaa's high-resolution studies were made on two kinds of receivers: swept-frequency receivers and multi-channel receivers. The earlier swept-frequency observations are presented first.

During the 1963 apparition of Jupiter, an experiment was carried out relating to the fine structure in the dynamic spectra of the Jovian decametric radiation (Riihimaa, 1964a,b). The swept-frequency receiver was swept electronically between 20 and 18 MHz with a sweep repetition frequency of 10 sweeps/sec. The bandwidth of the receiver was 80 kHz and the integration time constant was 0.1 milliseconds.

Generally the records showed groups of bursts lasting from a few seconds to a few tens of seconds. Sometimes a group of bursts could be resolved into very short bursts with durations down to about 5 milliseconds. On several occasions storms consisting of several intense short bursts

were recorded. These high intensity bursts showed bandwidths narrower than the operating range (18-20 Mhz) and they gathered into bands which drifted negatively in frequency at rates varying between 0.1 and 0.8 MHz/min. The structure of the very short bursts was thus seen to be very complex and more refined apparatus was needed to study these bursts effectively.

During 1964 Riihimaa (1966a) repeated his earlier fine structure experiment but used different techniques of observation. He used a high-resolution multi-channel spectrograph to observe a 0.7 MHz band centered at 19.0 MHz. The individual receivers were spaced at 50 kHz intervals and had bandwidths of 5 kHz. The dynamic spectra were recorded photographically from intensity-modulated indicator lamps, the integration time constant being 30 milliseconds.

Most recordings showed similar variations of intensity with time from channel to channel, indicating radiation bandwidths of the order of 500 kHz or more, the durations of the bursts ranging from a few seconds to a few tens of seconds. Some of his records had portions showing fine structure composed of bursts with bandwidths of 50 kHz or less. The duration of the bursts varied from the resolution limit of the equipment (30 milliseconds) to a few seconds.

Riihimaa (1966b,c) repeated his multi-channel high-resolution experiment during 1965. The equipment was essentially the same as that for the previous experiment and

consisted of a 14-channel spectrograph with channel to channel spacing of 50 kHz and a centre frequency of 19.1 MHz.

The new results supported the earlier ones and there were indications of three types of dynamic spectra. The most common type of spectrum had practically no fine details, had typical bandwidths of 0.5 MHz or more and had bursts of a few seconds duration. The second type of spectrum showed more detail. The storms were composed of bursts which often had bandwidths of the order of 50 kHz and the durations of the individual bursts were about 1 sec. The third type of spectrum was very complex. It was composed of pulses which had bandwidths down to 50 kHz while the pulse durations often went down to the resolution limit of the equipment (30 milliseconds). The first type of spectrum occurred most often when the Main or A source was in the central meridian. The second type occurred most often for the early or B source while the third type occurred most often for the B and C sources.

The experiment showed that there were considerable variations in the bandwidth properties of Jupiter's decametric bursts. Riihimaa suggested that it was therefore doubtful whether a classification of the bursts could be made only on the basis of their duration and suggested further that the classification of radio bursts from Jupiter should be based on their high-resolution dynamic spectra.

In two recent papers Riihimaa (1968a,b) reported

high-resolution swept-frequency observations made during 1967/1968 in the 21 to 23 MHz frequency range. The receiver was swept electronically and had a bandwidth of 50 kHz. The integration time constant was 1.25 milliseconds and the sweep repetition rate was 20 sweeps/second.

Riihimaa found that the dynamic spectra of Jupiter's decasecond bursts consisted mostly of parallel but irregularly spaced bands of emission, separated by 200 to 300 kHz. These bands drifted in frequency and the drift rate magnitudes appeared to cluster around 100 kHz/second and the direction of drift usually depended on the central meridian longitude. Practically all the positively drifting bursts were from source B while almost all the source A storms were negatively drifting.

Riihimaa and Warwick (1968) reported a systematic search for these parallel lanes of emission in the Arecibo spectra taken in 1964. They found that the drift patterns exist on the Arecibo records and that the magnitudes and signs of the drift rates are in agreement with the results reported by Riihimaa in 1968.

Swept-frequency observations of Warwick and Gordon:

Using a receiver originally designed by Riihimaa (1961) for solar studies and subsequently modified for Jupiter observations, Warwick and Gordon (1965) and Gordon and Warwick (1967) made simultaneous measurements of the polarization and spectrum of Jupiter's radio bursts in the

frequency range from 24 to 36 MHz during the last quarter of 1964. The receiver was of the superheterodyne type using voltage-variable capacitance tuning of the radio frequency pre-amplifiers and the local oscillator. The radio-spectrograph tuned from 36 to 24 MHz at a sweep-repetition rate of 100 sweeps/second. The bandwidth of the receiver was 65 kHz and the integration time constant was 54 micro-seconds.

They used the 1000-foot telescope at Arecibo with broad-band, crossed log-periodic dipole antennas connected to give the left- and right-circular components of the radiation. By combining the left- and right-circular components they could measure the cross-correlation product between these components. The polarization of the incident radiation could thus be completely determined. The receiver was operated on a time-shared basis between the three modes and was programmed to sweep the left-circular, correlation, right-circular and correlation channels consecutively. Each sweep in a given mode took 10 milliseconds to complete. It is thus clear that the left- and right-circular components are not recorded simultaneously and that there is a 40 millisecond delay between successive sweeps on either the left- and right-circular channel.

The data was presented as an intensity-modulated display on 35 mm. film, the correlation channel occupying one half of the film and the left- and right-circular channels the other half.

Most of the records showed no variations on a time scale shorter than about 1 second and most bursts lasted for a few tens of seconds. These long bursts were often broad-band and drifted slowly in frequency at negative drift rates of about 0.9 MHz/min. These bursts were similar to the bursts observed on the Boulder records. They found that the long bursts were right-handed elliptically polarized with roughly constant axial ratio and orientation of major axis as a function of a frequency above 24 MHz.

Apart from these general observations of the long bursts, they also reported storms of very short bursts. In three of the nineteen storms recorded, bursts occurred which were less than 0.2 MHz in bandwidth and had durations of less than 20 milliseconds at a given frequency. These very short bursts drifted negatively in frequency at the large drift rates of 25 to 35 MHz/sec. One particular storm consisted of bursts of the order of seconds which occurred simultaneously with the very short bursts. The short bursts appeared super-imposed on the background of the long bursts. The long bursts and the short bursts appeared simultaneously for only a few minutes, after which the storm consisted entirely of short bursts. On the basis of this observation they concluded that the very short bursts must be a property of the source and could not be attributed to scintillations in the terrestrial ionosphere or the inter-planetary medium.

The polarization of the short bursts was generally

elliptical and changed very rapidly from one sense to the other as the bursts drifted down in frequency. In a particular section of one of the records the polarization of the short bursts was circular and varied in an unusual way. During a particular sweep there were alternations in the sense of the circular polarization with frequency and during subsequent sweeps there were alternations of the sense of the circular polarization at the same frequency. The polarization thus varied rapidly with both frequency and time; they called this specialised variation of polarization "polarization diversity".

The above discussion might appear to indicate that there is a wealth of high-resolution spectrographic data available. However, this is not really so. The only instrument capable of high-resolution polarization observations over a large frequency range (10 MHz or more), is no longer in operation and no studies of this nature have been carried out since 1964. The single record of the polarization diversity and the large drift rates of the short bursts have yet to be confirmed by other workers. The observations of Riihimaa, although more recent, cover only a narrow band of frequencies. It is thus clear that there is a large gap in our knowledge of the high-resolution swept-frequency polarization characteristics of Jupiter's decametric radiation.

1.4 FARADAY EFFECT ON THE DECAMETRIC EMISSIONS

Electromagnetic waves from Jupiter must pass through the Earth's ionosphere (and the interplanetary medium) to reach our receivers. The ionosphere is a strongly doubly-refracting plasma at decametric wavelengths. A partially polarized wave is split into two independent modes of propagation, each of which has a different phase velocity. The polarization ellipse of the emergent wave is therefore rotated with respect to the incident wave; but the axial ratio and sense of rotation remain unaltered if there is no preferential absorption.

1.41 Discovery of the Faraday effect for Jupiter

During 1963 the Boulder spectrographic records of emission from Jupiter contained an unusual amplitude modulation as a function of frequency (Warwick and Dulk, 1964; Dulk, 1965b). This modulation was evident as alternate light and dark bands lying, in most cases, nearly parallel to the time axis of the dynamic spectral records. The bands were more closely spaced at low frequencies than at high frequencies and were visible over the frequency range from approximately 35 to 15 MHz.

The structure of the bands suggested that they may be caused by the reception of elliptically polarized radiation on a linearly polarized antenna, when the direction of the major axis of the ellipse is rotated as a function of frequency. The maxima and minima of intensity on the

records are produced as the major and minor axes of the ellipse are successively aligned with the linearly polarized antenna. The crowding of the bands towards lower frequencies is almost inversely proportional to the square of the frequency. The above observations suggested that the alternate light and dark bands were caused by Faraday rotation in the Earth's ionosphere, the interplanetary medium or Jupiter's ionosphere, or in all three. Faraday rotation would be apparent on the Boulder records since the antennas were vertically polarized corner reflectors.

Warwick and Gordon (1965) and Gordon and Warwick (1967) reported Faraday fringes on their Arecibo records of the cross-correlation product of the left- and right-circular components of the radiation. Riihimaa (1966c) reported Faraday fringes in his records obtained with a low-resolution phase-switched swept-frequency interferometer in the frequency range 20 to 15 MHz.

1.42 Analysis of the data

From the Faraday fringes on the Boulder spectrographic records Warwick and Dulk (1964) and Dulk (1965b) determined the orientation of the polarization ellipse at the receiver over the frequency range from 20 to 35 MHz. Then they determined the total amount of Faraday rotation from the source to the receiver. With the total amount of Faraday rotation known, they checked its origin by attributing all the rotation to effects in the

Earth's ionosphere, computing the electron content of the ionosphere, and then comparing the results with estimates of electron content made by other means.

They neglected the effect of Faraday rotation in the interplanetary medium since this would not exceed 0.3 radian, due to the low electron densities and small magnetic field in the interplanetary medium, and this is minute compared to the total Faraday rotation. They found fairly good agreement ($\pm$10%) between the two values for the electron content of the Earth's ionosphere and concluded that practically all the Faraday rotation occurs in the Earth's ionosphere. This result was entirely unanticipated since it was expected that, on the basis of estimates of electron densities in Jupiter's ionosphere and the predicted values for the magnetic field, the Faraday rotation at Jupiter would be as much as or even more than that of Earth.

From the measured position of the major axis of the polarization ellipse at the receiver and a knowledge of the total Faraday rotation in the Earth's ionosphere, they extrapolated backward to find the position of the major axis of the polarization ellipse at the source.

1.43 Implications of the observed Faraday effect

The non-existence of Faraday rotation in Jupiter's ionosphere does not necessarily indicate that the estimates of electron density and magnetic field intensity were in error

but rather that there might be special propagation conditions in Jupiter's ionosphere under which the waves do not experience Faraday rotation. Warwick and Dulk attempted to explain the lack of Faraday rotation in Jupiter's ionosphere by requiring that the waves leaving Jupiter are entirely in a single mode. Since the waves impinging on the Earth's ionosphere are eliptically polarized (as they must be if we are to observe the terrestrial Faraday effect), the base modes for wave propagation in Jupiter's ionosphere must be elliptical rather than circular. In the Earth's ionosphere the base modes are circular for the frequencies at which Jupiter's decametric radiation is observed.

They suggested that the radiation is generated in the extraordinary mode, and since only one mode is present the radiation passes through Jupiter's ionosphere unaffected by Faraday rotation. The radiation thus arrives at the top of the Earth's ionosphere with a fixed orientation of major axis i.e. the orientation is independent of frequency. On entering the Earth's ionosphere the radiation splits into the two characteristic (circular) modes, undergoes Faraday rotation and arrives at the ground with the observed Faraday rotation. They concluded that the major axis of the polarization ellipse is approximately parallel to the magnetic equator of Jupiter, and that the polarization properties at Jupiter show no radical changes over the frequency range from

15 to 39 MHz.

Parker, Dulk and Warwick (1969) reported a further analysis of the Faraday effect on Jupiter's radio bursts. Using all the Boulder spectrographic data of the early source emissions from 1960 to 1967, they found that at Jupiter, the ellipse has an orientation independent of frequency over the range 15 to 35 MHz, and that its major axis has an average position angle of $-25^{\circ} \pm 15^{\circ}$ from the magnetic dipole axis. The orientation angle is measured from Jupiter's magnetic north pole to the ellipse, north through east. This value differs from the preliminary result reported by Warwick and Dulk. Parker, Dulk and Warwick also reported the observations of Bennett et al. (1965), who found that the alignment was very nearly parallel to Jupiter's rotational equator. (This reference is unfortunately not available).

New experimental evidence is needed to clarify the problem of polarization ellipse orientation at Jupiter.

CHAPTER II

THEORIES OF JUPITER'S DECAMETRIC RADIATION

2.1 INTRODUCTION

The present chapter describes some of the theories which have been proposed to explain the origin of the observed decametric radiation. No attempt will be made to describe the theories in detail, but we will indicate what the predictions for the observed decametric radiation are and how, in some cases, the predictions agree with the experimental results.

The earlier suggestions of lightning flashes or volcanic stimulation of the Jovian ionosphere were soon discarded and attention was focused on methods of generation by particles streaming through the ionosphere or magnetosphere. To account for the observed circular polarization it was assumed that the planet possesses a magnetic field which strongly affects either the generation process or the escape of the generated radiation.

The first two theories presented are those of Warwick and Ellis. These theories describe many of the observed effects fairly well, but have certain inherent difficulties.

The most recent theoretical work has centered around the question of how Io, Jupiter's first Galilean satellite, modulates the emission. The Gledhill theory gives a model which describes the longitude and frequency dependence well and includes the Io-effect as an integral part of it, but as yet it lacks a developed theory of the generation

mechanism. The most comprehensive theory of the interaction between Io and the Jovian magnetic field is that of Goldreich and Lynden-Bell.

2.2 WARWICK'S RADIATION MODEL

Warwick (1961, 1963a,c, 1964) based his model on a group of dynamic spectra taken on the Boulder swept-frequency spectrograph. These spectra were later shown to be Io-related, which implies therefore, that even if Warwick's model should be correct it only explains the spectrum of the Io-related emission.

2.21 Description of the theory

The radiation is assumed to be produced by fast electrons precipitated from Jovian radiation belts by magnetic disturbances. The electrons move down lines of force and generate Cerenkov radiation in the ionosphere. The emission is assumed to take place at frequencies close to the gyro-frequency and to be beamed in the direction of motion of the electrons, escaping after reflection either by a denser layer of ionosphere or else by the solid surface of the planet. The magnetic field is assumed after Morris and Berge (1962), to be due to a dipole inclined at 9^{o} to the rotation axis. The geometry of these reflections together with the asymmetric field accounts for the observed longitude-spectrum profile.

Using the above assumptions, Warwick found, by trial

and error, that profiles similar to the observed ones require the dipole to be located:

1) near the axis of rotation but well away from the equatorial plane (to achieve a slowly drifting spectrum);
2) roughly 0.7 Jupiter radii south of the equatorial plane and displaced by a lesser amount from the axis, in the direction of Earth when the central meridian longitude is 200° (to achieve the correct senses of frequency drift either side of longitude 200°), and
3) displaced slightly from the plane specified by the rotational axis and the central meridian longitude of 200° (to achieve the small asymmetry of the spectra about the 200° central meridian longitude).

The sense of the dipole field is also determined by the theory. The Cerenkov radiation is generated in the extraordinary mode so that to produce right-handed polarization for the reflected waves received at the Earth, the northern pole of the planet must be a magnetic north seeking pole - i.e. the magnetic field has the opposite sense to that of the Earth.

2.22 Predictions and criticisms of the theory

The synthetic spectra produced on the basis of the above assumptions reproduced quite closely the observed, Io-related,

spectral features. The model explained the two major sources (A and B) of the decametric bursts above 20 MHz and their frequency drifts.

At the time Warwick proposed his theory, polarization observations were still rather few. The theory predicted the presence of a single polarization sense (right-handed) at all longitudes and cannot explain at all the recent observations of variations of axial ratio with frequency and longitude.

According to Ellis (1965), there are several difficulties in Warwick's theory, not the least of which is the requirement of a highly asymmetric dipole location, although this was supported to some extent by the observations of Morris and Berge. Recent very accurate measurements at decimetric wavelengths (Branson, 1968) have shown that it is unlikely that displacements of the magnitude required are present.

Warwick's original theory was proposed before the discovery of the Io-effect and has recently been updated to include the Io-effect (Warwick,1967). Warwick believes that hydromagnetic waves or particle disturbances generated near Io must move from the radius of Io's orbit to smaller radii in order to generate radiation beamed towards the Earth.

2.3 THE DOPPLER-SHIFTED CYCLOTRON THEORY

One of the most detailed theories of the Jupiter

emission is that of Ellis (1962a,1963,1965) and Ellis and McCulloch (1963). An attractive feature of this theory is that it is based upon conditions similar to those which are known to exist in the Earth's upper atmosphere. The theory is able to make predictions about the polarization and the spectral variations of the bursts observed at the Earth. Some of the predictions can be tested experimentally.

2.31 Description of the theory

The theory assumes that the Jovian decametric radiation is due to cyclotron radiation emitted by bunches of electrons travelling through a postulated Jovian magnetosphere as a result of disturbances near the outer boundary of the exosphere. The electrons travel in helical paths down high-latitude magnetic field lines and in so doing emit electromagnetic radiation.

If the electrons are not highly relativistic, they will radiate mainly at the cyclotron frequency and the higher harmonics of the cyclotron frequency may be neglected. The observed frequency will be the Doppler-shifted cyclotron frequency. Much of the radiation emitted by the spiralling electrons will be unable to escape, as to do so it would have to pass through a magneto-ionic stop region, i.e. one in which the refractive index is imaginary. If, however, the electrons have sufficient velocity, the forward radiation will be Doppler-shifted to a frequency greater than the extraordinary wave critical frequency, and will therefore escape.

Cyclotron radiation can also occur backwards and radiation in the Cerenkov mode is always possible. Neither of these can escape from the Jovian exosphere, however, as this would require propagation through a region for which the refractive index is imaginary and the attenuation is very great.

Radiation may therefore be received from bunches of electrons moving toward the planet and from bunches moving away from the planet after reflection at the mirror point. Inward-travelling bunches produce bursts of increasing frequency due to the increasing magnetic field. These bursts escape after reflection at the appropriate extra-ordinary mode reflection level. Outward travelling bunches produce bursts of decreasing frequency. In both cases, after refraction the emerging radiation is mainly confined to the surface of a cone whose axis is the magnetic field. The angular radius of the cone can be determined from Snell's Law on the assumption that surfaces of constant refractive index are plane and perpendicular to the magnetic field direction. It can be shown that the cone angle decreases with increasing frequency.

Using as an example the generation of whistlers in the Earth's magnetosphere by the above mechanism, they assume that the radiation will only take place from field lines with a high magnetic latitude. Activity will only be observed on Earth when the cone of the radiation is swept over the

Earth.

The Io-control is introduced into the Doppler-shifted cyclotron theory by requiring that either the occurrence of electron streams or the momentum distribution of the electrons within the streams is modified by Io, possibly via hydromagnetic or electromagnetic radiation from Io. These disturbances in the electron distributions must propagate through the large difference in Jupiter longitude between the position of Io and the source region of the decametric radiation.

2.32 Predictions of the theory

The present discussion will be confined to the predictions which have bearing on the polarization and dynamic spectra, although many of the other observed properties of the decametric radiation are also predicted.

The distribution of the polarization of the bursts is contained in the foregoing theory since the axial ratio, r, of the polarization ellipse will depend mainly on the half angle of the emission cone, α . That is

$$r = \pm \cos\alpha \qquad (2.1)$$

The cone angle depends strongly on the pitch angle of the spiralling electrons (the angle between the electron velocity and the magnetic field) and the refractive index of the magneto-ionic medium. Since the pitch angle of the spiralling electrons depends on the magnetic latitude, the distribution of axial ratios can be changed considerably by a small change in the magnetic latitude of the source.

It can be shown from the theory that the sum of the axial ratios is related to the number of bursts by

$$\Sigma |r| = N^p \qquad (2.2)$$

where p as predicted by the theory is 1.05 and N is the number of bursts.

Ellis computed a synthetic dynamic spectrum in the 18 to 40 MHz frequency range for the early source (Jupiter emission in the central meridian longitude range 70^o to 190^o). His spectrum contains a number of bursts drifting successively from low to high frequencies and back to low frequencies. These drifting burst groups have the appearance of a number of overlapping loops in the dynamic spectrum. Large numbers of these overlapping loops produce an envelope similar to the positive drift profile of early source emission as observed at Boulder.

Finally, Ellis derives a schematic dynamic spectrum for the 18 to 20 MHz frequency range and the central meridian longitude range from 95^o to 115^o. This schematic spectrum represents the start and end points of some of the loops in the larger spectrum described above. The spectrum exhibits structure on several time scales - tens of minutes, seconds and milliseconds. He suggests that the longer duration structures are composed of millisecond bursts so that a normal burst (0.2 to 2 seconds duration) is due to the random superposition of millisecond bursts. He predicts that these fine structures in time will have negative

(decreasing in frequency) drift rates in the range from 30 to 50 MHz/sec.

2.33 Comparison of theory and observations

The observational results give good agreement with the theoretical predictions for a number of cases.

Dowden (1963) found that observations at 10.1 MHz gave an axial ratio distribution similar to that predicted by equation (2.1). To test the prediction for the sum of the axial ratios in equation (2.2), Dowden used the following technique. He divided his records into 60° central meridian longitude ranges and calculated r for each of the N bursts in a 60° range. He then obtained $\sum|r|$ in each range and plotted $\sum|r|$ against N in each 60° range for the left- and right-handed bursts separately. His observations at 10.1 MHz gave a value of 1.10, with an estimated error of about 10%, for p in equation (2.2).

Sherrill (1965b), using a technique similar to Dowden's, reported good agreement with equation (2.2). He obtained p values between 0.92 and 1.14 at four frequencies between 16 and 24 MHz.

Barrow and Morrow (1968) reported extensive polarization studies at 18 MHz. They found good agreement with the theory, the value of p being of the order of unity.

The predictions of the theory regarding the polarization thus seem to be well supported.

Warwick (1967) pointed out that Ellis' synthetic spectrum for the early source resembles the early source spectra obtained at Boulder in form but not in detail. The chief objection to Ellis' spectrum is that it shows successive positive and negative drifts for a particular group of bursts. Although the Boulder spectra of the early source show complex details, they are not of this type.

A particular triumph of the Doppler-shifted cyclotron theory came when Warwick and Gordon (1965) reported short bursts with negative drift rates of up to 35 MHz/sec in the fine structure of their Arecibo records.

In conclusion, the Ellis and McCulloch theory explains many of the observed characteristics of the polarization and the dynamic spectra quite well. It experiences some difficulties with features not discussed in detail here, among these being the Io-effect. This theory is by far the most comprehensive of the theories for the generation of the decametric radiation and it appears attractive because of its use of mechanisms which are known to apply to the terrestrial magnetosphere.

2.4 THE GLEDHILL MODEL

Gledhill (1967a,b) proposed a model of Jupiter's magnetosphere which is capable of explaining some of the observed properties of the radiation from Jupiter, rather than giving a detailed theory of the generation mechanism.

2.41 Description of the model

Jupiter rotates very rapidly about its axis and completes a rotation in about 10 hours. If Jupiter's magnetospheric plasma co-rotates with the planet, the co-rotating plasma trapped in the magnetic field will be thrown out to those points on the field lines furthest from the axis of rotation. The effect of the centrifugal force is to confine the plasma to a region shaped like a discus about a plane inclined at 7° to the equatorial plane. As the planet rotates the discus of plasma rotates with it, and Io, the orbit of which lies in the equatorial plane, must pass obliquely through the discus twice every revolution. Thus the plasma frequency in the vicinity of Io will rise to a maximum and fall again during each such passage.

From a study of typical B source spectra taken at Boulder, Gledhill selects 40 MHz as the maximum plasma frequency. He assumes that a mechanism exists whereby Io generates radio waves at or near the plasma frequency, which depends on the local plasma density.

A discus of plasma distributed as above would imply that the positions at which Io passes through the plasma are separated by 180° central meridian longitude. Experimental evidence shows that the Io positions for A and B source emissions are separated by 140° central meridian longitude. To achieve this asymmetry he assumes that the dipole is not only tilted but also displaced 0.4 Jupiter

radii north of the equatorial plane.

2.42 Discussion of the model

The displaced dipole model gives a good fit to the dynamic spectra of the various sources, predicting quite well the maximum frequency reached by emission from each of the source regions and also the slow drifts in frequency.

Since the theory lacks a developed generation mechanism for the decametric emission, no predictions have been made about the polarization of the radiation.

In a recent review paper Carr and Gulkis (1969) criticised the model on the basis that there is no apparent source for the high plasma densities required by the model. The decimetric observations made by Branson (1968) seem to rule out a dipole displacement as large as 0.4 Jupiter radii.

The Gledhill model has the attractive feature that the Io-control of the dynamic spectra is introduced very simply and in fact forms a basic part of the theory.

2.5 THE THEORETICAL WORK OF GOLDREICH AND LYNDEN-BELL

The most recent investigation of how Io stimulates Jupiter's decametric radiation is the detailed theoretical study by Goldreich and Lynden-Bell (1969). The theory is involved and has many intricate calculations which will not be presented here. The general sequence of their discussion will however be outlined and some of their predictions will be mentioned.

2.51 Description of the theory

They assume that Jupiter is successively enclosed by a co-rotating, electrically insulating atmosphere, an ionosphere and a low density (0.1 to 10 electron/cm^3), collisionless magnetosphere which extends beyond Io's orbit. Io itself is assumed to be magnetically inert. They assume further that Io is a good conductor so that the electric field in its interior vanishes (as seen from Io's rest frame).

Perfect conductivity along the magnetic field lines outside of Io implies that the electric field must vanish everywhere within the tube of magnetic flux which passes through Io (the magnetic field is assumed to have permeated Io). The plasma contained within this flux tube moves as though it were attached to the satellite and the flux tube is "frozen" to Io. The two feet of the flux tube (in the northern and southern magnetic hemispheres) are forced to slip relative to Jupiter's co-rotating ionosphere. As seen from Io's frame the plasma outside the flux tube flows around it almost as an incompressible fluid flows past a solid tube.

A very large emf (roughly 1 million volts) develops across Io's radial diameter as seen from a co-ordinate system fixed to Jupiter. This emf causes a large current (roughly 1 million amperes) through the ionosphere. The current flows up from the one foot of the flux tube near

Jupiter's ionosphere along the half surface of the flux tube which faces Jupiter, crosses the magnetic field in Io and then flows back down to the ionosphere along the opposite half of the flux tube's surface.

Since the number density of charge carriers in the magnetosphere is low, the current must be carried by kilo-electron-volt electrons which are electrostatically accelerated at Io and the top of Jupiter's ionosphere. They argue, on the basis of the beaming of the low frequency bursts, that coherent cyclotron radiation produced by these current-carrying electrons is responsible for the decametric radiation.

2.52 Discussion of the theory

Goldreich and Lynden-Bell explain the negative frequency drifts of the very short bursts as being caused by radiating electron bunches which flow up to Io from the feet of the flux tube. The negative drift rate (because of the decreasing magnetic field) is then interpreted to be the rate of change of the local gyro-frequency. Using typical values they find a negative drift rate of 25 MHz/sec in the range near 24 MHz. This value compares very well with those reported by Warwick and Gordon (1965). The highly asymmetrical longitude dependence of the drifting storms cannot be explained by the theory. The theory does predict consistent results for the angle of the cone into which the radiation is beamed.

Since the radiation is produced by cyclotron emission this theory might be a logical extension of the Ellis and McCulloch Doppler-shifted cyclotron theory and could, presumably, make similar predictions about features such as the polarization of the radiation.

CHAPTER III

SWEPT-FREQUENCY POLARIMETERS

3.1 INTRODUCTION

We have so far discussed some of the properties of Jupiter's decametric radiation as observed by an experimenter on Earth. A brief review of the theories and their predictions has been given. The present chapter gives a description of some of the techniques which may be used to make swept-frequency polarization measurements.

Section 2 reviews the Stokes parameters as a means of describing the state of polarization of radio noise. It is shown how the parameters are related to quantities which can be measured with antennas. Section 3 gives a description of the swept-frequency apparatus used by other observers. Their specifications are presented as well as a discussion of their possible limitations. Section 4 outlines the need not only for more observations of the swept-frequency characteristics of the radiation but also for high-resolution swept-frequency polarimetry studies. Section 5 describes our proposed swept-frequency polarimeter and indicates how it may overcome some of the limitations of the earlier apparatus and how observations with it may bridge some of the gaps in our present knowledge of the radiation.

3.2 POLARIZATION AND ITS MEASUREMENT

The polarization of a partially polarized wave can be

completely specified by four quantities. These four quantities can be described by the Stokes parameters which are in turn closely related to measurable quantities. If the wave is completely polarized, there is considerable simplification and only two quantities need be measured to determine the axial ratio of the polarization ellipse.

Cohen (1958) treats radio astronomy polarization measurements in detail. We shall describe some of the derivations as far as they will help our further discussion.

3.21 Polarization Parameters

The radio waves of concern are partially polarized noise signals. Such waves can be uniquely resolved into polarized and unpolarized (randomly polarized) components. The electric vector of the polarized part traces out an ellipse which is continually fluctuating in size but maintains a constant orientation, axial ratio, and sense of rotation for intervals long compared with the period.

Definition of parameters:

The polarized part of the radiation is specified by its intensity (I_e), orientation of major axis (X), relative to some system of co-ordinates of the observer, and axial ratio (r). The sense of rotation is contained in the sign of r: $r>0$ means left-handed in the radio sense, and $r<0$ means right-handed. The axial ratio is usually defined as the ratio of the minor axis of the polarization ellipse to

the major axis. The unpolarized part of the wave has components at right angles which are independent; it is specified by a single parameter, its intensity (I_u). The total intensity (I) is the sum of I_e and I_u. The polarization fraction (m) is defined as the ratio of the polarized and unpolarized intensities (I_e/I_u). The four parameters that specify the wave are thus I,m,r and X.

Stokes parameters:

The Stokes parameters are a set of four numbers that define the wave and have the advantage of being closely related to antenna measurements. They may be defined by

$$I = I_e + I_u \qquad (3.1)$$

$$Q = I_e \cos 2\beta \cos 2X \qquad (3.2)$$

$$U = I_e \cos 2\beta \sin 2X \qquad (3.3)$$

$$V = I_e \sin 2\beta \qquad (3.4)$$

where

$$\beta = \tan^{-1} r \qquad (3.5)$$

In terms of these quantities m,r and X are given by

$$m = (Q^2 + U^2 + V^2)^{\frac{1}{2}} / I \qquad (3.6)$$

$$\sin 2\beta = V/I_e \qquad (3.7)$$

$$\tan 2X = U/Q \qquad (3.8)$$

$$r = \tan\beta \qquad (3.9)$$

Stokes parameters in terms of circular components:

Elliptical polarization can be considered to be the

resultant of either two linearly polarized components at right angles or two oppositely rotating circular components. We shall confine our discussion to oppositely rotating circular components.

If the wave is resolved into circular components the intensities I_r and I_l, of these components are

$$I_r = R^2 + \tfrac{1}{2}I_u \qquad (3.10)$$

$$I_l = L^2 + \tfrac{1}{2}I_u \qquad (3.11)$$

$$I = I_r + I_l \qquad (3.12)$$

R and L are the mean amplitudes of the left- and right-circular components of the polarized part of the wave, and (RL) will be used to denote the phase difference between them.

In terms of these circular components the Stokes parameters are

$$I = I_r + I_l \qquad (3.12)$$

$$Q = 2RL \cos (RL) \qquad (3.13)$$

$$U = 2RL \sin (RL) \qquad (3.14)$$

$$V = I_l - I_r \qquad (3.15)$$

Equations (3.12) to (3.15) can therefore be regarded as defining the Stokes parameters in terms of signals induced on antennas of opposite circular polarization.

3.22 Measurement Techniques

If two circularly polarized antennas are used as a polarimeter, the Stokes parameters can be found from equations (3.12) to (3.15) and the polarization parameters, from equations (3.6) to (3.9), are

$$m = \frac{\left[(I_l - I_r)^2 + 4R^2L^2\right]^{\frac{1}{2}}}{(I_l + I_r)} \qquad (3.16)$$

$$\sin 2\beta = \frac{(I_l - I_r)}{\left[(I_l - I_r)^2 + 4R^2L^2\right]^{\frac{1}{2}}} \qquad (3.17)$$

$$r = \tan\beta \qquad (3.18)$$

$$X = \tfrac{1}{2}(RL) \qquad (3.19)$$

The measurements required for complete determination of the polarization with the aid of a polarimeter are thus seen to be

I_r, the intensity of the right-circular component,

I_l, the intensity of the left-circular component,

RL, the cross-correlation product of the mean amplitudes of the right- and left-circular components,

and (RL), the phase difference between the right- and left-circular components.

These four quantities may be measured using suitable receiver electronics.

If the wave is assumed to be 100% polarized i.e. no unpolarized component is present, the axial ratio may be determined simply from the amplitudes of the right- and left-circular components, and it is given by

$$r = \frac{L - R}{L + R} \qquad (3.20)$$

Thus if the incident radiation is 100% polarized, the axial ratio may be determined from the outputs of two receivers connected to oppositely polarized circular antennas. If the receivers have square-law detectors i.e. the receiver outputs are proportional to the square of the incident amplitudes, the following alternate form of (3.20) must be used

$$r = \frac{D_l^{\frac{1}{2}} - D_r^{\frac{1}{2}}}{D_l^{\frac{1}{2}} + D_r^{\frac{1}{2}}} \qquad (3.21)$$

where D_r and D_l are the amplitudes of the receiver outputs and are porportional to I_r and I_l respectively.

If only left- and right-circular components are recorded however, certain ambiguities occur when assessing the state of polarization. It is impossible, for example, to distinguish between circular polarization plus random polarization and complete elliptical polarization. The ambiguities can be resolved by measuring the polarization fraction and the possible polarimeter responses are

summarised in Table 1, where the intensity of the right-handed circular component is given the arbitrary value of I.

From the above it will be clear that a complete determination of the polarization parameters (I,m,r, and X) may require quite sophisticated receiver circuitry. However, complete polarization greatly simplifies matters since the axial ratio can then be determined by simple two-component measurements.

Type of Polarization	$\|r\|$	m	I_r	I_l	RL
Right-handed circular	1	1	I	0	0
Linear	0	1	I	I	I
Random	0	0	I	I	0
Random + linear	0	$0<m<1$	I	I	$0<RL<I$
Right-handed elliptical	$0<\|r\|<1$	1	I	$0<I_l<I$	$0<RL<I$
Random + right-handed circular	1	$0<m<1$	I	$0<I_l<I$	0
Random + right handed elliptical	$0<\|r\|<1$	$0<m<1$	I	$0<I_l<I$	$0<RL<I$

Table 1 : Summary of Polarimeter Responses.

3.3 APPARATUS USED FOR SWEPT-FREQUENCY OBSERVATIONS OF JUPITER

A brief description of the apparatus used by other workers has already been given in Chapter 1. The characteristics of their instruments will be summarised here, particular attention being paid to type of apparatus (i.e. polarimeter, interferometer or total-power receiver), swept-frequency receiver specifications, antenna specifications, sensitivity of the complete receiving system (where possible) and possible limitations.

The sets of apparatus to be described are (i) the Boulder spectrograph, (ii) Riihimaa's swept-frequency apparatus, (iii) the Arecibo swept-frequency polarimeter and (iv) an earlier swept-frequency polarimeter operated at Rhodes University.

3.31 The Boulder spectrograph

The Boulder apparatus is a swept-frequency interferometer operating in the 7.6 to 41 MHz frequency range.

Receiver specifications: The receiver is of the superheterodyne type with two tracking radio-frequency stages and two intermediate-frequency stages. The frequency range was swept in 0.65 seconds every 1.3 seconds. The effective bandwidth of the receiver was 0.6 MHz and the integration time constant was roughly 3 seconds. Thus the receiver is best suited to studying bursts lasting several seconds. Interference from terrestrial sources below

30 MHz (mainly radio communications signals) was markedly reduced by the inclusion of minimum-level detection circuits in the receiver.

Antenna specifications: The two antennas were fully-steerable corner reflectors, each having a collecting area of approximately 500 m^2 and a gain of 8 to 10 dB over an isotropic radiator. The antenna feeds were vertically polarized conical monopoles and the antennas were connected as an interferometer on a northeast baseline of 263 m.

Sensitivity: The overall sensitivity of the receiving system i.e. antenna plus receiver, was sufficient to observe the intense radio source Cassiopeia A which has been measured to have flux density between 5 and 4 x 10^{-22} jansky in the frequency range from 18 to 40 MHz (Wells,1958).

Limitations: From the above specifications it is clear that this is a low-resolution instrument. Because of the relatively large receiver bandwidth, fine structure in frequency on a scale smaller than 600 kHz was "smeared out". The poor time-resolution of the receiver and the small transport speed of the recording paper did not allow individual bursts of durations less than several seconds long to be resolved. The minimum-level detection scheme reduced the possibility of observing millisecond bursts since the receiver discriminated against rapid changes in amplitude.

The swept-frequency spectrograph cannot give any detailed information about the polarization of the radiation.

The Boulder spectrograph is thus seen to be entirely unsuitable for swept-frequency studies of the millisecond bursts. However, it has been useful for studying the coarse spectral characteristics of Jupiter's decametric radiation and has produced several important results. The apparatus has one great advantage in that day-time observations are possible because of the minimum-level detection scheme.

3.32 Riihimaa's swept-frequency apparatus

Riihimaa (1964a,b) reported the first continuous high-resolution spectral observations of Jupiter's decametric radiation. We shall present the improved version of this apparatus as described by Riihimaa (1968a,b).

Receiver specifications: The receiver was tuned electronically over the frequency range from 23 to 21 MHz. The receiver used a relatively narrow bandwidth of 50 kHz and a tuning rate of 20 sweeps/sec. The integration time constant was 1.25 milliseconds. Bursts shorter than 0.05 sec would not be resolved by this apparatus.

Antenna specifications: The antenna consisted of eight full-wave dipoles and a reflecting screen. The theoretical midband gain was approximately 15 dB over an isotropic radiator.

Sensitivity: The theoretical sensitivity of the spectrograph was close to 0.4×10^{-21} jansky at the midfrequency. The variation of the standing-wave ratio in the antenna network as the receiver was swept over the frequency range somewhat reduced the effective spectral sensitivity.

Limitations: The most obvious limitation of the apparatus is the narrow band of frequencies over which it operates. The maximum drift rate that could be measured with any certainty is about 10 MHz/sec. The very short bursts (millisecond bursts) are known to have bandwidths of 50 kHz or less and durations of a few milliseconds - these millisecond bursts cannot be resolved with this apparatus. The apparatus can however resolve the short bursts (0.05 to 0.2 seconds' duration) in time. No indication of the polarization properties of the radiation can be given by this apparatus.

3.33 The Arecibo swept-frequency polarimeter

This is the only swept-frequency polarimeter ever operated with any success. The polarimeter investigated the high time-resolution of the Jupiter's radio spectrum with as complete a determination of the state of polarization as possible.

Receiver specifications: The receiver was of the superheterodyne type with two swept radio-frequency stages as well as a swept local-oscillator stage. The tuning through

the 36 to 24 MHz frequency band was accomplished by means of voltage-variable capacitance tuning of the local oscillator. The sweep took 10 milliseconds to complete but because of the time-shared operation of the receiver (see section 1.3) a component measurement was only repeated every 40 milliseconds. The intermediate-frequency bandwidth was 65 kHz and the receiver integration time constant had the very low value of 54 micro-seconds.

Antenna specifications: The antenna system consisted of two crossed log-periodic dipole antennas at the focus of the 1000-foot reflector. The outputs of these antennas were combined to obtain the left-and right-circular components of the radiation. The effective area of the antenna was found to be of the order of 3×10^4 m^2 throughout the operating range. The isolation between the crossed log-periodic dipole antennas was 20 dB.

Sensitivity: The primary calibration of the sensitivity of the overall receiving system was a record of the radio star Taurus A which has a flux density equal to 0.245×10^{-22} jansky. An instrument of this sensitivity would be able to detect even very weak bursts in the emission from Jupiter.

Limitations: The individual sweeps are not made simultaneously because of the time-shared operation of the receiver; there is a 40-millisecond delay between successive

sweeps on the left- and right-circular channels. For this reason changes in the sense of polarization which occur on a time scale shorter than 40 milliseconds are not observable. In addition bursts shorter than 40 milliseconds would not be recorded in successive sweeps on one of the circular channels. Warwick and Gordon (1965) reported three cases of bursts shorter than the 40-millisecond resolution of the instrument.

Although this is the most extensive swept-frequency polarimetry experiment of high-resolution yet conducted, it only gives information about bursts and storms above 24 MHz. The experiment was conducted for only three months since it used the 1000-foot reflector at Arecibo to obtain the required sensitivity.

3.34 The earlier Rhodes University swept-frequency polarimeter

A swept-frequency polarimetry experiment was carried out at Rhodes University during 1965. The apparatus was described by Gruber (1966) and will be discussed briefly here. The left- and right-circular components of the wave were obtained by combining the output signals from crossed log-periodic dipole antennas. The axial ratio was calculated on the assumption of complete polarization.

Receiver specifications: The superheterodyne receiver was swept electronically between 15 and 25 MHz. The local oscillator was tuned between 45 and 55 MHz and its output

was mixed with the input signals from the antennas to give the intermediate frequency of 30 MHz, which then contained all the required information in the 15 to 25 MHz range. The intermediate-frequency output was mixed with a second local oscillator signal of 29.4 MHz giving output frequencies from 0 to 600 kHz. A filter was then used to define the bandwidth and this was followed by a linear detector and an audio-frequency amplifier. The sweep rate was 10 MHz in 60 milliseconds repeated every 250 milliseconds. The receiver bandwidth was 100 kHz and the time constant was 1 millisecond.

The receiver was switched alternately between left- and right-circular inputs at a rate of 5 kHz in order to sample each polarization a number of times during a sweep. The receiver was thus operated on a time-shared basis somewhat different to that of the Arecibo receiver.

Antenna specifications: The log-periodic dipole antennas each had a predicted gain of 7 dB over an isotropic radiator. The antennas were arrayed in the form of an "X" above the ground with the high-frequency ends (the thin ends of the wedge-shaped antennas) pointing up to Jupiter. The antenna supporting structure was mounted on a semi-circular track and Jupiter could be tracked in azimuth while the axis of the antennas pointed at Jupiter. An antenna arrangement such as the above is, in the opinion of the author, unsuitable for use as a polarimeter. When the antenna is

arrayed with its ground image the direction of the main reception lobe is displaced off the axis of the antenna in the vertical plane. This could mean that when the axis of the antenna points at Jupiter, Jupiter in fact does not lie in the main lobe of the antenna. Also, since the long elements are near the ground, the height of the elements above ground in terms of their resonant wavelengths will be a function of frequency. This means that the antenna will not have frequency-independent impedance characteristics.

Sensitivity: No specification of the system sensitivity was given. Since Jupiter bursts were observed on only a few nights during the observing season, it seems that the system sensitivity was probably quite low, of the order of 10^{-20} jansky which means that only the stronger bursts in the emission were recorded. The misdirection of the main lobe could also account for the relatively few storms recorded.

Limitations: Because of the comparitively low sweep repetition rate (4/sec) fast drift rates and rapid changes in polarization could not be observed. The instrument was suitable for studying the long bursts (durations greater than 2 seconds) and possibly some of the normal bursts (durations between 0.2 and 2 seconds) provided they did not drift in frequency at a rate greater than about 1 MHz/sec. A great deal of interference was caused by spurious signals in the pass-band of the receiver. These signals did not

appear to be terrestrial stations in the 15 to 25 MHz band, but rather to be the result of beating between the harmonics of the local oscillator and strong signals from a frequency-modulated transmitting station.

3.4 THE NEED FOR MORE DATA

We have reviewed the spectral and polarization characteristics of Jupiter's decametric radiation as well as describing some of the apparatus which has been used to obtain this information. We are now in a position to consider the type of information that is needed to supplement our present knowledge.

A large amount of information about the fixed-frequency polarization characteristics of the radiation in the frequency band between 16 and 25 MHz has been presented. No swept-frequency observations of the polarization of the radiation in this frequency band have been forthcoming. The numerous high-resolution studies of Riihimaa gave indications of complex spectral characteristics for Jupiter's decametric radiation in the frequency band between 18 and 23 MHz. The observations of Warwick and Gordon at Arecibo have emphasised the need for high-resolution swept-frequency polarimetry studies of the short bursts.

The need for more experimental observations is emphasised by some of the concluding remarks at the end of an extensive review paper by Warwick (1967). He says ".....

the principal information needed is more refined data, especially on the fast-time resolution polarimetry and spectroscopy of millisecond bursts. The polarization diversity on these bursts as recorded at Arecibo needs confirmation." Warwick further suggests that in order to detect the possible variation of the orientation of the polarization ellipse at Jupiter with Jupiter's rotation, the terrestrial Faraday effect should be studied with greater precision. The results of such a study have recently been published by Parker, Dulk and Warwick (1969).

Further to this Barrow (1968) in his recommendations for future work states, " A swept-frequency polarimeter, ideally operating in the frequency range 10 to 30 MHz, is perhaps the most needed new instrumentation." Such an instrument, if of high enough resolution, would bridge the gap between the fixed-frequency polarization measurements and the swept-frequency observations of Warwick and Gordon, and Riihimaa. If the bursts of Jupiter's radio noise are to be classified according to their duration and bandwidth as suggested by Riihimaa (1966b) more high-resolution dynamic spectral studies are needed to clarify the possible classifications.

3.5 SPECIFICATIONS OF OUR PROPOSED SWEPT-FREQUENCY POLARIMETER

3.51 General

Bearing in mind the type of data required, we decided

to construct a swept-frequency polarimeter to cover as wide a band of frequencies as possible. The frequency range over which Jupiter's decametric radiation has been observed lies between 43 MHz (Kraus, 1958) and 4.8 MHz (Ellis, 1962b). One of the lessons learnt from the earlier Rhodes swept-frequency polarimeter and from fixed-frequency observations at Rhodes was that terrestrial interference, even at night, made observations of Jupiter at Grahamstown below 15 MHz almost impossible. The low-frequency limit of the polarimeter was thus set at 15 MHz. The high-frequency limit was set at 45 MHz, which includes the highest frequency reported.

The primary objective of the polarimeter was to enable variations of polarization sense with frequency to be studied rather than to enable a detailed determination of axial ratios. The limitations introduced by switching a single receiver between the left- and right-circular inputs have been mentioned and it was thus decided that the polarimeter should have independent left- and right-circular channels, i.e. separate receivers for the left- and right-circular components of the radiation. This has the advantage that the circular components of the wave are recorded simultaneously and no information is lost as is usually the case with switching.

No cross-correlation channel was to be included. Axial ratios can still be determined on the assumption of completely polarized incident radiation. The assumption of completely polarized radiation in the 16 to 24 MHz range is partially justified by the observations of Sherrill (1965a) and Barrow (1968) that some 80% of the bursts in this range have polarization fractions greater than 0.7. To obtain consistent values for the amplitudes of the left- and right-circular components, the two antenna-receiver systems would have to be gain-matched or accurately calibrated so that the frequency response of each system is known.

At the outset of the project it was decided that the electronic circuitry would be constructed using only semi-conductor devices (i.e. no valves would be used as had been the case with all the apparatus previously described). The reliability of these devices is generally good and they have low power requirements.

The proposed specifications of the swept-frequency receivers, the broadband antennas and the data display will now be given.

3.52 Swept-frequency receiver

In view of the problems experienced with heterodyning in the earlier Rhodes polarimeter, a receiver with no intermediate-frequency stages had to be devised. The receiver consisted of parallel-tuned radio-frequency stages,

a detector and then an audio-frequency amplifier. The tuning of the radio-frequency stages was to be accomplished with varactor diodes and the frequency sweeping was to be as linear with time as possible. A receiver of this type is, to the best of the author's knowledge, unique for Jupiter observations.

Early experiments indicated that tuning over the full frequency range could not be accomplished with a single receiver using the available varactor diodes. It was therefore decided to sweep the band in two parts with separate receiving systems for the 15 to 26 MHz and the 30 to 45 MHz ranges. The receiver covering the 15 to 26 MHz band will in future be referred to as the "low-frequency (or LF) receiver", while the receiver for the 30 to 45 MHz band will be known as the "high-frequency (or HF) receiver". It will be clear that the complete polarimeter requires two low-frequency receivers and two high-frequency receivers, i.e. four receivers in all.

The polarimeter was intended to be a high-resolution instrument with a sweep period of 10 milliseconds. However, it was decided to test a prototype receiver with a sweep period of 100 milliseconds and then, if these initial tests proved successful, to improve the resolution with a sweep period of 10 milliseconds.

3.53 Antenna specifications

General description of broadband antennas:

Since the polarimeter was to operate over a wide

frequency range, broadband antennas were needed to receive the incident radiation. Two of the most popular broadband antennas for our frequency range are the log-periodic dipole (LPD) antenna and the helical beam antenna. A broadband antenna must have the property that its radiation patterns and impedance characteristics are essentially frequency-independent over the operating band of frequencies. Helical antennas and LPD antennas can only operate effectively over a band of frequencies of about 1.7 to 1. This fact also made it necessary to sweep the band in two parts and to have separate antennas for the low-and the high-frequency receivers. The helical antenna and the LPD antenna both have good free-space frequency characteristics and there appears to be little to choose between them as far as polarimeter antennas are concerned.

Certain difficulties arise, however, as a result of the frequencies at which we wish to observe Jupiter. In general the antenna structures will be large at the frequencies at which we work because they must have dimensions of the order of a wavelength. Since the antenna structures are large they have to be erected near the ground - it is this erection over ground which causes considerable complication. We will not describe the design of these antennas in detail in this section but rather indicate why we selected helical antennas and not LPD antennas for our polarimeter.

The log-periodic dipole antenna:

A brief description of how a LPD antenna operates may clarify some of the subsequent discussions. A LPD antenna consists of an array of dipoles with lengths and spacings arranged in a log-periodic manner. Successive dipoles are connected alternately to opposite sides of a transmission line, called the "feeder", to produce the required element phasing. The antenna will be discussed for transmission of radiation; the discussion for reception is similar by the reciprocity theorem.

Radio-frequency energy, at a given frequency, travels along the feeder until it reaches a section of the structure where the electrical length of the elements and the phase relationships are such as to produce radiation. The resulting beam from this "active region" is directed towards the end of shortest elements so that the beam always passes through elements which are shorter than one-half wavelength at the operating frequency.

A horizontally-polarized LPD antenna can be oriented over ground in such a way that its vertical radiation pattern and impedance characteristics will be independent of frequency. This is possible because the active region can be located at a constant height in wavelengths above the ground. To ensure that the height of the active region in wavelengths remains constant the low-frequency end of the antenna must point up while the high-frequency end

points to the ground in such a way that the virtual apex falls on the surface of the ground. The main direction of propagation is in the direction of the virtual apex and the radiated wave is transmitted upwards after ground reflection.

Unsuitability of crossed LPD antennas:

Two crossed LPD antennas are required to obtain the left- and right-circular components of a wave. To achieve symmetry with respect to the ground reflections these antennas have to be arrayed in the form of an "X" above the ground. This means that the height of the active region in wavelengths above the ground will not be constant as a function of frequency since the active region is inclined to the ground. This will degrade the frequency-independent characteristics of the antenna.

A further unsuitable feature of crossed LPD antennas arrayed over ground was noticed in 1967 when the author tested a 1/10 full-scale model of crossed LPD antennas for the 15 to 25 MHz frequency range. When the crossed LPD antennas were arrayed with their earth images, the author noticed the following effects. There was no longer a single radiation lobe along the axis of the crossed LPD antennas, but the lobe had been split into two parts. The main radiation lobe of one LPD section was displaced at some angle to the side of the axis and the main radiation lobe of the other LPD section was displaced to the other side of the axis. There was thus no lobe in the direction

of the axis. The vertical direction of these main lobes was also a function of the angle at which the axis of the LPD antennas was inclined to the ground. The above considerations make ground-arrayed crossed LPD antennas unsuitable for use as polarimeter antennas.

The crossed LPD antennas used by Warwick and Gordon at Arecibo were suitable since they were located at the focus of the 1000-foot reflector at a distance of 435 feet from the reflecting screen. In this way the ground-reflection problem was eliminated and the crossed LPD antennas functioned as free-space antennas.

Suitability of helical beam antennas:

When a vertically polarized wave is reflected from a smooth surface it does not experience a phase change. When a horizontally polarized wave is reflected from a smooth surface, there is a 180° phase change. When a circularly polarized wave is reflected from a smooth surface its horizontal component is altered by 180°; hence the sense of polarization is reversed. Circularly polarized helical antennas are unique in being entirely unable to "see" their own images in a plane reflecting surface. This is so since the reflected wave has its sense reversed and is therefore orthogonal in polarization to the direct wave and the antenna will be insensitive to the reflected wave. This is confirmed by Sherrill (1965a) who used a two-helix

polarimeter, with the helices erected close to ground, for discrete-frequency observations in the 15.5 to 24.2 MHz range. He observed a significant number of circularly polarized bursts - it is unlikely that a polarimeter which is greatly affected by ground reflections will observe completely circularly polarized radiation.

3.54 Data display system

The data was to be presented as a 3-dimensional frequency-time-intensity plot. The left- and right-circular components were to be photographed simultaneously and displayed side by side permitting easy comparison of the outputs of the two channels. As it was unlikely that filming could be done at the observing site, there had to be some facility for recording the receiver outputs on magnetic tape so that the data could subsequently be processed. The amplitudes of the left- and right-circular components could be regained from the film by microdensitometry of the film and this would require an intensity calibration of the film.

CHAPTER IV

ANTENNAS

4.1 INTRODUCTION

In this chapter we shall describe the design and performance of the antennas which have been used by us for swept-frequency observations of Jupiter.

The first antenna to be presented is a horizontally polarized log-periodic dipole (LPD) antenna for the 15 to 25 MHz frequency range. It may seem strange that anLPD antenna was constructed after it was decided that crossed LPD antennas were unsuitable for a polarimeter. The horizontally polarized LPD antenna was constructed to enable us to see whether the original swept-frequency receiver constructed in 1967 for the 15 to 25 MHz range was suitable for swept-frequency observations of Jupiter. The author had conducted model studies of a 1/10 scale model LPD antenna for the frequency range from 15 to 25 MHz during 1967. Because a design was available and since a horizontally polarized LPD antenna of suitable design is comparatively simple to erect, it was decided to use an LPD antenna to test the receiver.

Once the receiver had proved suitable for Jupiter observations it was decided that circularly polarized helical beam antennas (helical antennas radiating in the axial mode) would be suitable for use as polarimeter antennas. Helical antennas of about 6 turns have been well discussed in the

literature, but it was soon clear that the engineering problems involved made the construction of a 6-turn helix at our frequencies prohibitive. The design specifications quoted in the literature apply only to helices of more than 3 turns and we decided to test a 4-turn model helix to see whether the radiation patterns were well enough defined to be suitable for Jupiter observations.

Once the model helix proved satisfactory, we constructed a right-handed polarized helical antenna for the 30 to 45 MHz frequency range. Since this structure is not as large as the equivalent structure for a helix in the 15 to 26 MHz range, we constructed a 5-turn helix as this would give better characteristics than a 4-turn helix. After the first helix had been successfully tested with the HF receiver, a left-handed polarized helix was also constructed for the 30 to 45 MHz frequency range. Finally, right- and left-handed polarized helices of 4 turns were constructed for the frequency range from 15 to 26 MHz. We shall describe each stage of the development of the antennas and present their respective characteristics.

4.2 LOG-PERIODIC DIPOLE ANTENNA

The design and construction of LPD antennas has been extensively treated in a handbook edited by Smith (1966). The design of the LPD antenna presented here closely follows the design procedure laid down in this reference and the design procedure will therefore not be described in detail.

The operation of an LPD antenna has been described in Chapter 3 and this description will not be repeated here.

4.21 Design of the antenna

A schematic diagram of the LPD antenna together with a definition of the design parameters is given in figure 1. As shown on the schematic the successive dipoles are connected alternately to opposite sides of the feeder. The feeder consists of two parallel pipes with the dipole elements connected to alternate sides of the pipes. The co-axial cable, which connects the antenna to the receiver, is fed up one of the pipes from the low-frequency end and at the high-frequency end the outer shield of the cable is connected to the one pipe while the core of the cable is connected to the other pipe.

The characteristic impedance of the antenna is controlled by the ratio of the length of any element to its radius, as well as the ratio of the separation of the centres of the feeder pipes and the radius of the pipes. Smith gives a complete set of graphs for determining the characteristic impedance of the antenna in terms of its dimensions.

The design of the LPD antenna was made bearing in mind the following points. The horizontal and vertical beamwidths of the main lobe had to be quite wide so that Jupiter could be observed within the half-power beamwidths of the main lobe for periods of a few hours without having to move the antenna. The angle relative to the ground at which the main

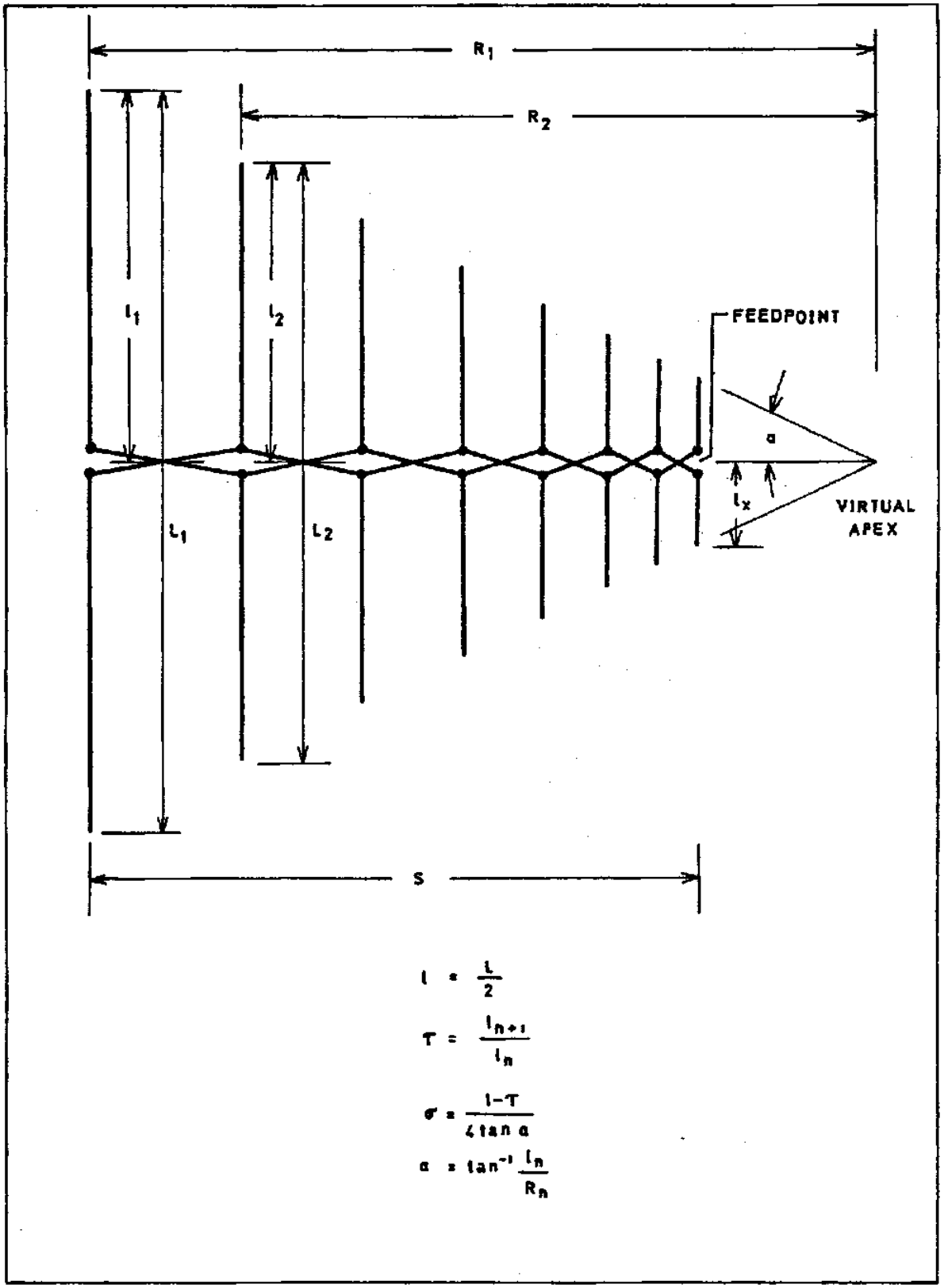

$$l = \frac{L}{2}$$

$$\tau = \frac{l_{n+1}}{l_n}$$

$$\sigma = \frac{1-\tau}{4 \tan \alpha}$$

$$\alpha = \tan^{-1} \frac{l_n}{R_n}$$

FIG. 1. SCHEMATIC DIAGRAM OF THE LOG-PERIODIC DIPOLE ANTENNA, SHOWING THE DESIGN PARAMETERS.

lobe points into space must be such that Jupiter can be observed when it is still quite low above the horizon and when near transit. An excessively large antenna could not be constructed due to space limitations at the observing site and the engineering problems associated with making a large antenna structure steerable. Fortunately the above considerations point to the selection of similar sets of design parameters. Low values of the element length scaling factor and the element spacing factor are associated with the wide beamwidths, high main lobe elevation angles (greater than 30° and less than 60°) and relatively short antenna structures. Once trial values of the spacing constants had been selected these were used with the design curves presented by Smith to check if the desired performance could be obtained. The number of dipole elements in the antenna is determined by the bandwidth of the antenna and the element length scaling factor. The final design of the antenna is as follows:

Lowest frequency	15 MHz
Highest frequency	25 MHz
Element length scaling factor, τ	0.81
Element spacing factor, σ	0.10
Half-angle of antenna structure, α	25.5°
Characteristic impedance	75 ohms
Number of elements	8
Ratio of half-length of elements to radius	450

Plate 1. The ground-arrayed log-periodic dipole antenna.

Ratio of separation of feeder pipes to radius of pipes	1.3
Total length of longest element, L_1	11.6 m
Total length of shortest element, L_x	2.66 m
Overall feeder length, S + 2.5 m	12.2 m

The total length of the longest element is usually slightly longer than half the wavelength at the lowest frequency while the shortest element is considerably shorter than half the wavelength at the highest frequency. The exact fractions are determined by the spacing and scaling constants. The feeder length is the length of the pipes from the longest to the shortest elements and to this must be added 1/8 of the longest wavelength (i.e. 2.5m) since a shorting plate must be placed across the feeder pipes within 1/8 of a wavelength from the low-frequency end.

4.22 Antenna characteristics

The angle at which the antenna is inclined to the ground (usually called the structure elevation angle) determines the angle to the horizontal at which the radiation progresses into space (usually called the take-off angle). Plate 1 shows the ground-arrayed LPD, the direction of maximum radiation is towards the shortest elements. From the design curves given by Smith it is found that a structure elevation angle of 32^{o} gives a take-off angle of 42^{o} and a vertical radiation beamwidth of 52^{o}. This means that

Jupiter can be observed within the half-power vertical beamwidth of the antennas for all elevation angles between 16° and 68°. The horizontal beamwidth is virtually unaltered from its free-space value by ground arraying and this is found to be about 63° from the free-space radiation patterns plotted by Smith. The antenna directivity is predicted to be 9.8 dB over an isotropic radiator.

Experimental determination of the radiation patterns and the directivity is not possible because of the physical size of the antenna. However, figure 2 shows predicted radiation patterns for the LPD antenna.

The antenna was constructed and mounted on top of a 7.7 m pole. The method used for supporting the antenna feeders and the dipole elements can be seen in plate 1. The antenna can pivot about the main supporting pole as axis and can be moved in azimuth into four fixed positions (only three positions are shown on the plate.) In this way Jupiter can be kept in the beam of the antenna throughout the period of observations.

Figure 3 shows the voltage standing-wave ratio of the antenna as a function of frequency measured at the receiver (i.e. at the end of 30 m of 75 OHM co-axial cable). The standing-wave ratio was found to be independent of the position in which the antenna was placed. The standing-wave ratio is everywhere less than 1.5 but the comparatively

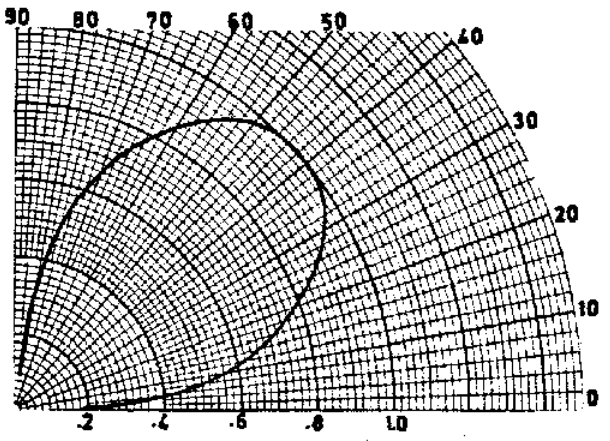

VERTICAL PATTERN

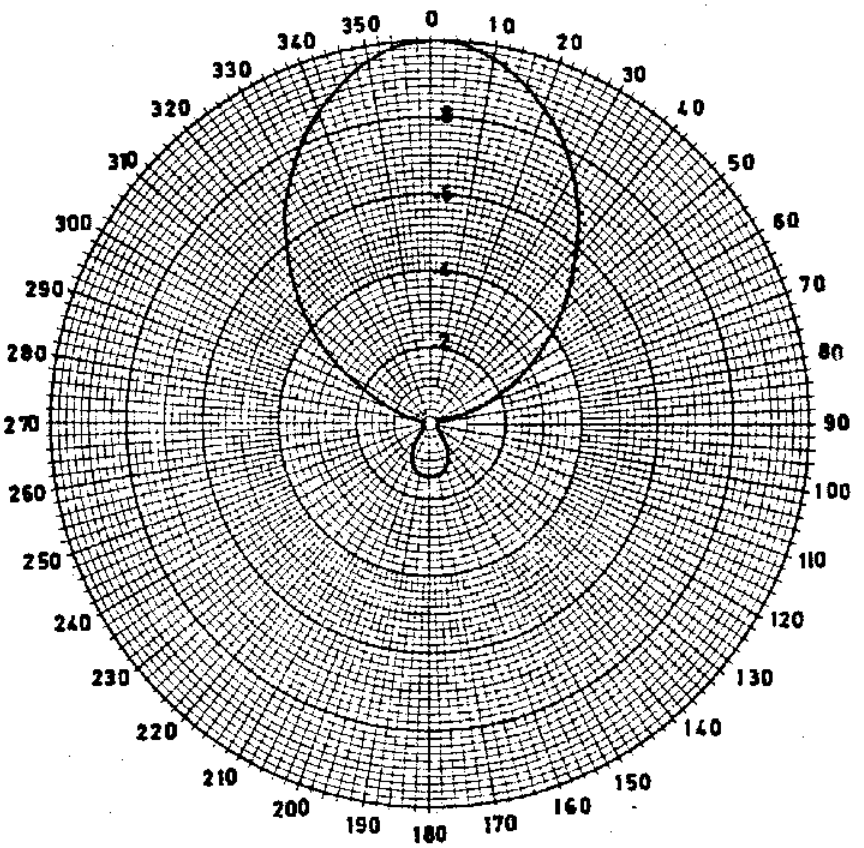

HORIZONTAL PATTERN

(CONICAL CUT AT 42° ELEVATION)

FIG. 2. PREDICTED GROUND-PLANE PATTERNS FOR THE LOG-PERIODIC DIPOLE ANTENNA.

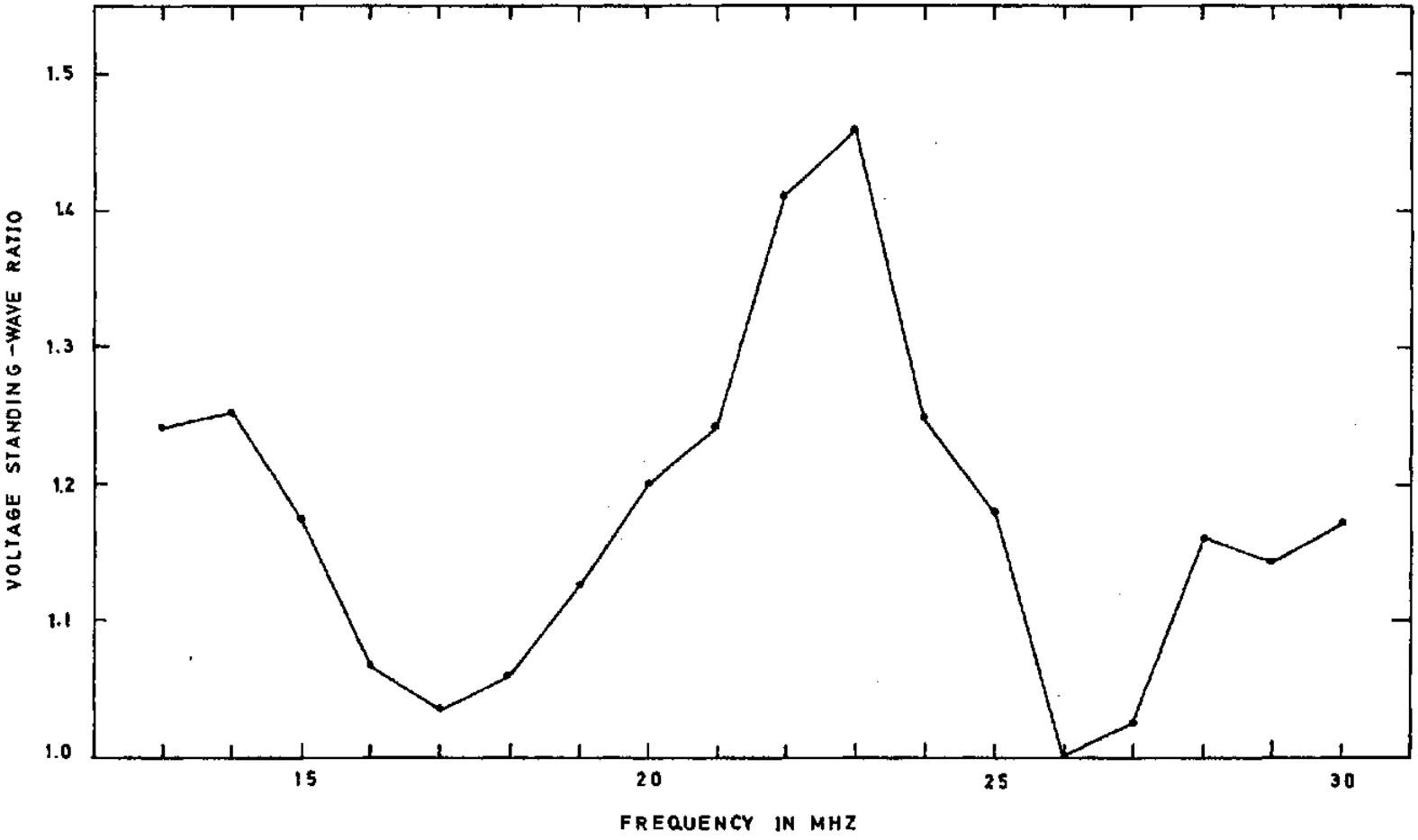

FIG. 3. MEASURED VOLTAGE STANDING-WAVE RATIO OF THE LOG-PERIODIC DIPOLE ANTENNA AS A FUNCTION OF FREQUENCY.

high standing-wave ratio between 21 and 24 MHz somewhat degrades the performance of the antenna.

Since its construction in December 1967 the LPD antenna has been used continuously with the various LF swept-frequency receivers for observations of Jupiter. During 1968 a single spectral record of Jupiter's decametric radiation was obtained using this antenna. In 1969 about 15 storms were observed with the LPD antenna and one of these storms is of considerable interest and will be presented later. The LPD antenna has now been replaced by a 4-turn helical antenna but it can still be used for observations since it can be steered to track Jupiter once the planet has moved out of the beam of the 4-turn helical antenna which is fixed in position.

4.3 MODEL STUDY OF A HELICAL BEAM ANTENNA

This study was conducted to test whether helical antennas of 4 turns would be suitable for use as swept-frequency polarimeter antennas. We shall indicate why scaling of the dimensions and frequency of a full scale antenna is permissible, thereby making model studies meaningful. The design of the antenna and the testing procedures will be discussed and finally the results of the study will be presented.

4.31 Model measurements

Radiation pattern and directivity measurements of a full-

scale helix for the decameter wavelength range is impractical because of the large size of the antenna system. It is therefore convenient to build a model of suitable size and then to make measurements on the properties of the model.

Model measurements in electromagnetic systems are based on the principle of electromagnetic similitude - a direct consequence of the linearity of Maxwell's equations (Stratton, 1941). A study of these equations relating to the media forming and surrounding an antenna shows that the following equations must hold if an electromagnetic system is to be exactly simulated on a different scale. They are

$$\mu\epsilon L^2 f^2 = K_1 \qquad (4.1)$$

$$\mu\sigma L^2 f = K_2 \qquad (4.2)$$

where K_1 and K_2 are constants, L is a typical linear dimension, f is the frequency and μ, ϵ, σ are the permeability, dielectric constant and conductivity respectively.

If we let the scaling factor be p, the following relations must be satisfied if equations (4.1) and (4.2) are to hold. Any dimension L_m of the model must be related to the corresponding dimension L of the actual antenna by

$$L_m = L/_p, \qquad (4.3)$$

the frequency f_m used to measure the model antenna must be

related to the frequency f used with the real antenna by

$$f_m = pf , \qquad (4.4)$$

and, finally, the conductivity σ_m of the metal used in the model must be related to the conductivity σ of the actual antenna by

$$\sigma_m = p\sigma . \qquad (4.5)$$

However, σ for good conductors like aluminium and copper is very large and the metal can be considered a perfect conductor and the conductivity need not be modelled, while ϵ and μ also retain their same values.

For accurate far-field or Fraunhofer radiation patterns of an antenna, the measurements must be made with a sufficiently large distance between the transmitting and receiving antennas. Ideally the transmitted wave should arrive at the antenna under test as a truly plane wave. Since the transmitter emits a spherical wave the phase front at any finite distance will be curved. If the variation of phase across the aperture of the antenna under test is to be less than $\pi/8$, it can be shown that the separation, r, between the transmitting and receiving antennas must obey the following

$$r \geq 2\frac{a^2}{\lambda} \qquad (4.6)$$

where a is the width or physical aperture of the antenna and λ is the wavelength to be used.

4.32 Design and construction

The design of a helical antenna operating in the axial or beam mode has been extensively discussed by Kraus (1947; 1948; 1949 a,b). In the axial mode of radiation the field is a maximum in the direction of the helix axis and is circularly polarized or nearly so. The axial mode of radiation occurs when the helix circumference is of the order of 1 wavelength and the helix pitch angle lies between 12^{o} and 15^{o}. The axial mode of radiation of the helix is most simply generated using the co-axial line and ground plane arrangement shown in figure 4, with the inner conductor connected to one end of the helix and the outer conductor to the ground plane. The bandwidth over which the antenna will radiate (or receive) in the axial mode is from 0.75 to 1.3 of the centre frequency giving a total bandwidth of 1.75 to 1.

Design of the antenna:

By deciding on a 4-turn helix for engineering reasons, the directivity of the helix is predetermined since the directivity is a function of the number of turns. The directivity and the beamwidths of the main lobe are inter-dependent therefore the beamwidths are also fixed by the selection of 4 turns. It is convenient to make the circumference of the helix one wavelength at the centre frequency of operation. The remaining parameter to be specified is the helix pitch angle; the difference in characteristics between antennas of 12^{o} and 15^{o} pitch angle is not large.

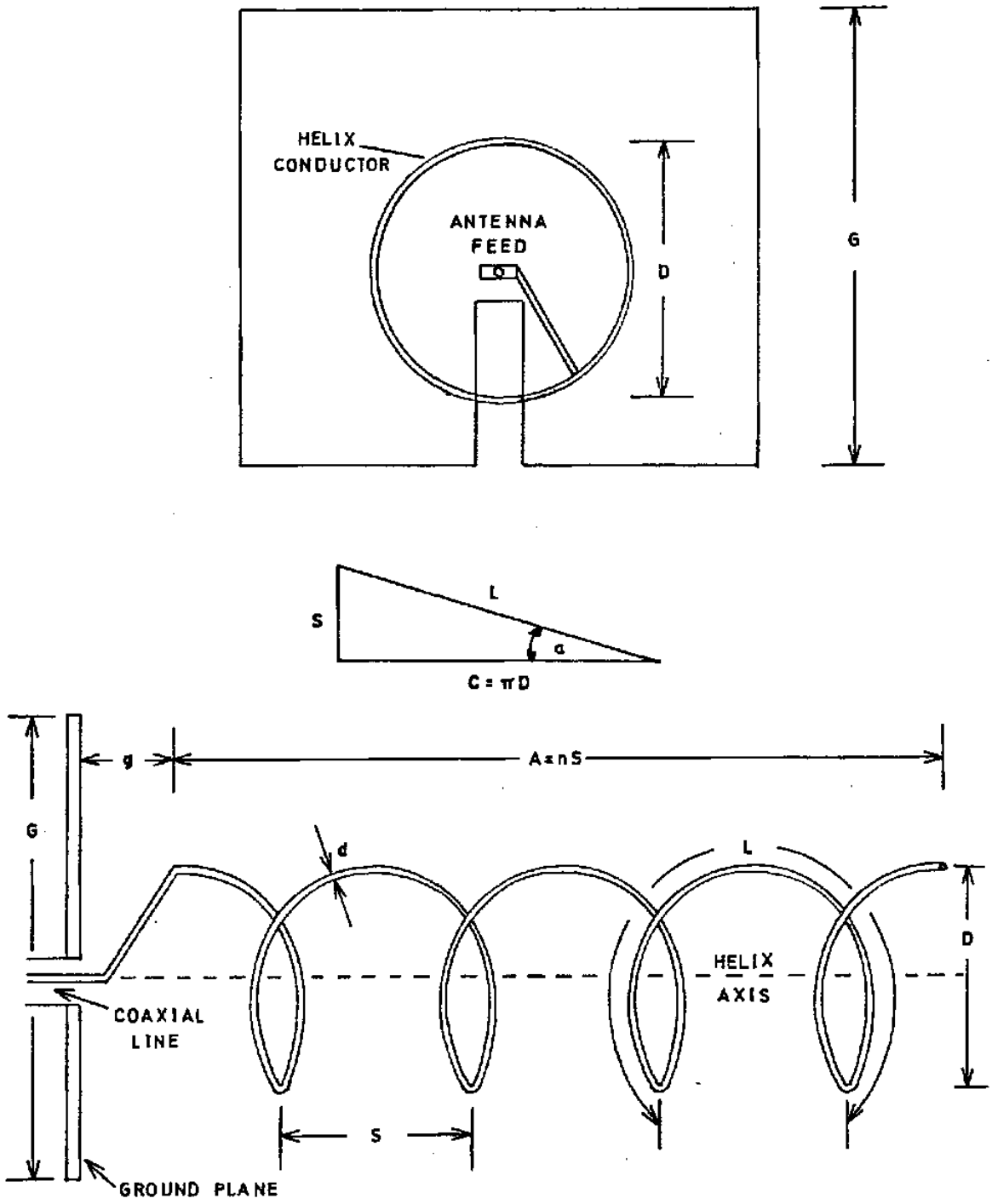

FIG. 4. THE HELICAL BEAM ANTENNA WITH DIMENSIONAL SYMBOLS.

The smaller angle gives slightly better patterns (sharper main lobe and smaller minor lobes) while the larger angle gives a slightly smaller impedance variation over the bandwidth. A value of 12.5° was selected. If one turn of the helix is unrolled on a flat plane the circumference (C), spacing (S), turn length (L) and the pitch angle (α) are related by a triangle as shown in figure 4.

The model helix was designed to be a 1/20 scale model of a full-scale helix antenna for the 15 to 25 MHz frequency range and thus had to operate over the frequency range from 300 to 500 MHz. The specifications of the helix are as follows:

Centre frequency	f = 400 MHz
Helix circumference	C = 75 cm
Helix diameter	D = 24 cm
Helix turn spacing	S = 16.5 cm
Length of turns	L = 76.8 cm
Number of turns	n = 4
Helix pitch angle	α = 12.5°
Overall helix length	$A = nS$ = 66 cm
Spacing of turns to ground plane	g = 8.25 cm
Overall antenna length	$A + g$ = 74.25 cm
Width of ground plane	G = 37 cm
Conductor diameter	d = 0.075 cm

With the feed arrangement shown in figure 4, the spacing, g,

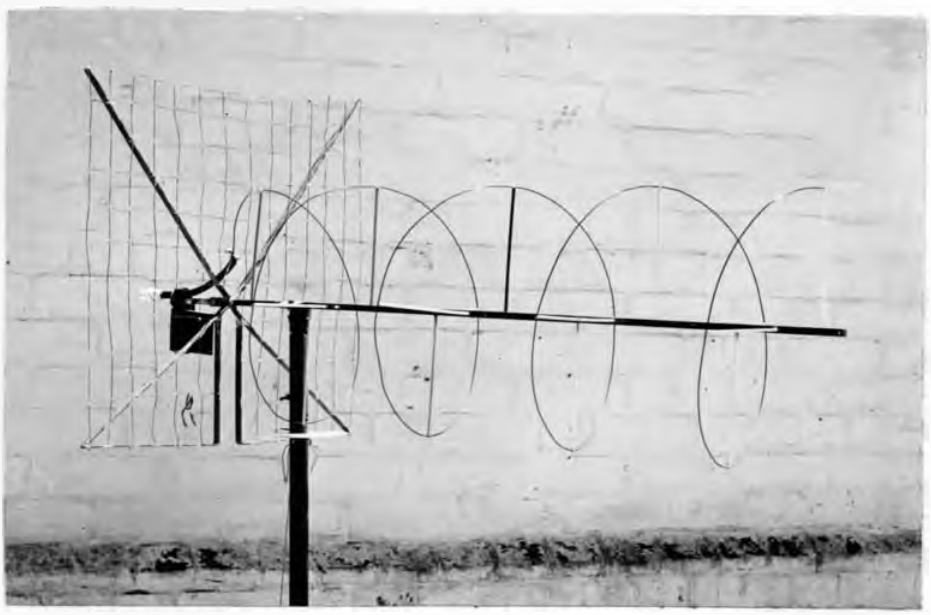

Plate 2. The model helix antenna.

between the ground plane and the helix proper (of length nS) is one half the turn spacing. The diameter of the helix conductor is not a critical specification.

Construction of the antenna:

Since the electric fields received by the helix are entirely transverse, the centre boom of the antenna was made out of a o.6 cm-square brass rod 75 cm long. The helix turns were wound from copper wire and were supported every quarter turn by 12-cm plastic rods fixed to the boom. The ground plane consisted of a frame as shown in figure 4. A cross-hatched mesh of copper wire on 5-cm centres was woven between the edges of the frame. Each mesh intersection was soldered to ensure maximum ground plane continuity. The co-axial line is co-incident with the helix axis and the connection between the centre of the co-axial line and the helix proper consists of a section of conductor which is simply a continuation of the helix proper. The model helix is mounted on a 75 cm long ebonite rod, can rotate about the rod as axis and can be raised in elevation above the horizontal. Plate 2 shows the completed model helix.

4.33 Results of the model helix study

The model was tested by using it as a receiving antenna for radio-frequency energy transmitted to it from a dipole antenna which was a half-wavelength at 400 MHz. The transmitting and receiving antennas were separated by a distance

of 7.5 m (10 wavelengths at the centre frequency) thereby satisfying the plane-wave condition in equation (4.6).

The horizontal and vertical radiation patterns were first plotted at 400 MHz, where the circumference of the helix in wavelengths ($C\lambda$) is equal to 1. After this pattern was found to be of the axial mode of radiation, two sets of patterns were plotted at the top and bottom ends of the frequency range to see whether the patterns were still axial mode patterns at the extremes of the design range. The set of 5 electric field patterns are shown in figures 5 till 9, the frequency and the circumference of the helix in wavelengths at that frequency are indicated on each figure. In each case the solid patterns are for the horizontally-polarized field component and the dashed patterns for the vertically-polarized field component. Both patterns were adjusted to the same maximum during testing and have been normalized to unity. These patterns in the 300 to 500 MHz frequency range are as expected for the axial mode of radiation.

The graphs of figure 10 give a summary of the performance of the model helix. The top graph gives the measured axial ratio in the direction of the helix axis as a function of frequency. It should be pointed out that the definition of the axial ratio used here is that recommended by the Institute of Radio Engineers (Kraus, 1950) and is in fact the inverse of the axial ratio used by radio astronomers i.e. the axial

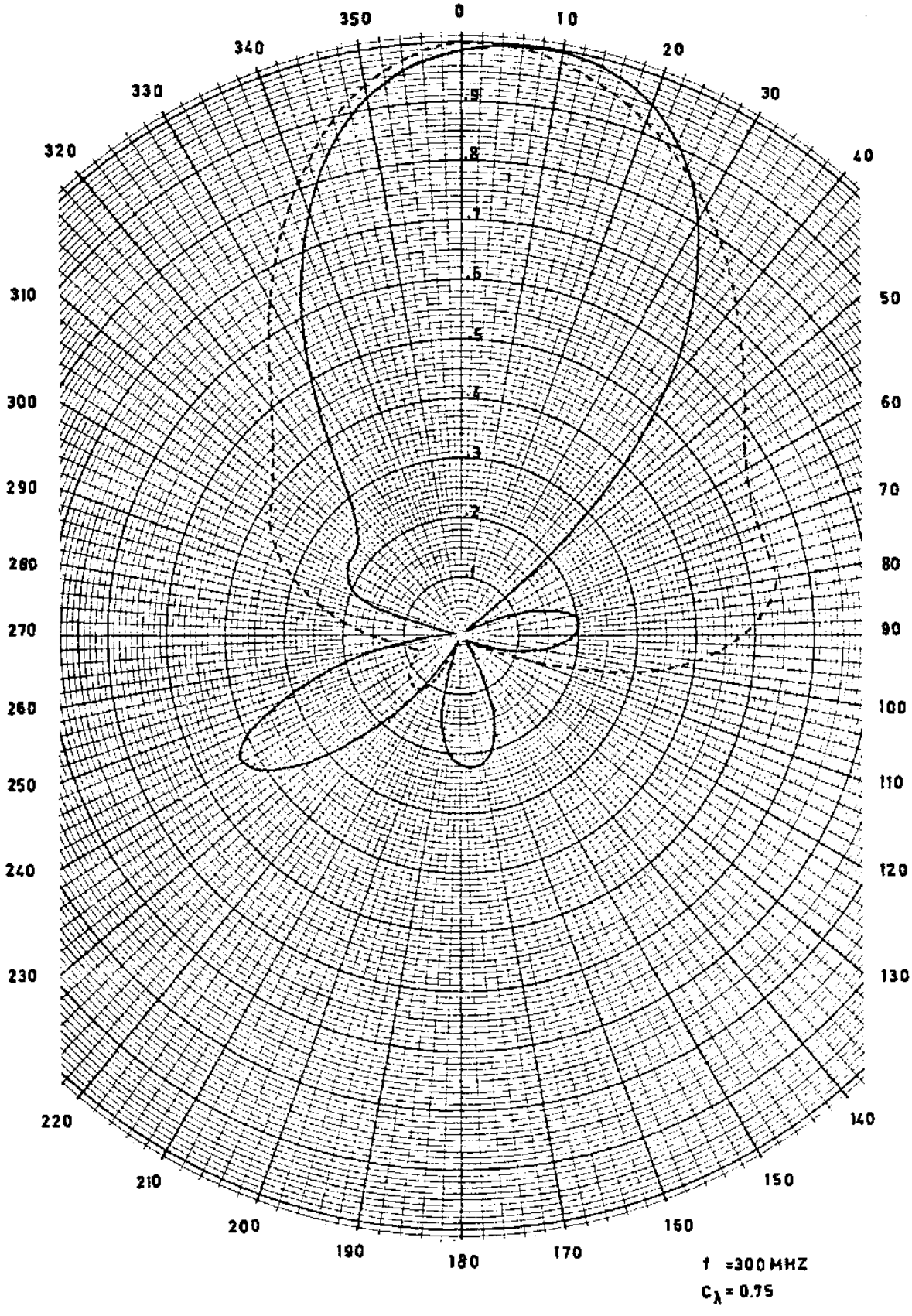

FIG. 5. MEASURED ELECTRIC FIELD PATTERNS.

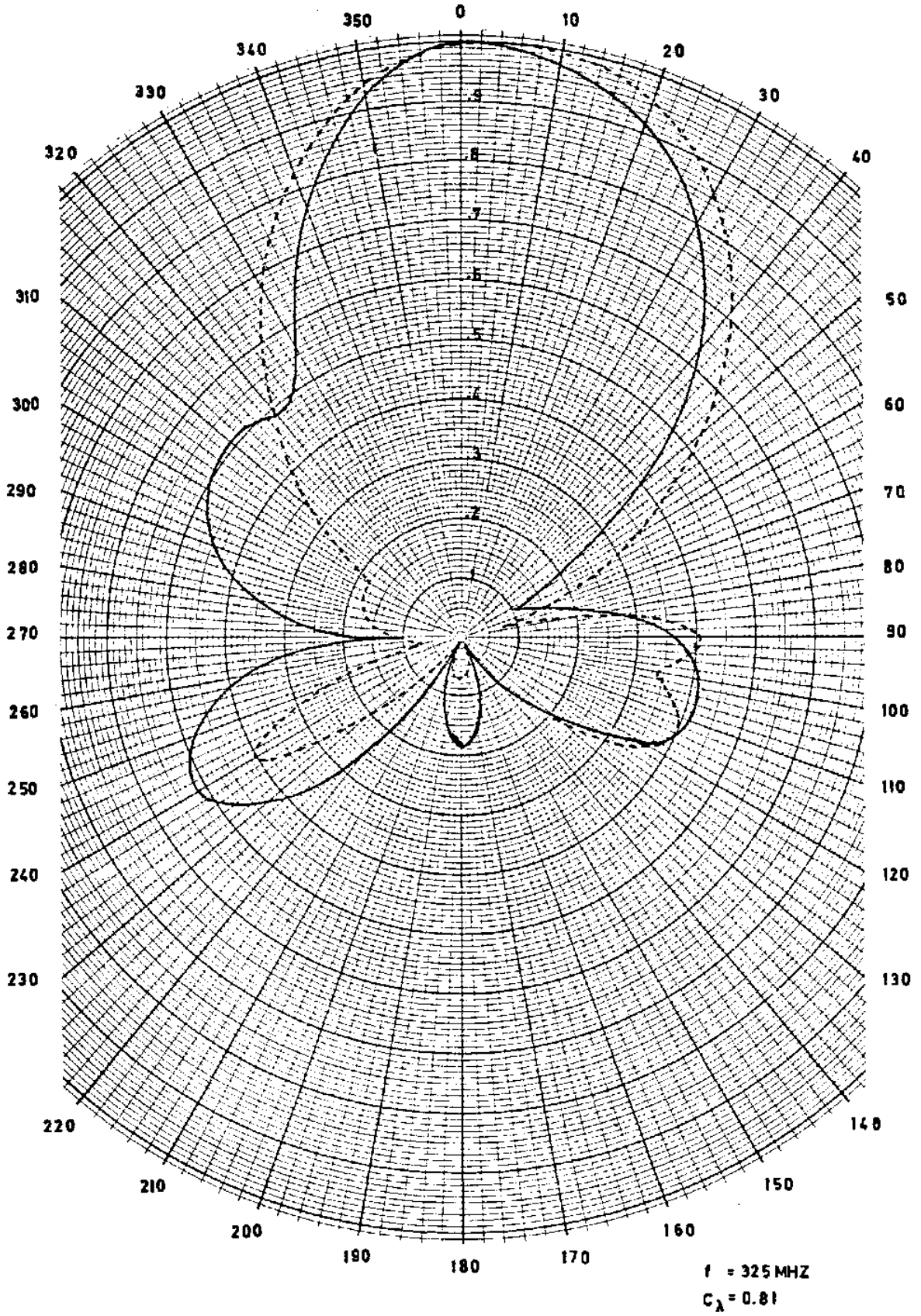

FIG.6. MEASURED ELECTRIC FIELD PATTERNS.

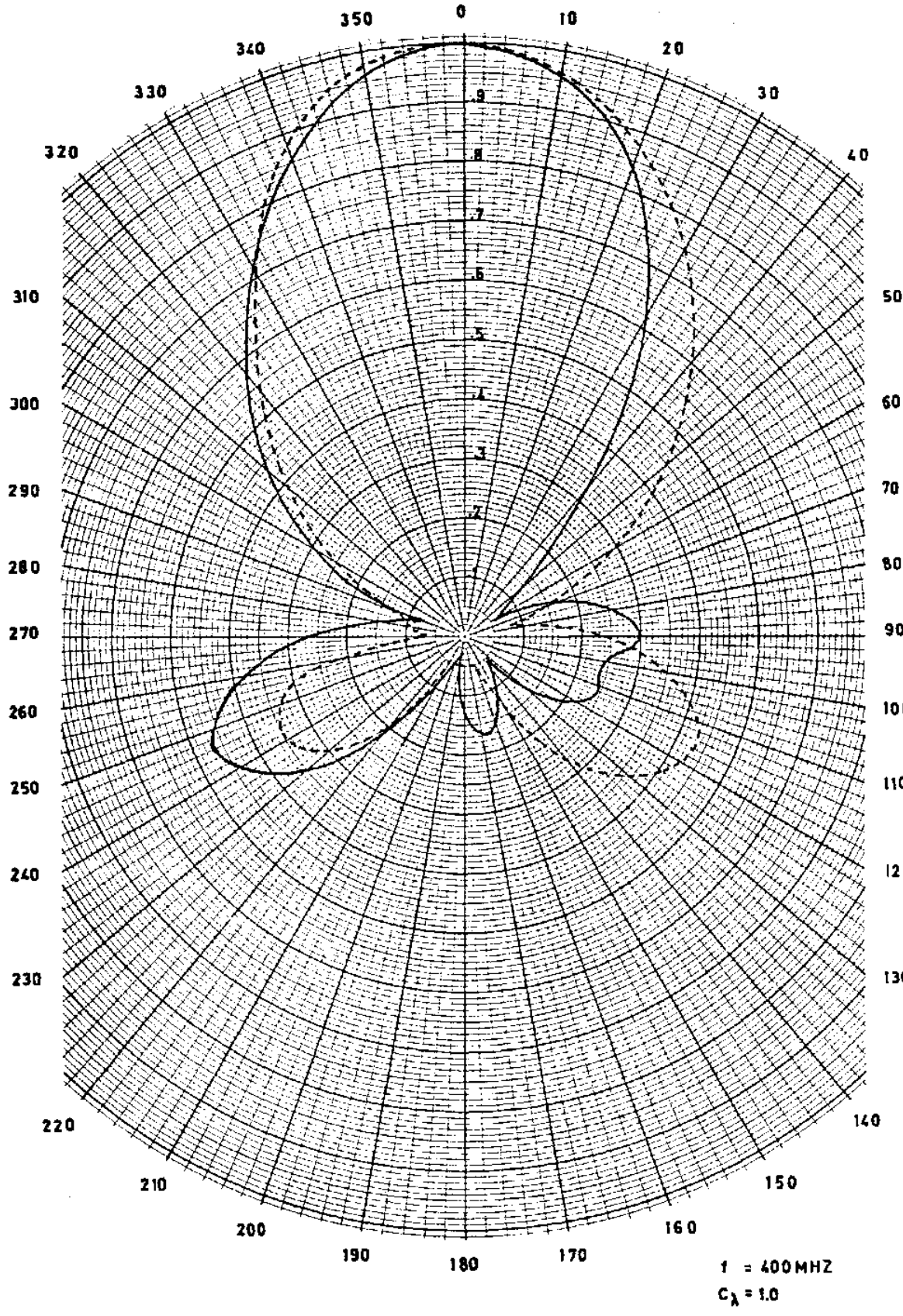

FIG.7. MEASURED ELECTRIC FIELD PATTERNS.

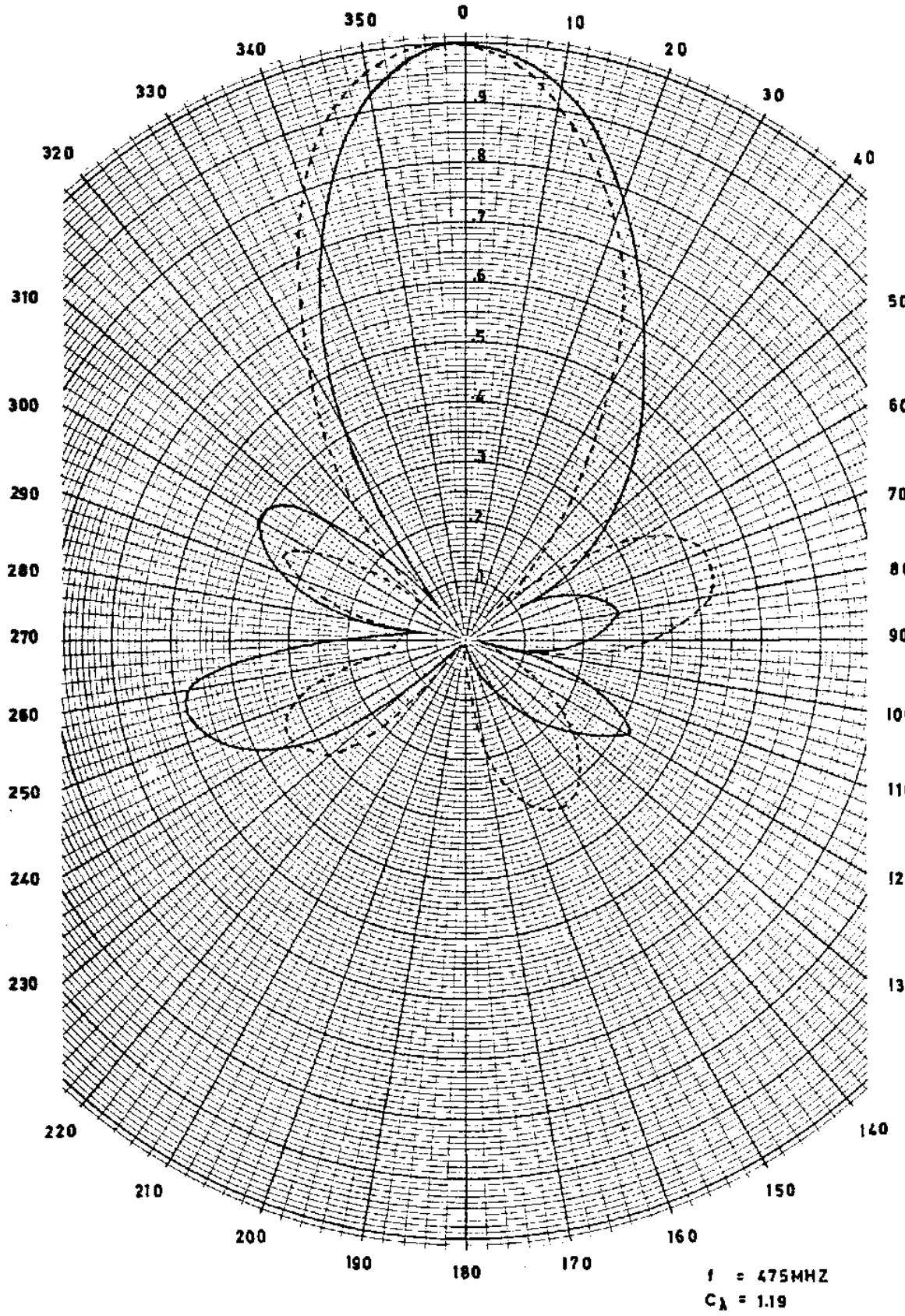

FIG. 8. MEASURED ELECTRIC FIELD PATTERNS.

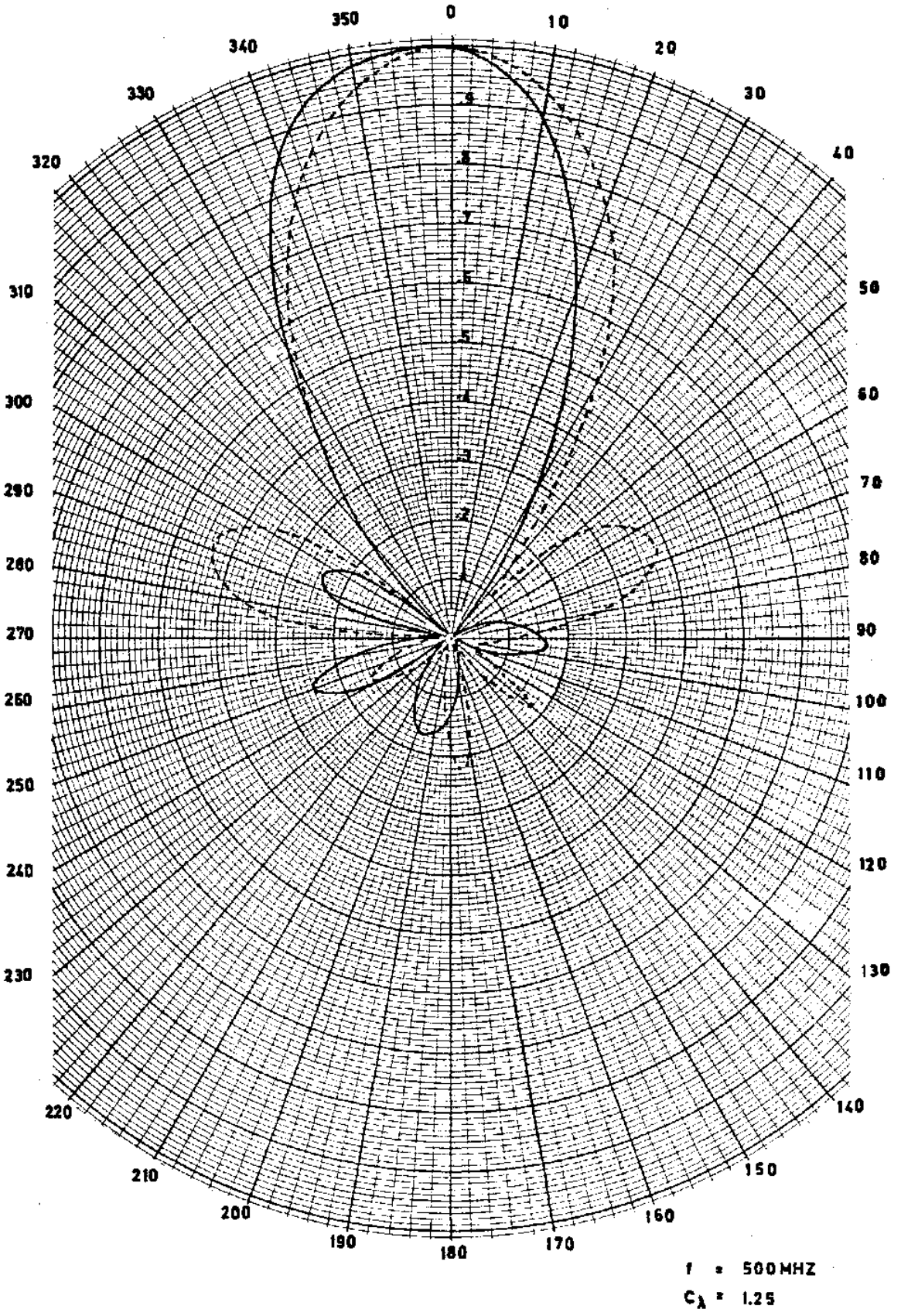

FIG. 9. MEASURED ELECTRIC FIELD PATTERNS.

ratio is equal to the ratio of the major axis to the minor axis of the polarization ellipse. We shall use this definition of axial ratio only as far as it helps our discussion of helical antennas. Circular polarization still has an axial ratio of magnitude 1 in this definition. The theoretical axial ratio of a helical antenna is given by

$$\text{axial ratio} = \frac{2n+1}{2n} \qquad (4.7)$$

where n is the number of turns. The predicted value for 4 turns is thus 1.125.

The middle graph gives the horizontal and vertical half-power beamwidths, measured from the curves of figures 5 to 9, as a function of frequency. The last graph gives the directivity in dB of the antennas as a function of frequency. The directivity (D) is calculated using the approximate formula (Kraus,1950)

$$D \text{ in dB} = 10 \log \frac{41253}{W_E W_H} \text{ dB} \qquad (4.8)$$

where W_E and W_H are the horizontal and vertical half-power beamwidths as measured above. The directivity calculated using this formula may in some cases be slightly high, since the formula does not take into account the effect of the minor lobes.

In summary, between 300 and 500 MHz the half-power beamwidth ranges from about 70° to 40°. Based on pattern integration, the directivity of the 4-turn, 12.5° helix

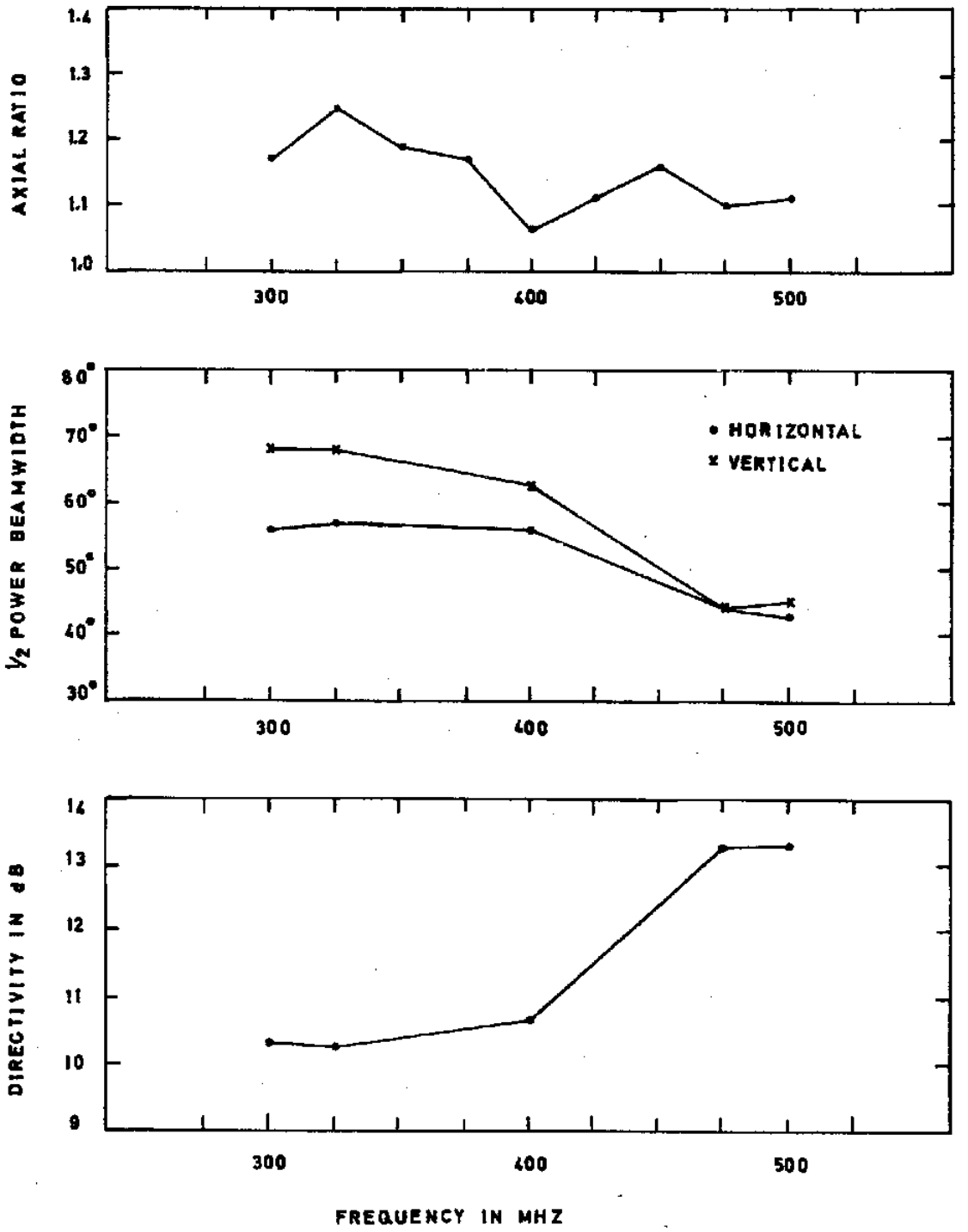

FIG. 10. MEASURED PERFORMANCE OF THE 4-TURN, 300-500 MHZ MODEL HELIX AS A FUNCTION OF FREQUENCY.

over an isotropic circularly-polarized antenna varies from about 10 dB at 300 MHz to 13.5 dB at 500 MHz. Between 300 and 500 MHz the axial ratio in the direction of the helix axis varies from 1.06 to 1.25, being less than 1.2 for most of the range. This represents a relatively small deviation from circular polarization. Considered altogether these pattern, directivity and polarization characteristics represent good performance over a wide frequency range and we decided that helical antennas of 4 turns would be suitable for use as polarimeter antennas in the 15 to 25 MHz frequency range. No measurements of the voltage standing-wave ratio as a function of frequency could be made since a sufficiently sensitive detector for the high-frequency admittance bridge was not available.

4.4 THE HIGH-FREQUENCY HELIX

After the model helix had been successfully tested a right-handed polarized helix was constructed for the frequency range from 30 to 45 MHz. The 5-turn right-handed polarized helix was completed in November 1968 and observations with an HF swept-frequency receiver commenced immediately. A left-handed polarized helix was constructed in February 1969 but no observations with it were possible until April 1969 when a second HF swept-frequency receiver was completed.

4.41 Design and construction

Design:

The design of the HF helix is similar to that of the

model helix shown in figure 4 (which, as it turns out, is a 1 in 10.67 scale model of the HF helix) and the specifications are as follows :

Centre frequency	$f = 37.5$ MHz
Helix circumference	$C = 8$ m
Helix diameter	$D = 2.56$ m
Helix turn spacing	$S = 1.76$ m
Length of turns	$L = 8.2$ m
Number of turns	$n = 5$
Helix pitch angle	$\alpha = 12.5^{o}$
Overall helix length	$A = nS = 8.8$ m
Spacing to ground plane	$g = 0.88$ m
Overall boom length	$A + g = 9.68$ m
Width of ground plane	$G = 4$ m
Conductor diameter	$d = 1.27$ cm

Construction:

The centre boom of the helix consisted of three 2.54 cm diameter aluminium tubes set in an equilateral triangle 10 cm on a side. The three tubes were held together as a rigid structure by means of aluminium spacers andthe boom was pre-stressed to help counteract the droop in the boom when it was pivoted near one end. The droop was further counteracted by running a 5 x 5 cm wooden support beam from the boom at a distance of about 3 m from the front of the antenna to a support pole fixed to the pivot of the antenna. The helix coil was made of 1.27 cm diameter aluminium tubing

Plate 3. The right- and left-handed polarized helical antennas for the 30 to 45 MHz range.

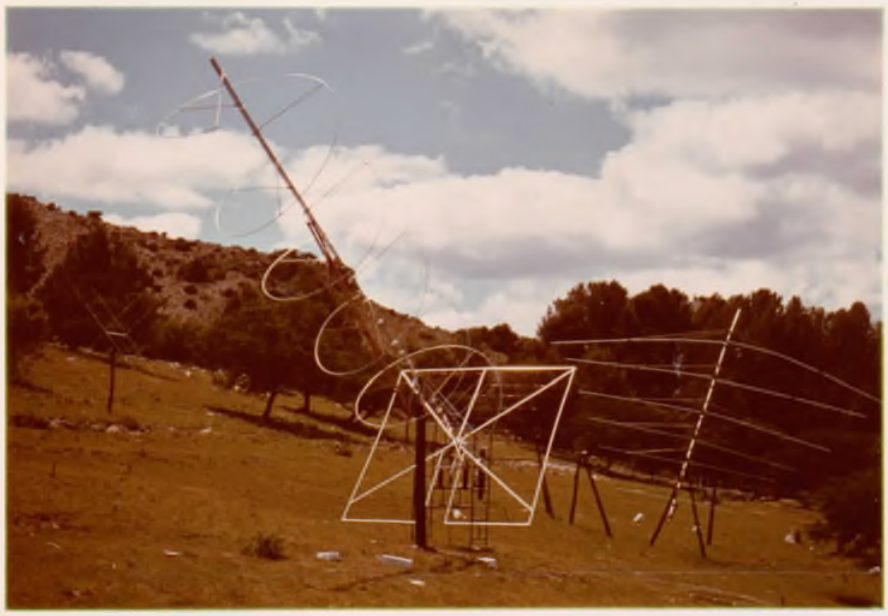

Plate 4. The right-handed helix for the 30 to 45 MHz range and the log-periodic dipole antenna.

and was rolled on a coiling machine specially designed for the purpose. The helix conductor was supported every 1/3 turn by means of 1.5 cm diameter wooden dowels fixed to the centre boom.

The antenna pivot-point is located at a distance of 1.85 m from the ground screen and the antenna is mounted on top of a 2.8 m pole. The ground screen was formed by weaving a cross-hatched mesh of copper wire on 0.3 m centres between the frame of the ground-screen. Each mesh intersection was soldered to ensure maximum ground screen continuity. The ground screen was loaded so that the centre of gravity of the whole system co-incided with the pivot-point. The antenna is steerable in both altitude and azimuth and the gap in the centre of the ground screen shown in figure 4 is to allow the support pole to pass through the ground screen for large elevation angles. The right-handed polarized helix is shown in plate 3 and the left-handed polarized helix can be seen in the background. Plate 4 shows another view of the right-handed helix with the LPD antenna in the background. Most of the constructional details are visible on these plates. The rope enclosure round the antennas is to prevent sheep from getting snarled up in the antenna stay ropes.

4.42 Predicted performance

The antenna structures are too large to enable us to make direct pattern and directivity measurements, however, the performance of the helices can be predicted by means of the

following formulae:

$$\beta = \frac{52}{\frac{C}{\lambda}\sqrt{\frac{nS}{\lambda}}} \quad \text{degrees} \qquad (4.9)$$

where β = half-power beamwidth

λ = free space wavelength

and the other symbols are as defined earlier,

$$\text{Directivity} = 15\left(\frac{C}{\lambda}\right)^2 n \frac{S}{\lambda} \qquad (4.10)$$

$$\text{or} \quad \text{Directivity in dB} = 11.8 + 10 \log \left[\left(\frac{C}{\lambda}\right)^2 n \frac{S}{\lambda} \right] \text{dB} \qquad (4.11)$$

$$\text{and} \quad \text{Characteristic impedance} = 140 \frac{C}{\lambda} \text{ ohms} \qquad (4.12)$$

The characteristic impedance of the antenna varies linearly with frequency between 112 ohms at 30 MHz and 168 ohms at 45 MHz and is 140 ohms at the centre frequency.

Figure 11 shows the calculated performance of the 5-turn helix as a function of frequency. The final graph shows the maximum effective aperture of the antenna as a function of frequency. The maximum effective aperture (A_{em}) is determined from (Kraus, 1950)

$$A_{em} = \frac{\lambda^2 D}{4\pi} \qquad (4.13)$$

where λ = free-space wavelength

and D = directivity from equation (4.10)

Although the performance of the antenna is frequency dependent to some extent, this turns out to be an advantage.

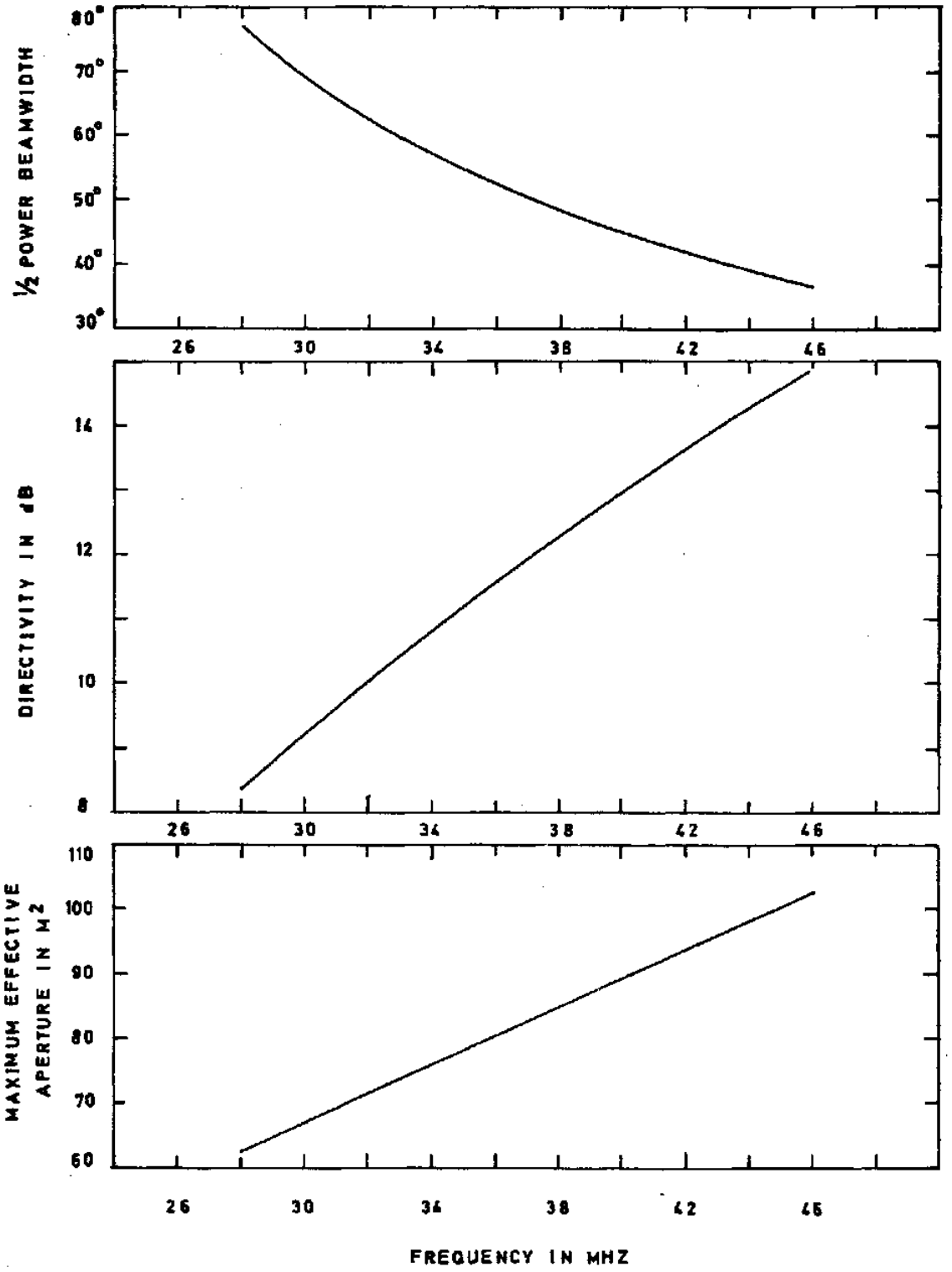

FIG.11. CALCULATED PERFORMANCE OF THE 5-TURN, 30-45 MHZ HELIX AS A FUNCTION OF FREQUENCY.

The maximum effective aperture is larger at higher frequencies and therefore the overall sensitivity of the polarimeter will be larger at the high-frequency end of the range. This helps to compensate for the smaller flux densities of signals at the high-frequency end of the range.

4.43 Measured performance

Figure 12 shows the voltage standing-wave ratio of the antennas as a function of frequency. There are three curves and we shall discuss the dashed curve first. Originally 40 m of low-loss 50 ohm co-axial cable was attached directly to the antenna and the standing-wave ratio was measured at the receiver. Several commercial wide-band baluns were used to try and improve the voltage standing-wave ratio but direct coupling appeared to give the best results. The antenna was operated like this with a swept-frequency receiver and the poor voltage standing-wave ratio produced considerable loss in sensitivity. It was subsequently realised that the poor standing-wave ratio was produced by the extreme mismatching of the antenna and feeder.

The following matching procedure was adopted. The antenna was terminated (shunted) with a 150 ohm resistor which gives a combined impedance of about 75 ohms at the centre frequency. As no 75 ohm co-axial cable was available at the time, a quarter-wave transformer at the centre frequency of 37.5 MHz was placed between the terminated

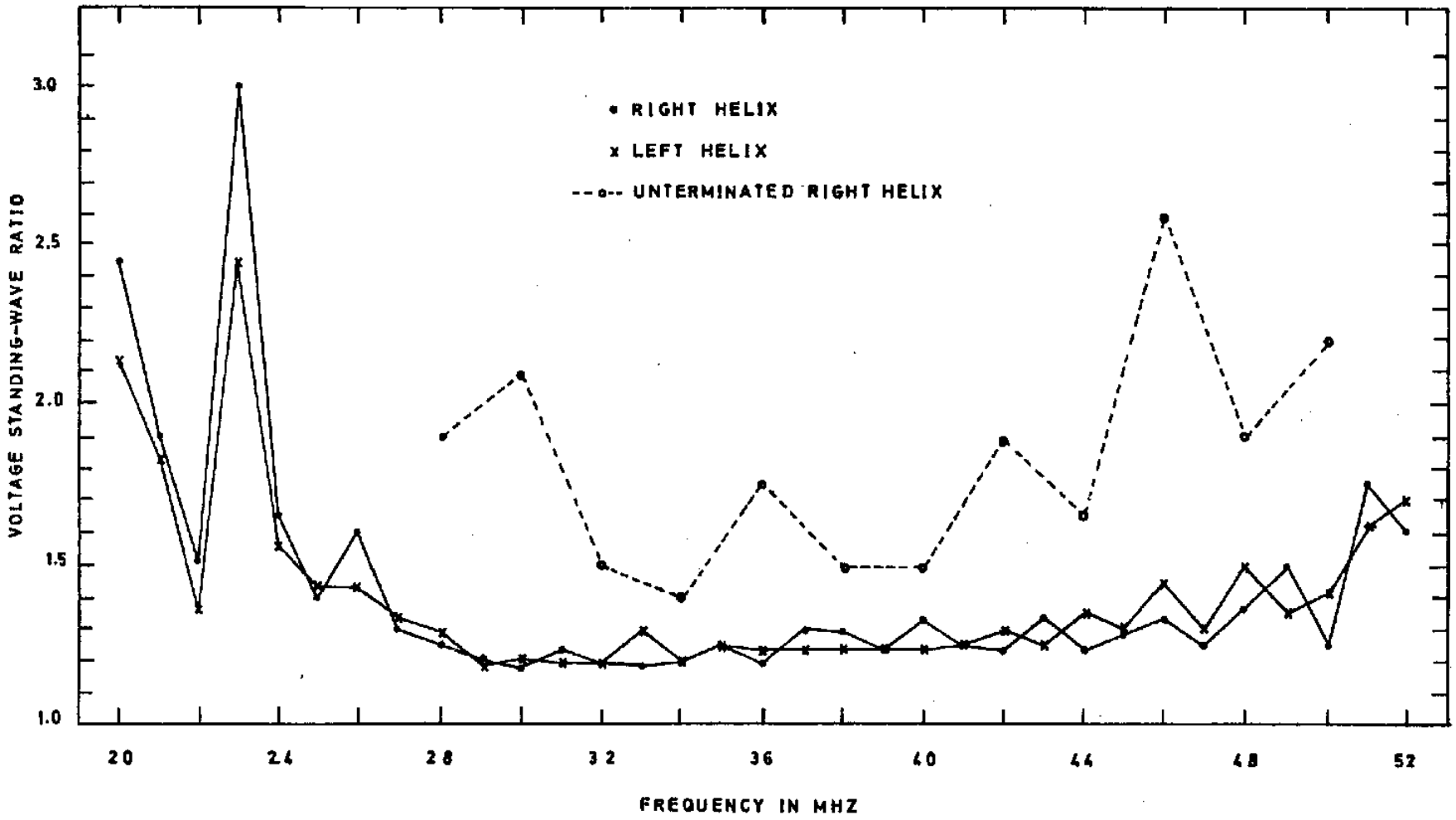

FIG. 12. MEASURED VOLTAGE STANDING-WAVE RATIO OF THE 5-TURN, 30-45 MHZ HELICES AS A FUNCTION OF FREQUENCY.

antenna and the 50 ohm cable and the standing-wave ratio was measured again. The standing-wave ratiosof the matched helices are shown by the lower curves in figure 12. The matching improved the standing-wave ratios considerably and thus also the frequency independence of the receiver system. It should be noted that the loss in the co-axial transmission line would give measured standing-wave ratios better than the true standing-wave ratios. This is not considered an important factor here since the cables have low losses (1 dB / 30 m).

The predicted and measured performance of the HF helices make them suitable for use as polarimeter antennas. Two, and possibly more, storms were observed using the right-handed polarized helix; unfortunately, there was no receiver for the left-handed polarized helix at the time the storms were recorded.

4.5 THE LOW-FREQUENCY HELIX

Once the HF right-handed polarized helix had been used successfully for Jupiter observations, the LF helices were designed. Unfortunately, as a result of an aluminium shortage caused by a fire in the aluminium factory, these helices could not be completed before June 1969 (near the end of the observing season). This is the most unfavourable time for Jupiter observations since Jupiter sets earlier than about 2400 hours U.T. during this period. Interference

from terrestrial radio stations during the early evening makes observations almost impossible. No storms have been recorded using the LF helices but the complete swept-frequency polarimeter sweeping the range 15 to 45 MHz is being run on a routine basis during the present 1969/1970 observing season. It is hoped that storms will be recorded as soon as conditions are favourable. The greatest single factor influencing observations at the moment is the frequent interference from the high-voltage power lines which supply electricity to the site. Swept-frequency observations are then almost impossible since the whole frequency band from about 20 to 45 MHz is saturated with power-line interference. This problem is being investigated at the moment.

4.51 Design and construction

Design:

Since the final LF swept-frequency receivers sweep the range 15 to 26 MHz, the LF helices were designed to cover this range. This is in order since the axial mode persists for frequencies between 0.75 and 1.3 of the centre frequency. The design of the LF helices can be obtained by scaling up the dimensions of the model helix by a factor of 20. There are two dimensions which are not scaled exactly; these are the helix conductor diameter and the width of the ground screen. The design is as follows:

Centre frequency	f = 20 MHz
Helix circumference	C = 15 m
Helix diameter	D = 4.8 m
Helix turn spacing	S = 3.3 m
Length of turns	L = 15.37 m
Number of turns	n = 4
Helix pitch angle	$\alpha = 12.5^{o}$
Overall helix length	A = nS = 13.2 m
Spacing to ground plane	g = 1.65 m
Overall boom length	A + g = 14.85 m
Width of ground plane	G = 9.2 m
Conductor diameter	d = 1.27 cm

Construction:

Originally the LF helices were to be fully steerable, but it was soon realised that a structure 15 m long and 5 m in diameter would present considerable engineering difficulties. The problems experienced in making the HF helices fully steerable also indicated that a fully steerable LF helix would be impossible for us to construct. The following compromise was reached: the helix was to be mounted in such a way that it could be moved at intervals during the observing season. Thus the helix is fixed in position during any particular observing night, but it can be moved to track the position of Jupiter at stages through the observing season. In this way observations, with Jupiter within the half-power beamwidths of the antenna, are

possible for about 4 hours a night throughout the observing season.

The central boom of the antenna was made out of three 2.54 cm diameter aluminium tubes set in an equilateral triangle with sides of 25 cm. The boom was held as a rigid structure by means of triangular spacers made from 1.5 cm diameter aluminium tubing. The spacers were placed at 1.5 m intervals along the boom and the structure was further strengthened by means of cross-bracing between the spacers. The helix coil was rolled in 5 m lengths on the coiling machine and every joint was welded to ensure maximum continuity. The helix conductor was supported every 1/3 turn by 5 x 2.5 cm wooden beams fixed to the centre boom. The coils were further supported by means of thin nylon ropes attached at every 1/6 turn.

The antenna structure was mounted as shown in figure 13. The upper sketch shows how the boom is supported by means of three 1.5 cm diameter ramoline ropes passing over pulleys mounted at various heights on a 10 m high pole. The elevation of the antenna can be adjusted by manually raising the antenna with the three ropes and the elevation of each antenna was set initially at 45° to the horizontal. The lower sketch shows how the antenna is pivoted on the ground. The pivot is set into a concrete slab and the pivot can rotate about its axis as well as in a vertical plane. The pyramid-shaped point of the antenna boom contains a 2.54 cm

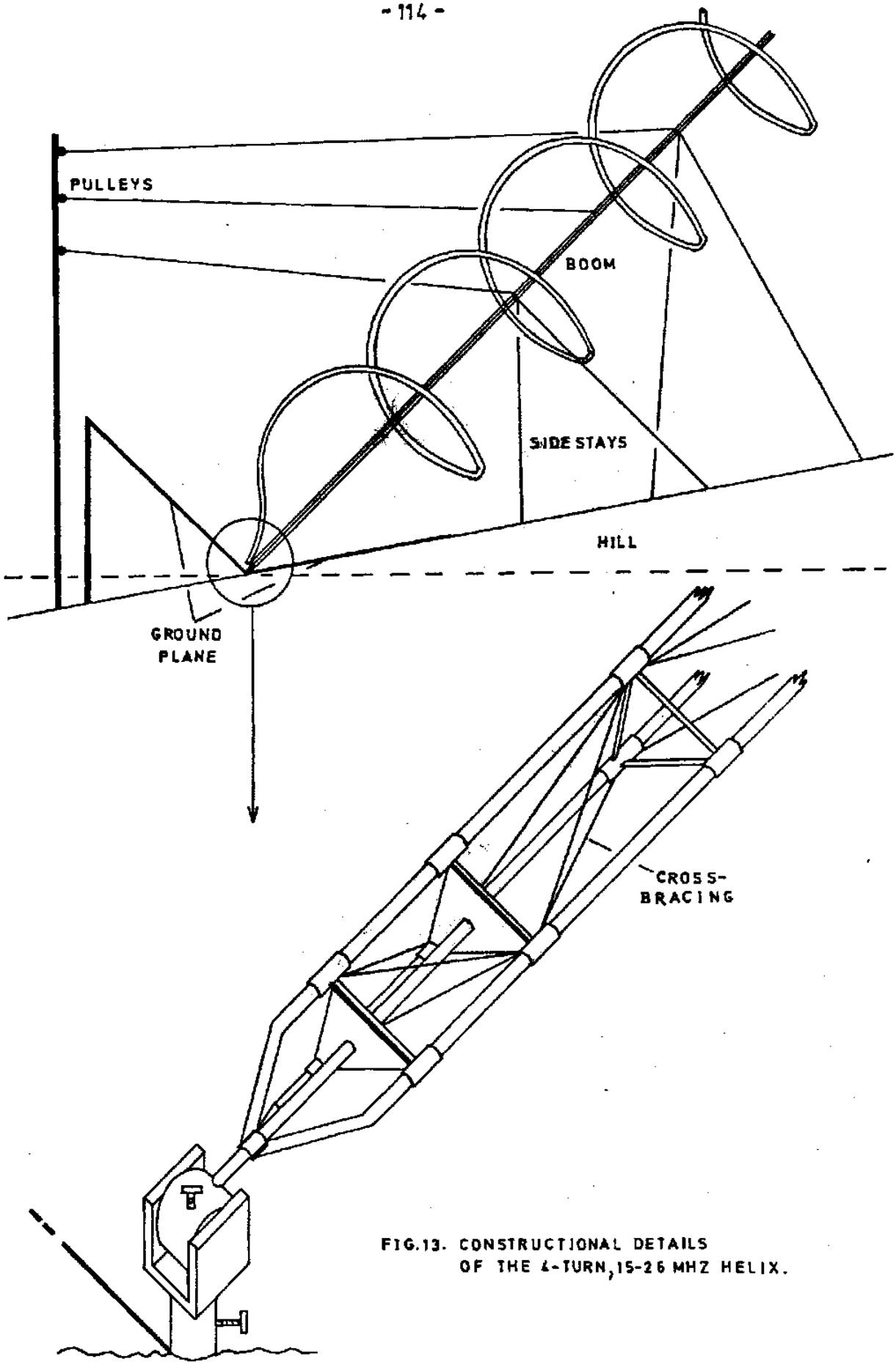

FIG.13. CONSTRUCTIONAL DETAILS OF THE 4-TURN, 15-26 MHZ HELIX.

Plate 5. The right-handed helix for the 15 to 26 MHz range.

steel rod which is set into the pivot. The triangular spacers and the method of cross-bracing can also be seen in this sketch.

As shown in the upper sketch the antenna is fixed in position by means of side stays of 0.6 cm diameter ramoline rope. Thin nylon ropes were also attached to the centres of the beams supporting the helix coil and were then fixed to the ground to prevent torsional oscillations of the helix structure. The ground plane consisted of half a ground plane, of length 9.2 m and width 4.6 m, at right angles to the helix axis and half a ground plane lying on the surface of the ground. This is shown in figure 13. A mesh of copper wires on 0.6 m centres was woven between the ground plane frame and all the mesh intersections were soldered.

Most of the features described above can be seen in plates 5 and 6. Plate 5 shows the right-handed circularly polarized antenna and plate 6 shows the left-handed circularly polarized antenna (the HF left-handed helix can be seen in the background). The size of the antennas can be gauged by remembering that the poles supporting the whole structure are 10 m high.

4.52 Predicted and measured performance

The performance of the LF helices is predicted by equations (4.9) through (4.13). The characteristic impedance of the antennas varies between 105 and 182 ohms in the frequency range from 15 to 26 MHz. Figure 14 summarises

Plate 6. The left-handed helix for the 15 to 26 MHz range.

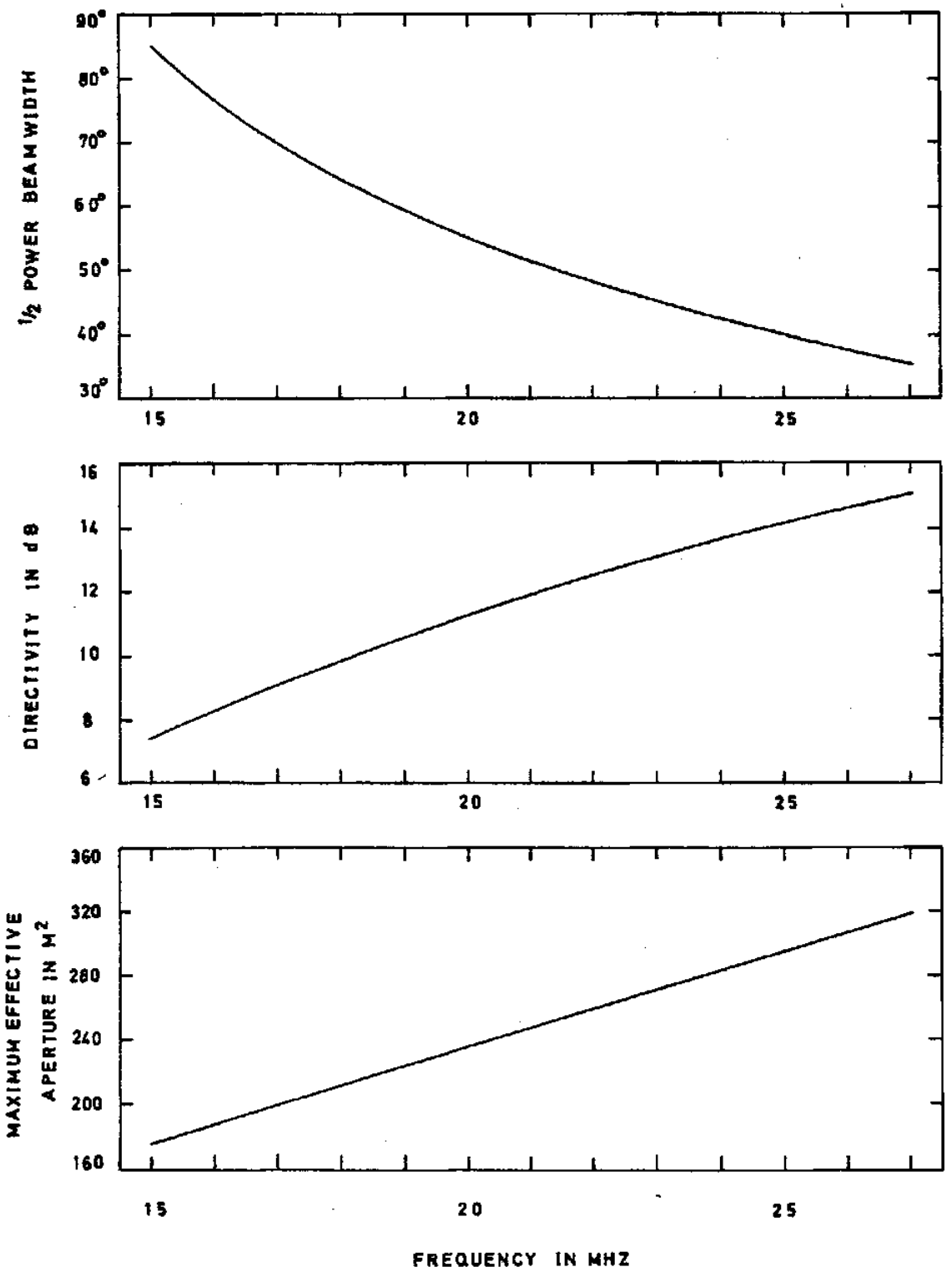

FIG.14. CALCULATED PERFORMANCE OF THE 4-TURN, 15-26MHZ HELIX AS A FUNCTION OF FREQUENCY.

the calculated performance for the LF helices. Notice that the maximum effective aperture of the LF helix is considerably larger than the maximum effective aperture for the HF helix. This results, of course, from the larger physical dimensions of the LF helix.

The antennas were both terminated with 150 ohm resistors and were connected to the receivers by low loss 75 ohm co-axial cable. The right-handed polarized helix needed 40 m of cable and the left-handed polarized helix needed 70 m of cable to reach the receivers. Figure 15 shows the voltage standing-wave ratio of the two antennas as a function of frequency as measured at the receiver ends of the cables. The voltage standing-wave ratio for both helices is better than 1.4 throughout the operating range and this is very good performance over such a wide band of frequencies.

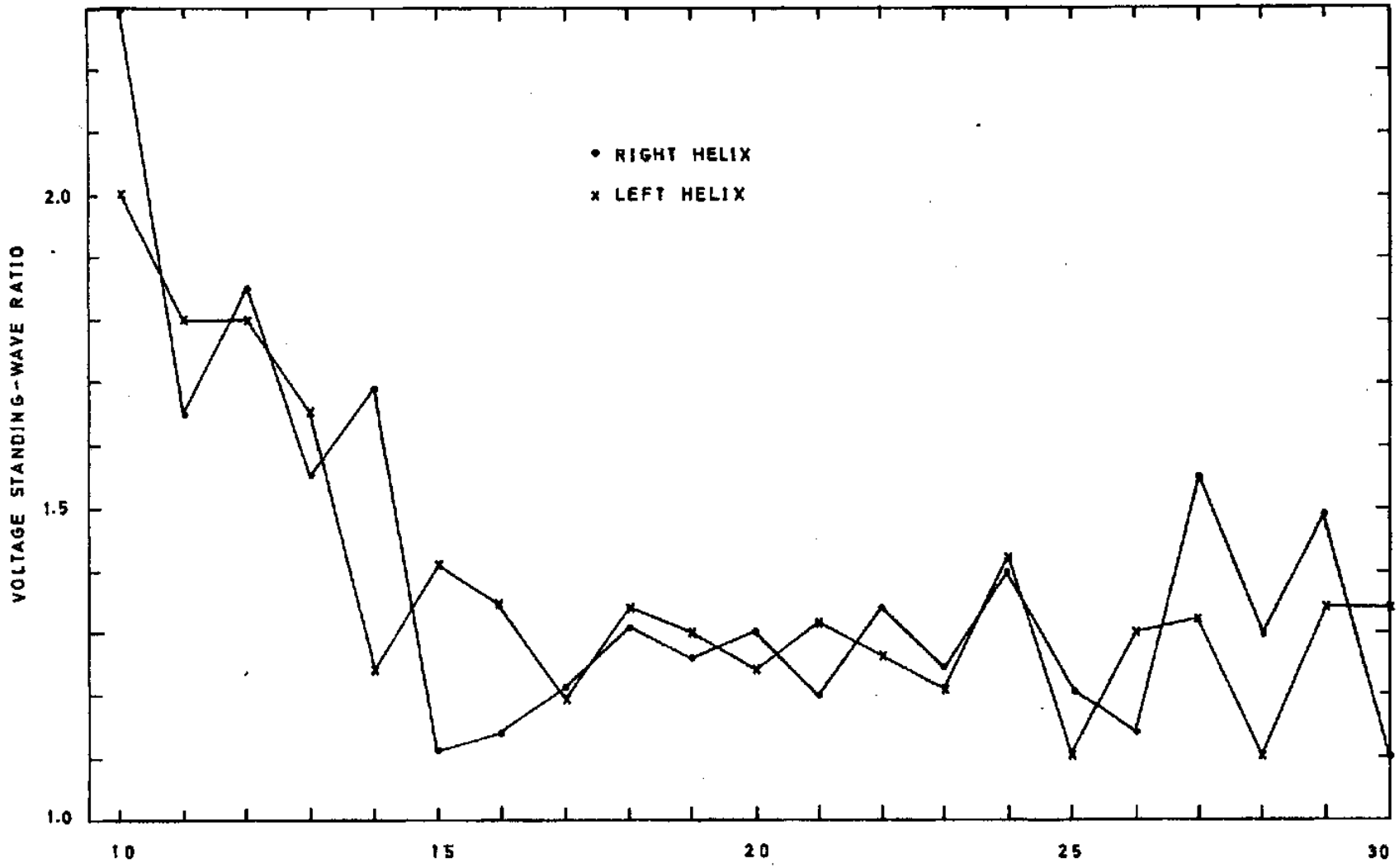

FIG.15. MEASURED VOLTAGE STANDING-WAVE RATIO OF THE 4-TURN, 15-26 MHZ HELICES AS A FUNCTION OF FREQUENCY.

CHAPTER V

ELECTRONIC CIRCUITRY OF THE SWEPT-FREQUENCY POLARIMETER

5.1 INTRODUCTION

In this chapter we shall present the circuit diagrams of the various electronic stages of the swept-frequency polarimeter. No attempt will be made to describe the design considerations of the various stages in detail, but a simple description of the types of circuits used and the purpose of some of the controls will be given. We shall first present the final versions of the polarimeter circuitry and then, when all the circuits have been discussed, we shall describe the development of the apparatus through its various stages. It will be appreciated that the final circuit diagrams are the end result of many modifications to the original circuit designs. A description of all the modifications made during the construction and experimental operation of the various stages is not feasible in this discussion; some of the more important modifications will be mentioned, however. Finally, photographs of selected waveforms from the receiver and from the intensity-modulation calibration system will be shown.

5.11 Block diagram

Figure 16 shows the block diagram of the swept-

frequency polarimeter. The complete swept-frequency polarimeter in fact comprises two polarimeters, one for the 15 to 26 MHz range and another for the 30 to 45 MHz range. Thus the block diagram should be seen as being duplicated - once for the low-frequency range and once for the high-frequency range. The discussions which follow apply equally well to the low- and high-frequency polarimeters. Details which are essentially different for the two polarimeters will be pointed out.

The input signals from the antenna are passed through a high-pass filter to a broadband radio-frequency pre-amplifier which is followed by an attenuator. From the attenuator the signals are fed to the swept-frequency receiver which is tuned by means of varactor diodes. The receiver is calibrated in frequency and time at one minute intervals by the harmonics from the harmonic generator. The tuning voltage for the varactor diodes is obtained from a sweep generator which also produces a pulse which is used to trigger the oscilloscopes monitoring the signals. The pulse is fed into the audio amplifier so that the pulse is present in the receiver output at the start of each sweep. The signals from the audio amplifier are fed into a range compressor which reduces the dynamic range of the output signals. This is necessary since the data recorder overloads on large signals. The final output signals are fed either to the data recorder so that the signals can be

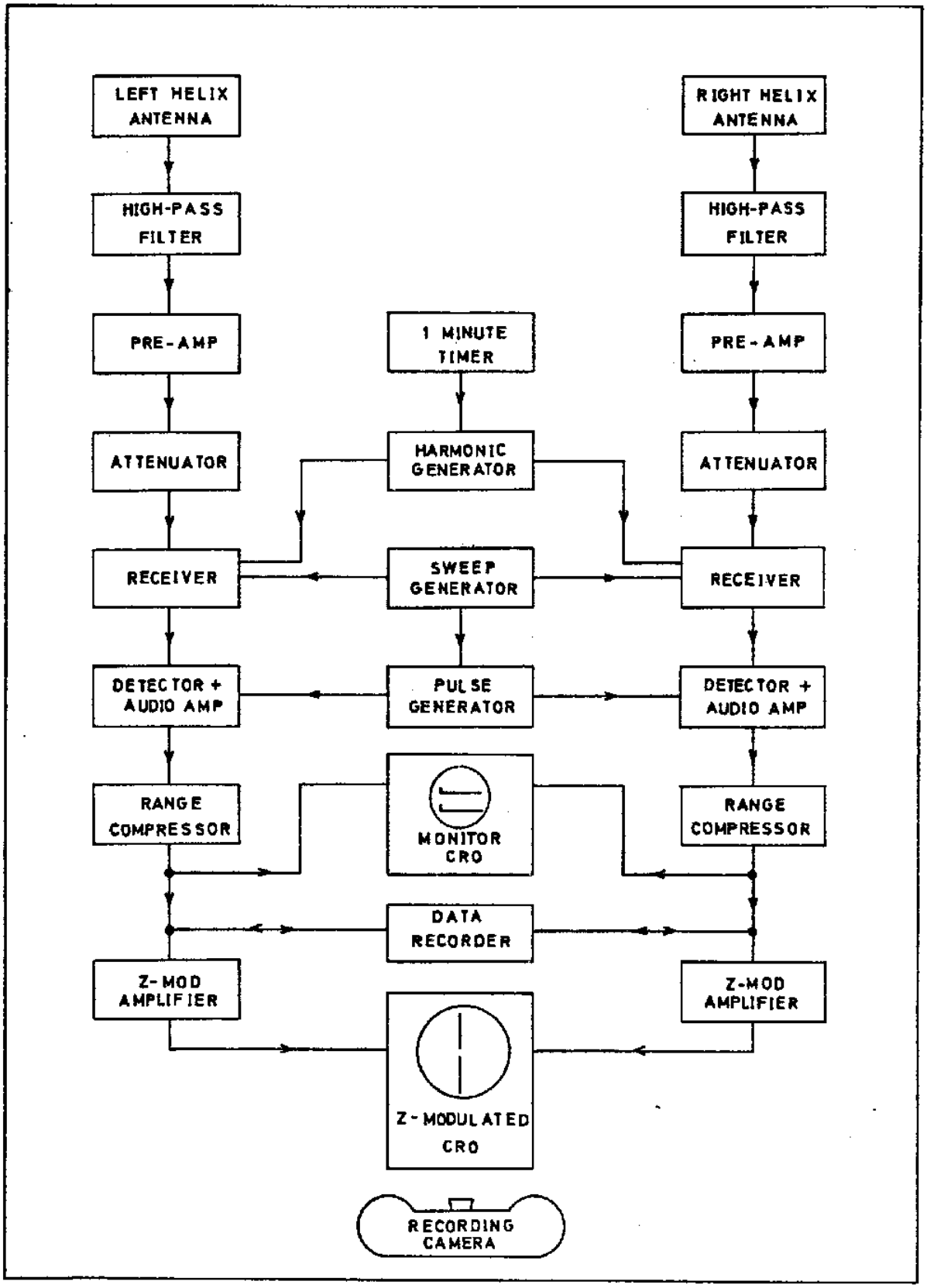

FIG.16. BLOCK DIAGRAM OF THE SWEPT-FREQUENCY POLARIMETER.

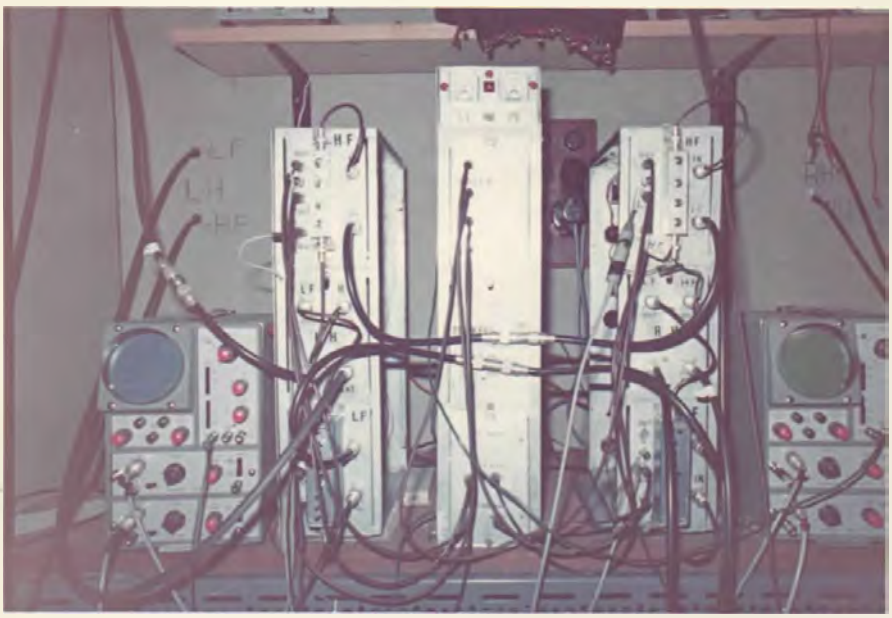

Plate 7. The receiving equipment of the swept-frequency polarimeter.

recorded and processed subsequently or to a Z-modulation amplifier which permits direct photographic recording of the signals from intensity-modulated oscilloscope traces at the observing site.

Plate 7 shows the installation of the various circuits into three different chassis holders. The left-hand holder contains the two left-circular receivers and their associated electronics; the centre holder contains the sweep generators and the time and frequency calibrators while the right-hand holder contains the two right-circular receivers and their associated electronics. The entire polarimeter circuitry is run off a stabilised supply which is shown on top of the centre holder. The DC power supply will not be discussed.

5.12 Notes on circuit diagrams

A note on certain conventions used in the circuit diagrams is necessary. Resistance values are denoted in the following way: values between 0 and 1000 ohms are written down with no symbol after them (thus 68 denotes 68 ohms), values in the kilo-ohm range are followed by the symbol k (2.2 k denotes 2.2 kilo-ohms) and values in the megohm range are followed by M (1 M denotes 1 megohm). Capacitance values are followed by the symbol μ (·1μ means 0.1 microfarads) and the symbol p (1000p means 1000 picofarads). The symbol μH is used to denote microhenries.

As can be seen from plate 7, the various stages of the

polarimeter are interconnected by means of co-axial transmission cable. The radio-frequency stages are coupled by means of radio-frequency connectors which are denoted by ⊙—, the outer shield being grounded. The low-frequency stages are connected by means of so-called "normal" low-frequency connectors which are denoted by ◑— ; the outer shield is usually grounded. Simple interconnections between circuits on the same chassis are denoted by o— .

Since specialised types of semiconductors are used, a complete list of devices in the ciruits is given at the end of the chapter. The devices are listed sequentially throughout the circuits, the symbol T denoting transistor, field effect transistor (FET) or unijunction transistor and the symbol D denoting various diodes. The specifications of certain inductances are also listed and these are given the symbol L. Stages will frequently be identified by the label of the active device in brackets, e.g. (T3).

5.2 RECEIVER AND ASSOCIATED ELETRONICS

5.21 High-pass filters

The signals from the antennas are passed through high-pass filters to eliminate strong signals in the band below the low-frequency limit of the receivers. Due to non-linearity in the pre-amplifiers these signals would

produce outputs at the harmonics. The m-derived high-pass filters for the low-frequency (LF) receivers were designed with m = 0.5 and cut-off frequency at 14 MHz for a terminating impedance of 75 ohms. The circuit diagram of this filter is shown in figure 17. Since the values of the capacitors resulting from the design are not identical with those available commercially, the capacitors in the end sections are made variable. In this way it is possible to tune the filter to give a suitable cut-off frequency. The measured frequency response of the filter is shown in figure 18. The m-derived high-pass filters for the high-frequency (HF) receivers have m = 0.316 and a cut-off frequency at 28 MHz for a terminating impedance of 75 ohms. The circuit diagram of this filter is shown in figure 19 and the measured frequency response is shown in figure 20.

5.22 Radio-frequency pre-amplifier and step-attenuator

Pre-amplifier:

The LF receivers use commercially-manufactured pre-amplifiers with a voltage gain of 30 dB. The HF receivers use pre-amplifiers designed by the author and their circuit is shown in figure 21. The input low-noise transistor T1 is used as a grounded-base stage which gives an input impedance of about 50 to 75 ohms for a wide range of frequencies and collector load resistors. The collector circuit contains a peaking network to peak the response of

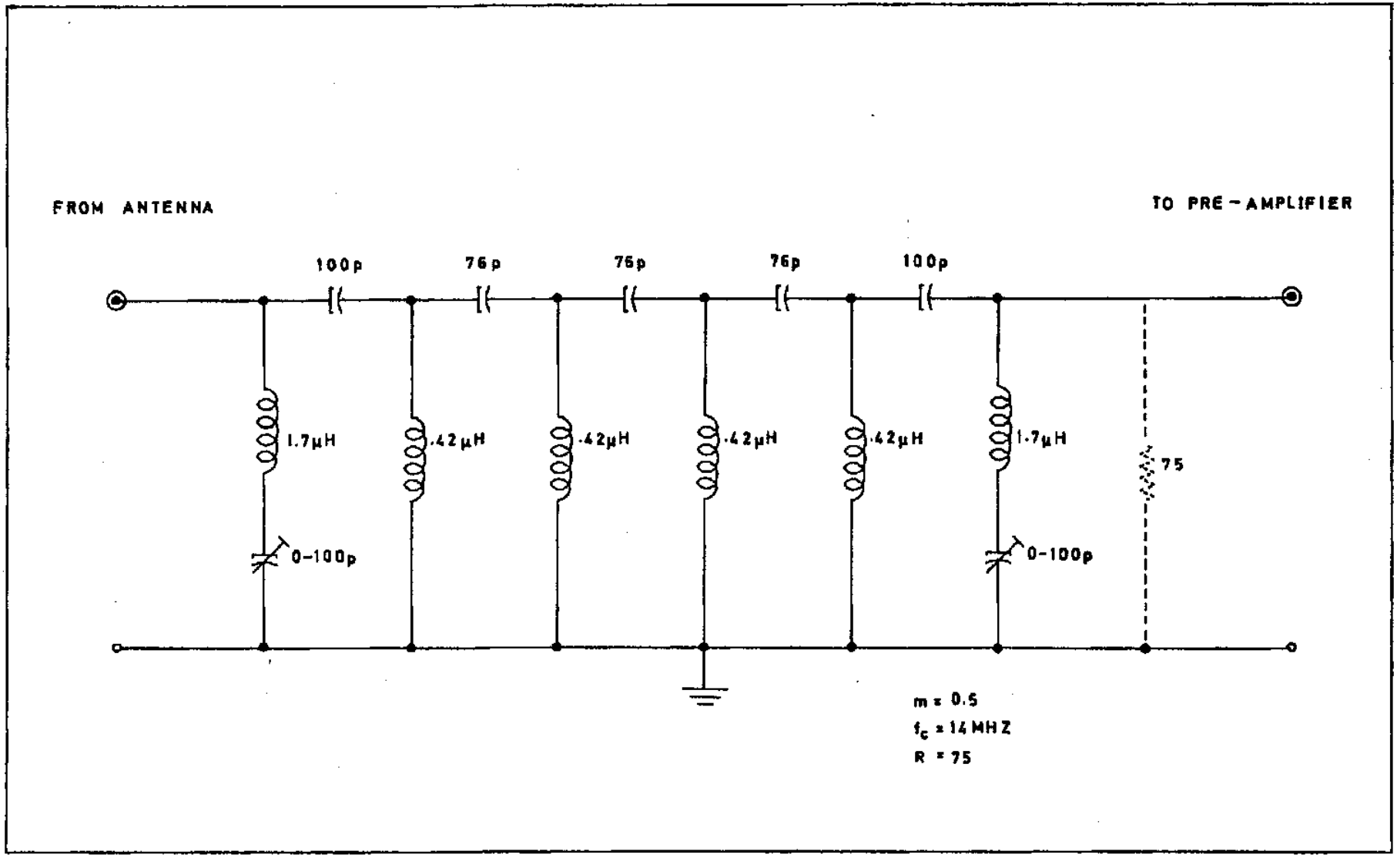

FIG.17. 14MHZ CUT-OFF FREQUENCY HIGH-PASS FILTER.

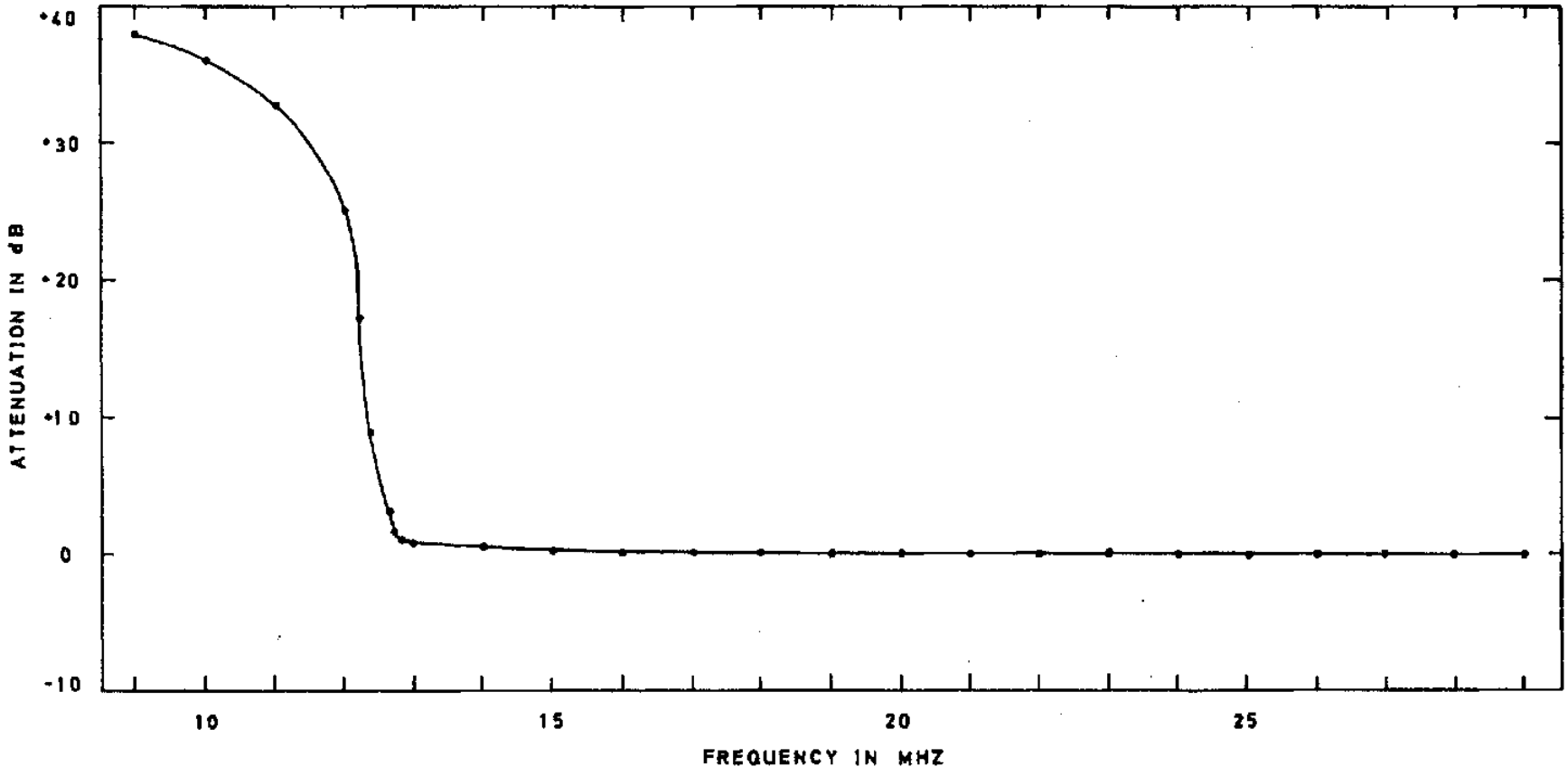

FIG.18. FREQUENCY RESPONSE OF THE 14MHZ HIGH-PASS FILTER.

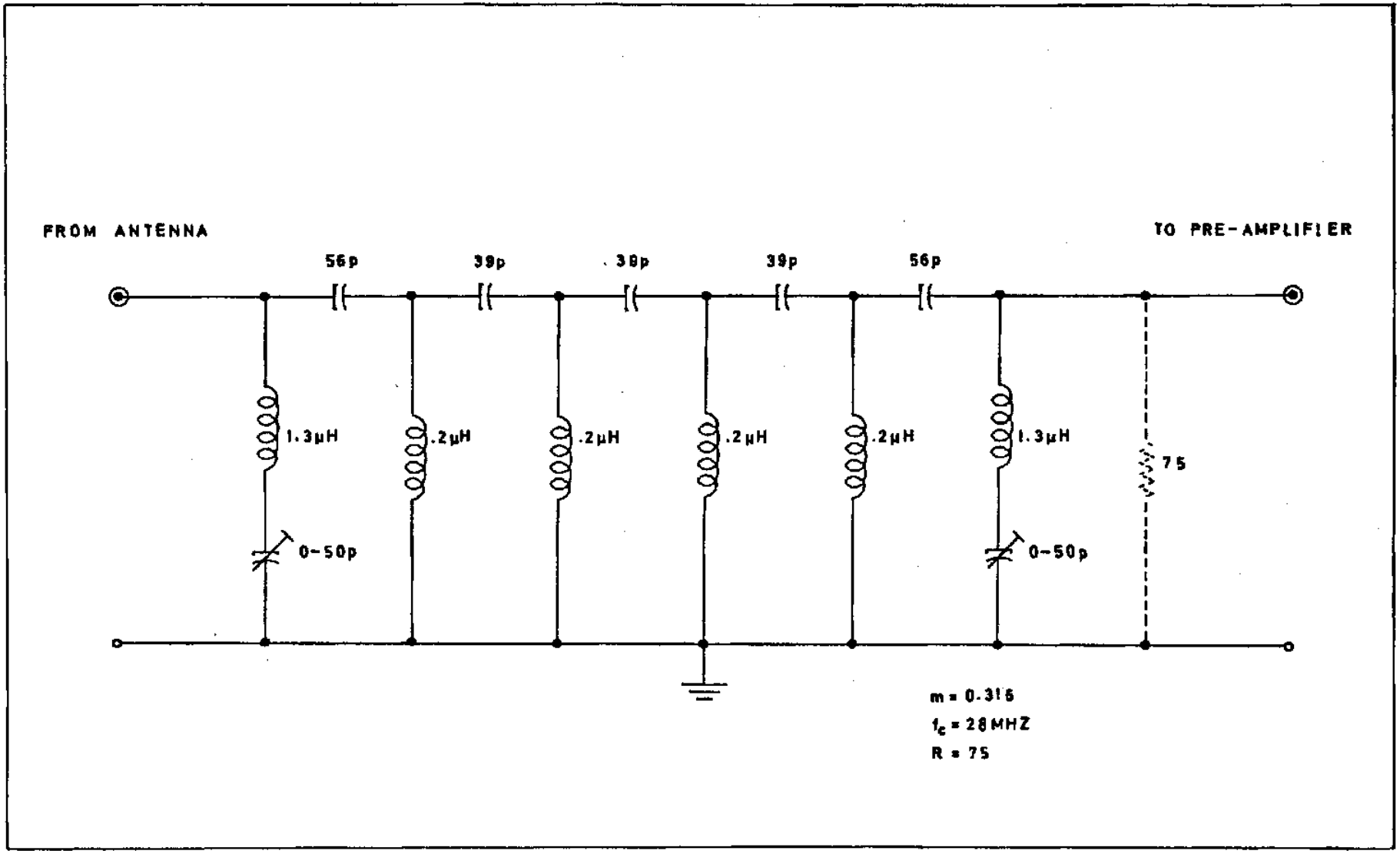

FIG.19. 28MHZ CUT-OFF FREQUENCY HIGH-PASS FILTER.

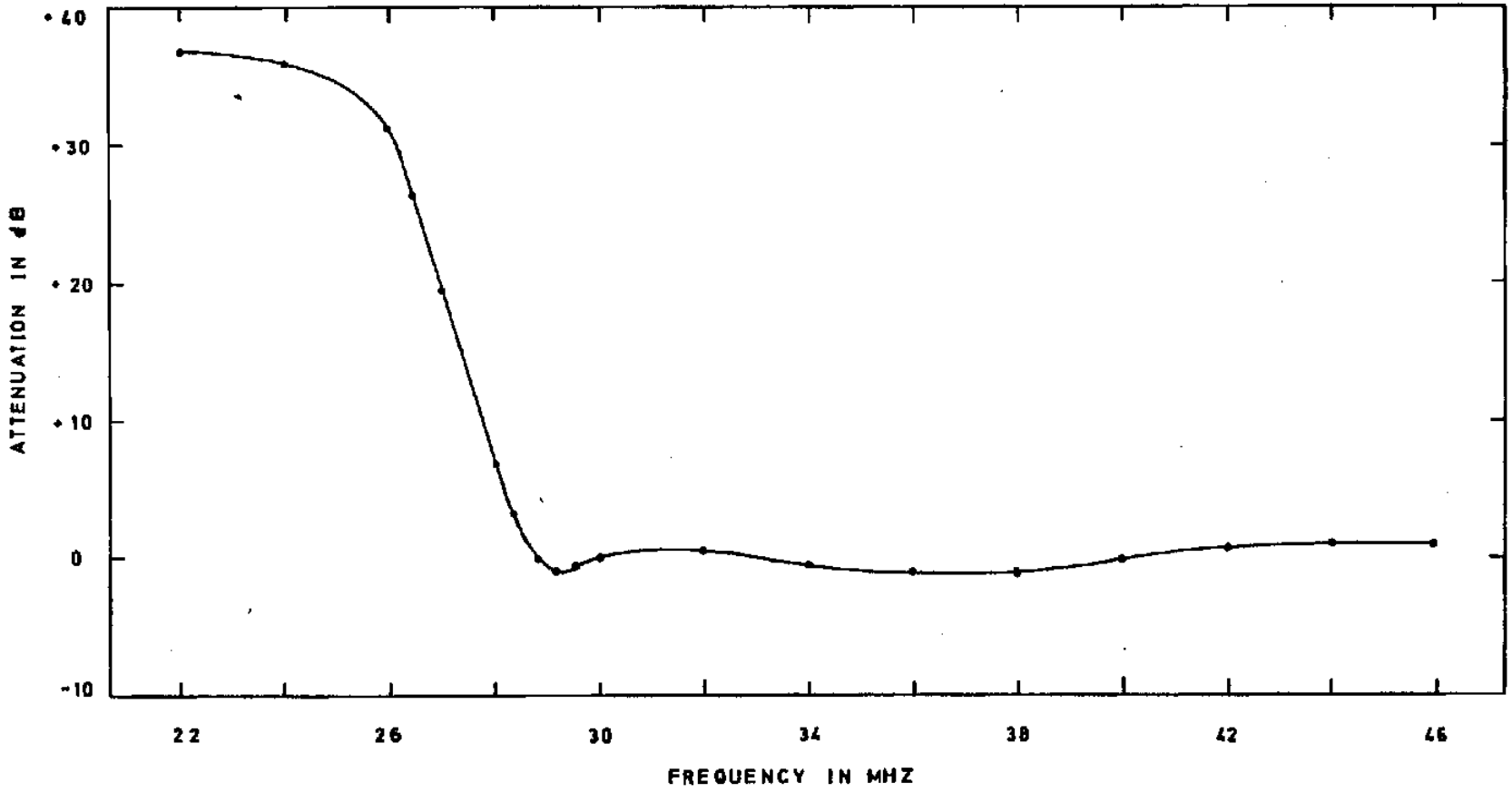

FIG. 20. FREQUENCY RESPONSE OF THE 28MHZ HIGH-PASS FILTER.

the amplifier once the response starts to "roll off" at about 20 MHz. The position of the fairly broad peak in the 30 to 45 MHz range can be adjusted by means of a slug-tuned inductance L2. The second low-noise transistor T2 is used as a conventional common-emitter amplifier with a low collector load resistance to reduce the effect of parasitic capacitances at high frequencies. The output of this stage is fed into a low-attenuation pad to give some isolation for the sake of stability. The pre-amplifier has a voltage gain of 30 dB and is enclosed entirely within a 1/16" thick brass box to ensure effective radio-frequency screening. The same is done for the attenuators and the harmonic generators.

Attenuator:

The output of the pre-amplifier is fed into a step-attenuator which allows a range of attenuations to be switched in as required. The LF receivers employ commercial attenuators with the following attenuation settings in dB: 1, 2, 2, 5, 10, 20, 20, 20 and 20. The HF receivers use symmetrical unbalanced π attenuator pads designed to give 50 ohms characteristic impedance. The attenuator has four attenuation settings which give the following dB range: 2, 2, 5 and 10. The circuit of figure 21 shows two of the unbalanced π sections; the switches can be set individually or in groups to give attenuations up to 19 dB. For the various attenuator settings the resistors of the pads have

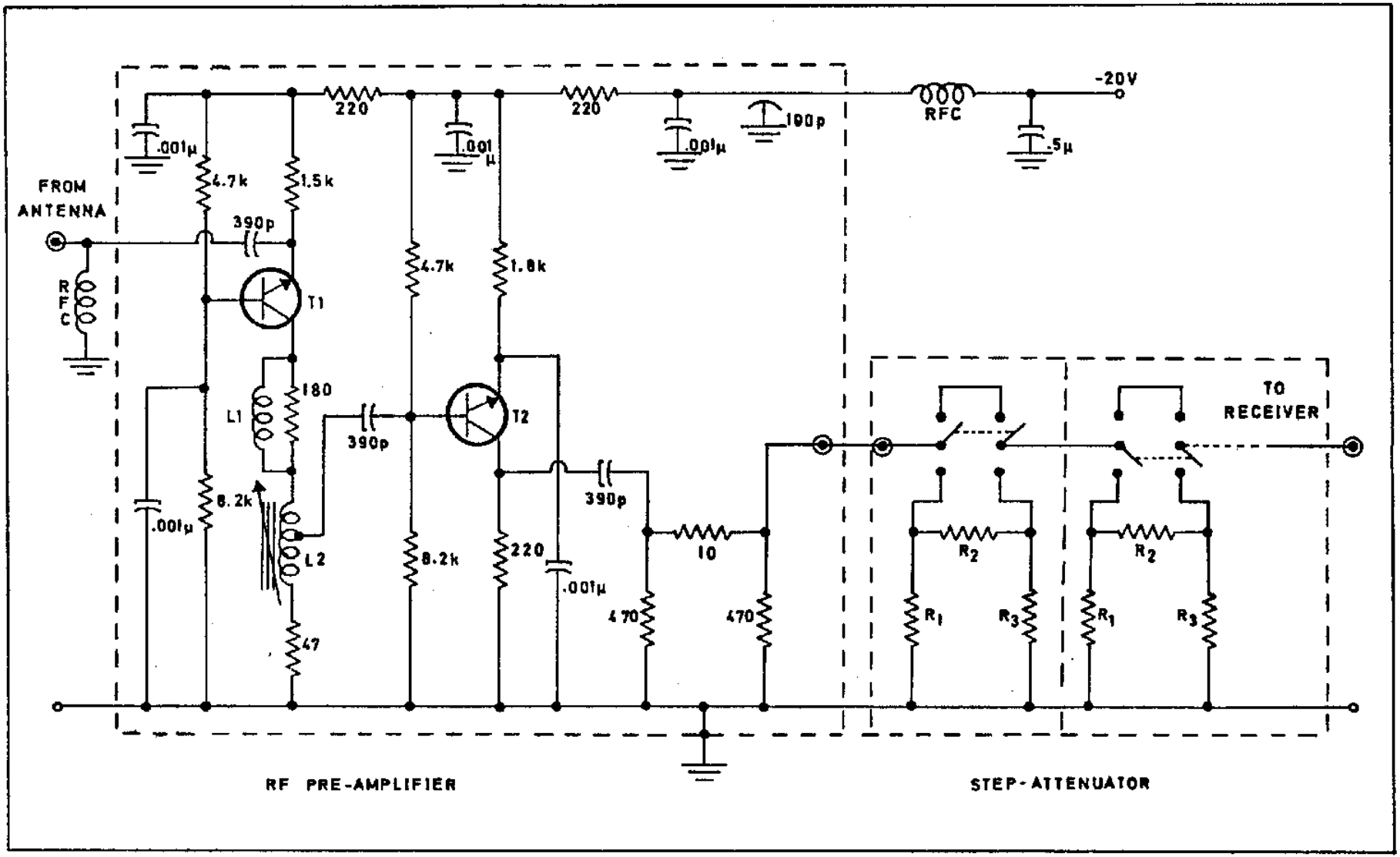

FIG.21. R.F. PRE-AMPLIFIER AND STEP-ATTENUATOR.

the following values:- for the 2dB positions $R_1 = R_3 = 425$ ohms and $R_2 = 12$ ohms, for the 5dB position $R_1 = R3 = 188$ ohms and $R_2 = 32$ ohms and for the 10dB setting $R_1 = R_3 = 105$ ohms and $R_2 = 75$ ohms.

5.23 Swept-frequency receiver

The circuit diagram of the LF swept-frequency receiver is shown in figure 22. There are two inputs which will be discussed in later sections; these are the sweep-voltage input from the sweep generator and the frequency-time calibration input from the harmonic generator. The first stage of the receiver is a grounded-base amplifier (T3) with collector peaking and it has an input impedance of about 50 ohms. The input from the harmonic generator is also connected to the emitter of the first transistor.

The tuned stages of the receiver are three identical common-emitter amplifiers (T4, T5, T6) with parallel-resonant circuits in their collector leads. The resonant frequency of the circuits is varied by varying the capacitance of varactor diodes D1, D2, D3 with a tuning voltage. We shall not discuss the problem of obtaining a linear frequency versus time output from the receiver at this stage, suffice to say that a linear output requires a tuning voltage which is not a linear function of time. The negative supply voltage is connected to the transistors through a tap on the coil of the resonant circuit to reduce capacitive loading of the

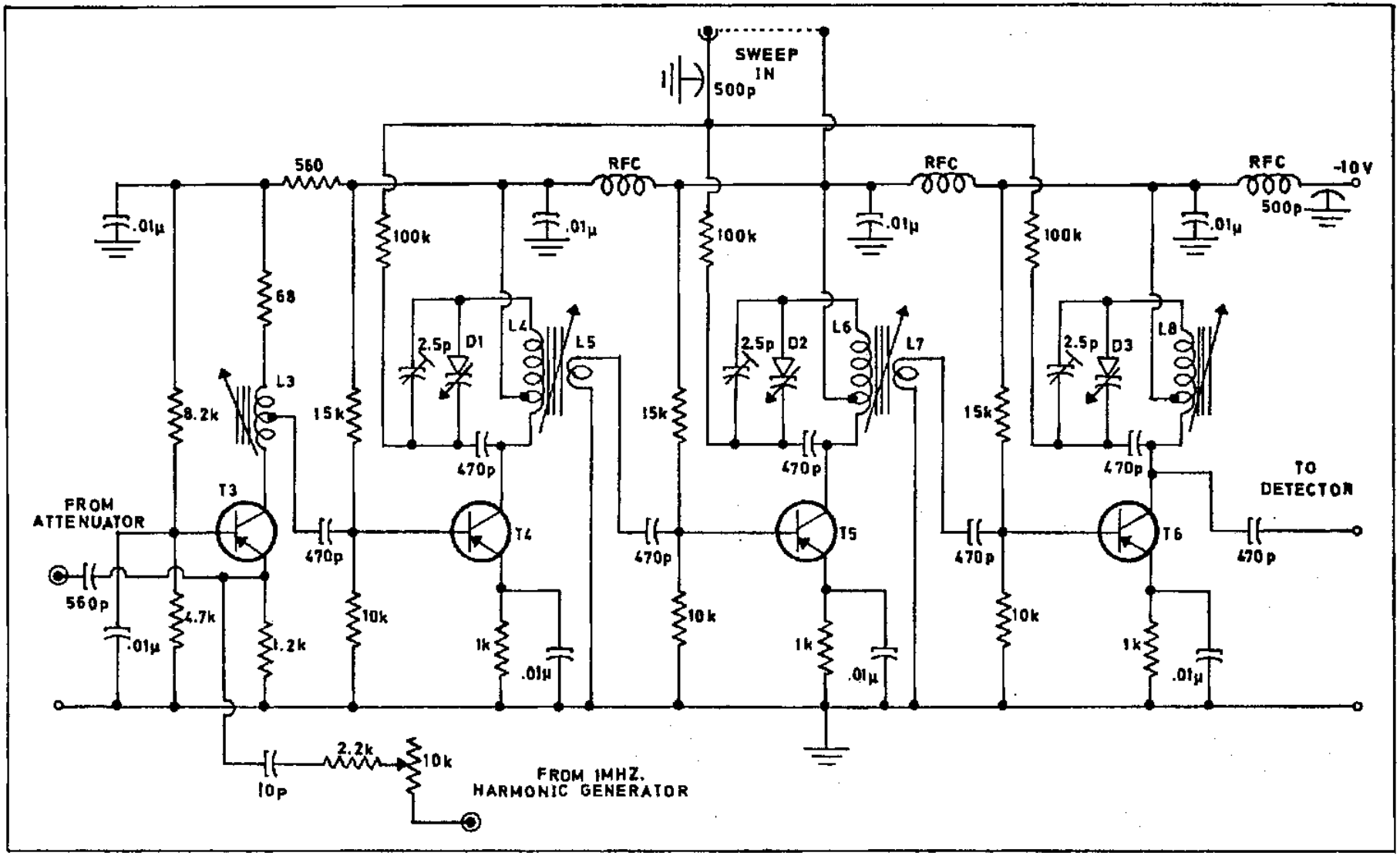

FIG.22. THE 15-26 MHZ SWEPT-FREQUENCY RECEIVER.

resonant circuit. It is important to keep stray capacitances as small as possible since the capacitance range of the varactor diodes is only from 14 to 21 picofarads.

Cascaded tuning stages:

If several tuning stages are cascaded and tuned with the same tuning voltage, they must all pass through the same resonant frequency at the same time to obtain effective selective amplification. To obtain the best "tracking" throughout the range the varactor diodes should have identical characteristics. Since commercially-manufactured matched triads of diodes were unobtainable the following procedure was used to select the best-matched diodes from a stock of about 50. A single tuning stage was set up and the diodes were inserted into this circuit in turn and their highest and lowest frequencies for two tuning voltages were noted. The diodes which had the most closely matched highest and lowest frequencies were selected for the final receiver. The complete receiver is tuned by the following procedure. The three tuning stages are tuned individually to cover the same frequency range (26 to 15 MHz, say). The three stages are then coupled inductively and are tuned at the low-frequency end by means of the inductances only and the high-frequency end is then tuned by using only the trimmer capacitors.

Feedback from the second tuned circuit via T5 produces

an effect on the first tuned stage similar to that which is observed with double-tuned amplifiers. If the two circuits are overcoupled the characteristic "double-humped" over-coupling peak is obtained and the bandwidth of the combination is broader rather than narrower for cascaded stages. The stages are therefore lightly coupled by means of a single turn of wire around the coil of the previous resonant circuit to eliminate this effect. By varying the coupling, the bandwidth of the receiver may be adjusted. The output of the final tuning stage (T6) is coupled directly to the detector stage through a capacitor since no feedback in the collector circuit is present.

High-frequency receiver:

The final HF receiver was constructed along similar lines to the LF receiver described above except that it has four rather than three tuned stages. This is necessary to obtain more gain and narrower bandwidths than are possible with only three stages. The component values are all identical to those of the LF receiver except for the values of the inductances and the coupling capacitors. The coupling capacitors are 270 rather than 470 picofarad capacitors. The specifications of the inductances are tabulated at the end of the chapter. (They are denoted by the symbol L').

The performance and specifications of the LF and HF receivers will be discussed when all the polarimeter

Plate 8. Constructional layout of the 15 to 26 MHz swept-frequency receiver.

circuitry has been presented. Plate 8 shows the constructional layout of the LF receiver in its chassis; the layout of the HF receiver is identical except that there is an extra tuned stage.

5.24 Detector, audio amplifier and range compressor

The circuit of these three stages is shown in figure 23.

Detector:

The detector consists of two diodes D4, D5 used as a voltage-doubling detector. The detector is a square-law detector i.e. the output voltage from the detector is proportional to the square of the input voltage from the receiver, and it gives positive-going output signals. The time constant of the detector is 1 millisecond for a 100-millisecond sweep period and 100 microseconds for a 10-millisecond sweep period.

Audio amplifier:

The audio amplifier consists of an integrated-circuit operational amplifier (Nexus type SQ10-a) with suitable feedback networks. The signals from the detector and the pulse generator are fed into the inverting input of the operational amplifier which is used as a summing amplifier. The non-inverting input is grounded. The amplitude of the negative-going pulse input signal is set

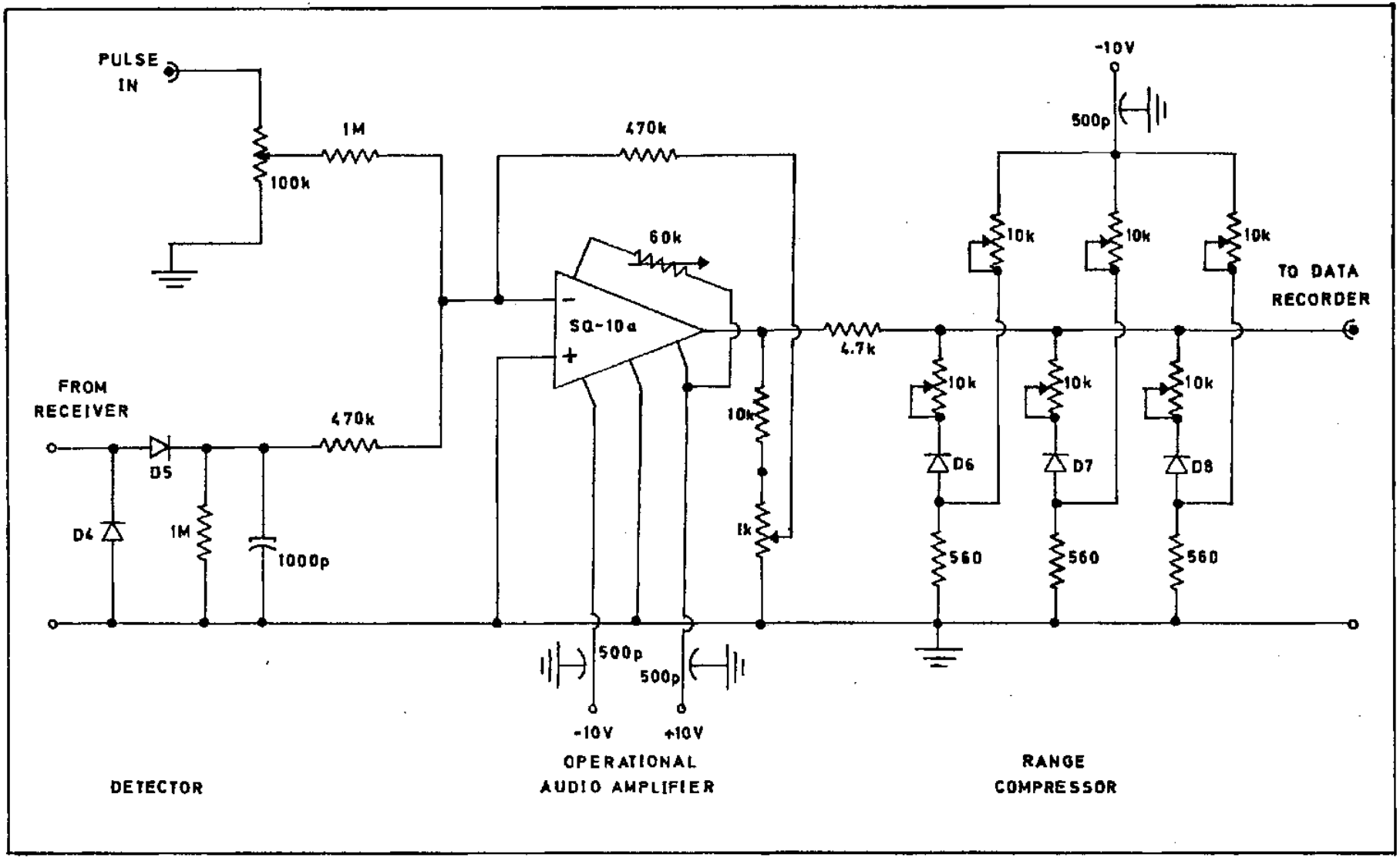

FIG.23. THE DETECTION AND AUDIO STAGES AND THE RANGE COMPRESSOR.

by the 100 k-ohm potentiometer and the overall gain of the operational amplifier is controlled by the 1 k-ohm potentiometer connected in series with a 10 k-ohm resistor between the output terminal of the amplifier and ground. The maximum distortion-free voltage gain is 150. The DC-offset voltage of the output signals is controlled by the 60 k-ohm potentiometer between the +10V line and the internal circuitry of the amplifier.

Range compressor:

The range compressor consists of three biased silicon diodes D6, D7, D8 which preferentially attenuate the high-level input signals. Under no-signal conditions the diodes are biased off. The 4.7 k-ohm resistor and the three lower potentiometers form a voltage divider across the output of the operational amplifier. By careful adjustment of the three upper potentiometers in the range compressor, the diodes can be made conducting one after the other for different negative input-signal levels and the large signals are attenuated smoothly rather than being clipped. The three lower potentiometers adjust the amount of attenuation. In this way an output signal of 9V is reduced to 1.5V while the low level signals (about 0.5V) are unaffected.

From the range compressor the signals can be fed either to the Z-modulation (intensity-modulation) circuitry or into the data recorder. Notice that no coupling capacitors

are used at all once the input signals have been detected. This means that the DC level of the output signals can be set so that the signals always deflect from a DC-zero level.

5.3 HARMONIC GENERATOR

The circuit of the 1 MHz harmonic generator for the LF receiver is shown in figure 24. Frequency and time calibration of the receiver is obtained when the harmonic generator is switched on once a minute by a relay (not shown). The harmonics are then displayed as signals separated by 1 MHz intervals along the frequency axis of the receiver output.

The harmonic generator is designed to give as many harmonics of the fundamental frequency of 1 MHz as possible. This is achieved by passing the output of the 1 MHz crystal-controlled oscillator (T14), which has been amplified by T13, into a Schmitt trigger through an emitter follower (T7). The Schmitt trigger contains two high-frequency transistors T8 and T10 with a third transistor T9 connected between the stages to act as a buffer amplifier. The mark-space ratio of the rectangular output waveform of the Schmitt trigger is set by the 1 k-ohm potentiometer connected to the base of T8. The square-wave output of the Schmitt trigger is fed into an operational amplifier which acts as a differentiator. The output from the differentiator is taken through an emitter

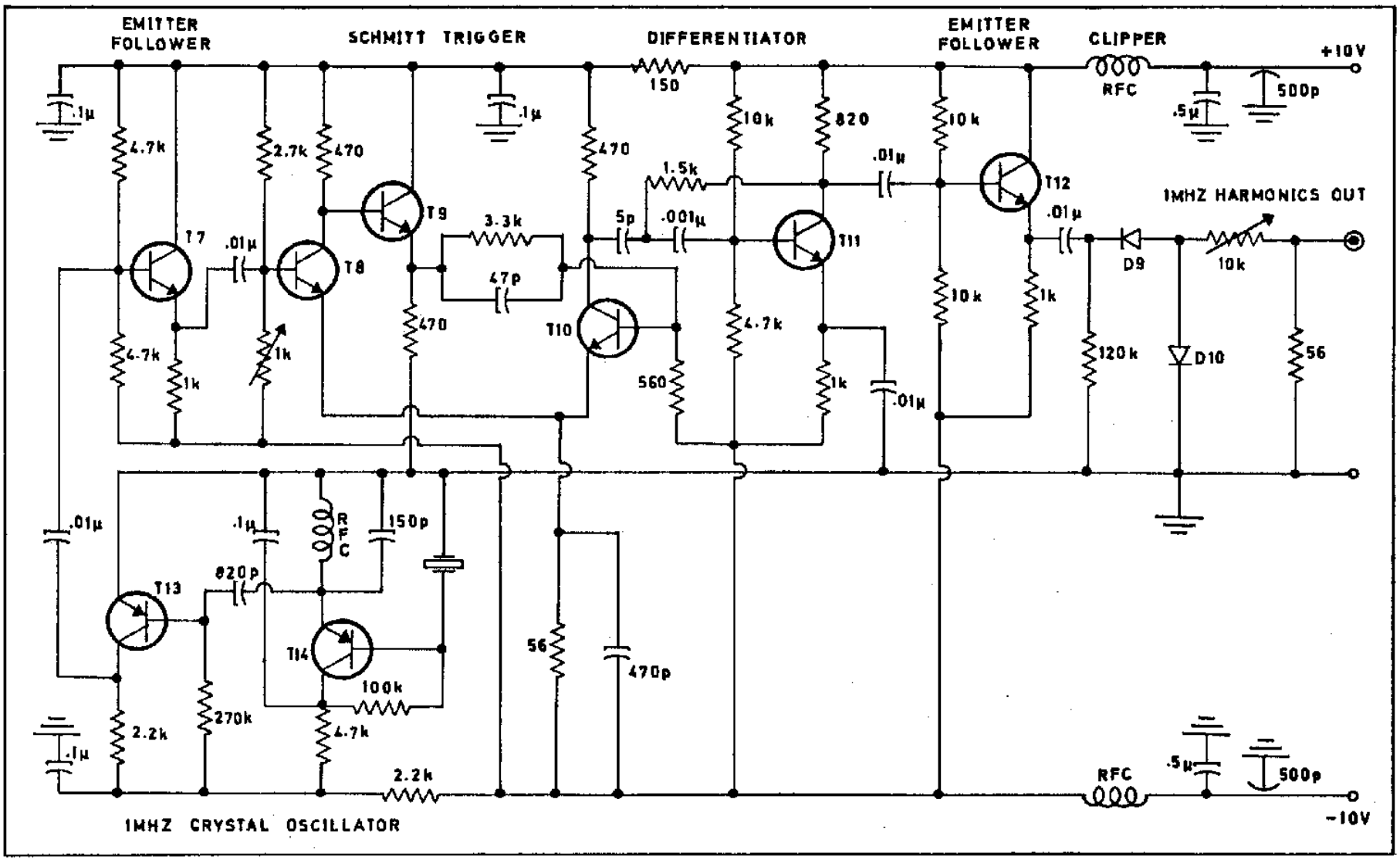

FIG.24. THE 1MHZ HARMONIC GENERATOR.

follower to a clipping circuit to remove the positive spikes. The output of the clipping circuit consists of a series of very sharp nagative-going pulses which contain all the 1 MHz harmonics.

The circuit diagram of the harmonic generator of the HF receiver is identical to the one in figure 24 except that the crystal-controlled oscillator has a frequency of 2,42 MHz.

5.4 TUNING-VOLTAGE AND PULSE GENERATORS

In this section we first describe the 100 millisecond-sweep generator and its associated pulse generator. The pulse fed to the audio amplifier produces a positive-going pulse at the output of the audio amplifier and can be regained to trigger the oscilloscopes when the receiver output is replayed from the data recorder. A method devised to obtain extremely good linearity of the receiver frequency-time output is described. Finally the circuit of the 10 millisecond-sweep generator is presented. As yet we have not operated a receiver for any length of time using the 10 millisecond-sweep, but it is hoped that the sweep will be used during the present observing season.

5.41 100 Millisecond-sweep and pulse generator

The circuit of the 100 millisecond-sweep and pulse generator is shown in figure 25. The basic circuit of the sweep generator is a hybrid timing circuit formed from a

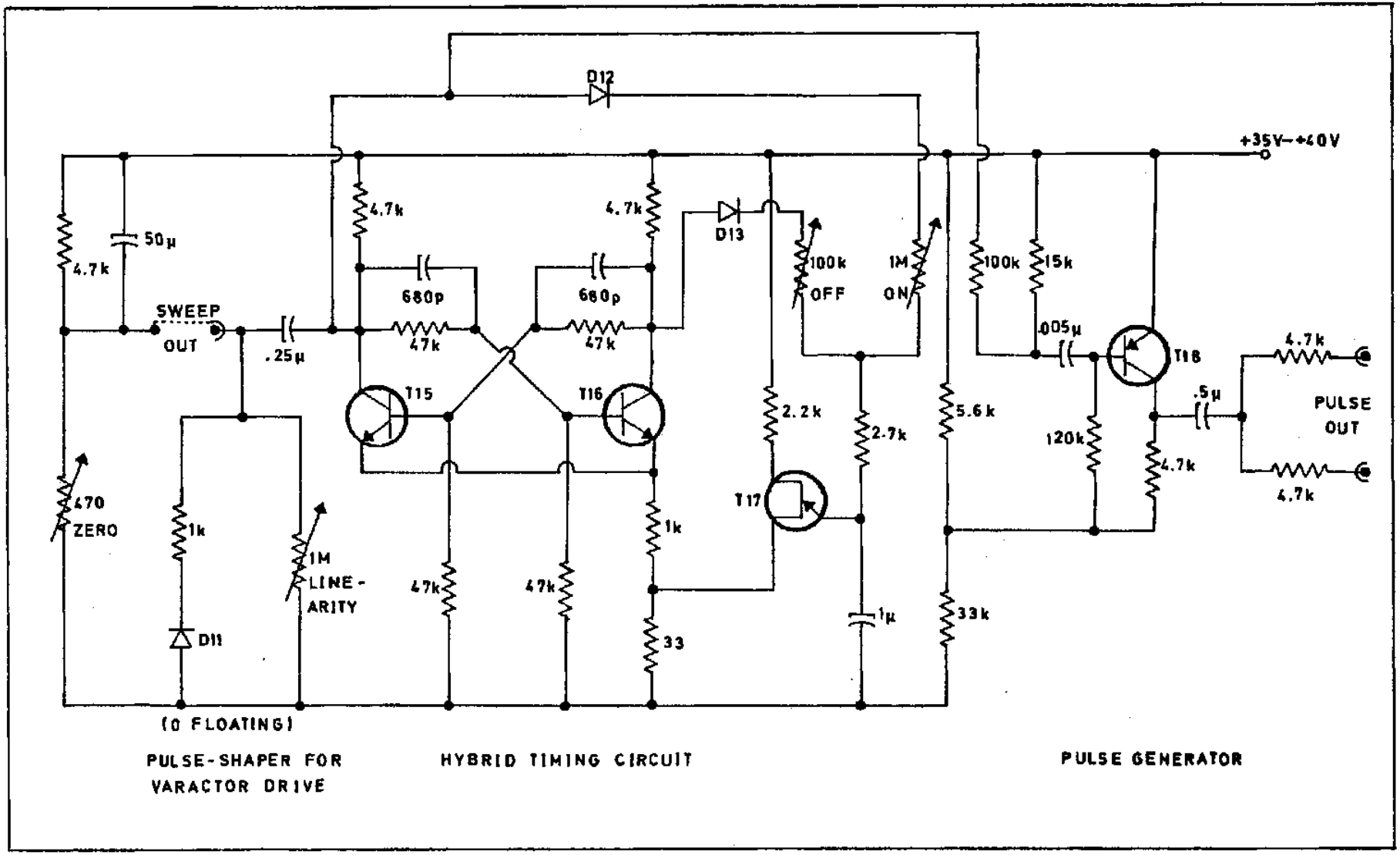

FIG.25. THE 100 m SECOND-SWEEP GENERATOR AND THE PULSE GENERATOR.

conventional bistable multivibrator (T15, T16) with a unijunction transistor T17 performing the timing and triggering functions. Each time the unijunction transistor conducts the discharge current from the 1 microfarad timing capacitor connected to its emitter develops a pulse across the 33 ohm resistor which triggers the bistable multivibrator from one state to the other. The timing capacitor charges through either the 100 k-ohm potentiometer or the 1 megohm potentiometer depending on which one is connected to the more positive collector. The diodes D12 and D13 isolate the other resistor from the timing capacitor. In this way the two parts of the period of the bistable multivibrator can be set independently.

The rectangular-wave output from the collector of T15 is shaped by means of a pulse-shaping network to give the required sweep voltage. The required starting value of the sweep voltage is adjusted by means of the generator power-supply voltage. The "on" time of the sweep is the "off" time of T15 which is set by the 1 megohm potentiometer which is thus labelled "ON". The 100 k-ohm potentiometer sets the time during which no sweep is present and is labelled "OFF". The sweep period was set at a 100 milliseconds and the off-time of the sweep was set at 15 milliseconds.

The pulse is obtained by differentiating the rectangular waveform at the collector of T15 and applying these pulses

to the base of T18 which is usually in the saturated conducting state. When a positive-going pulse is applied to the base of T18, the transistor is turned off and a negative-going pulse appears at its collector. A negative-going pulse at the base of T18 has no effect. Thus a synchronising pulse appears only at the start of the sweep and no pulse occurs during the off-time. The pulse has a duration of about 200 microseconds and this represents a very small fraction of the overall sweep time.

5.42 Receiver linearity

Low-frequency receivers:

The capacitance of the varactor diodes used in the receivers is a non-linear function of the reverse-bias voltage (the sweeping voltage) across the varactor diodes. Similarly the frequency to which the receiver is tuned is not a linear function of the sweep voltage. To obtain a linear frequency-time output for the receiver the curve of reverse bias versus time must duplicate the curve of reverse bias versus frequency (i.e. the linear frequency axis must be replaced by an axis along which time increases linearly).

Fortunately the relationship between reverse bias and frequency is almost exponential. The solid curve in figure 26 shows the measured voltages required to obtain the different frequencies. If we can obtain a voltage which

varies in exactly the same way but with increasing time instead of decreasing frequency, we will have a linear frequency-time variation. Superimposed on the same graph is a dashed curve showing the discharge with time of an RC circuit whose starting voltage has been adjusted to that required for 27 MHz. The time constant has been chosen to be 34 milliseconds so that three time constants will equal 102 milliseconds. As can be seen, the form of the two curves is very similar. There would however still be a detectable non-linearity in the frequency-time variation of the receiver. The linearity was improved by incorporating the reverse biased diode D11 in parallel with a 1 megohm potentiometer, labelled "LINEARITY", which could be used to vary the discharge time of the network. Using this arrangement the frequency-time variation could be made linear within the limits of the oscilloscope display.

It will be noticed that the final bias voltage reached by the sweep is not zero. This is arranged by having a floating power supply for the sweep generator and a 470 ohm potentiometer, labelled "ZERO", which references the sweep-generator voltage to the receiver.

High-frequency receivers:

Figure 27 shows the tuning voltage curve required for varying the frequency of the HF receiver (solid curve). The dashed curve shows how closely this curve can be approximated by an RC discharge network with a time constant of 45

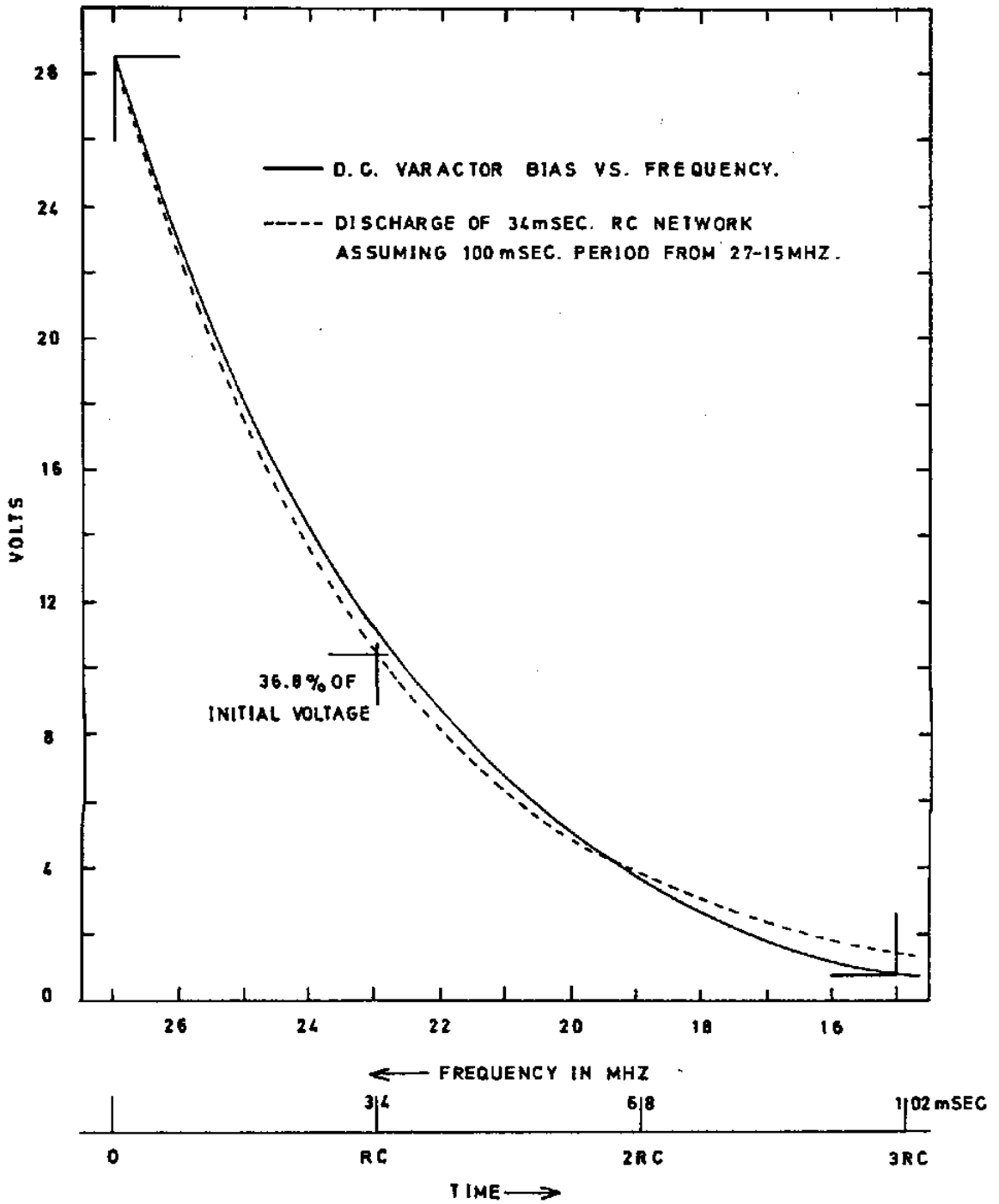

FIG.26. D.C. VARACTOR BIAS VS. RECEIVER RESONANT FREQUENCY AND VOLTAGE VS. TIME FOR RC NETWORK.

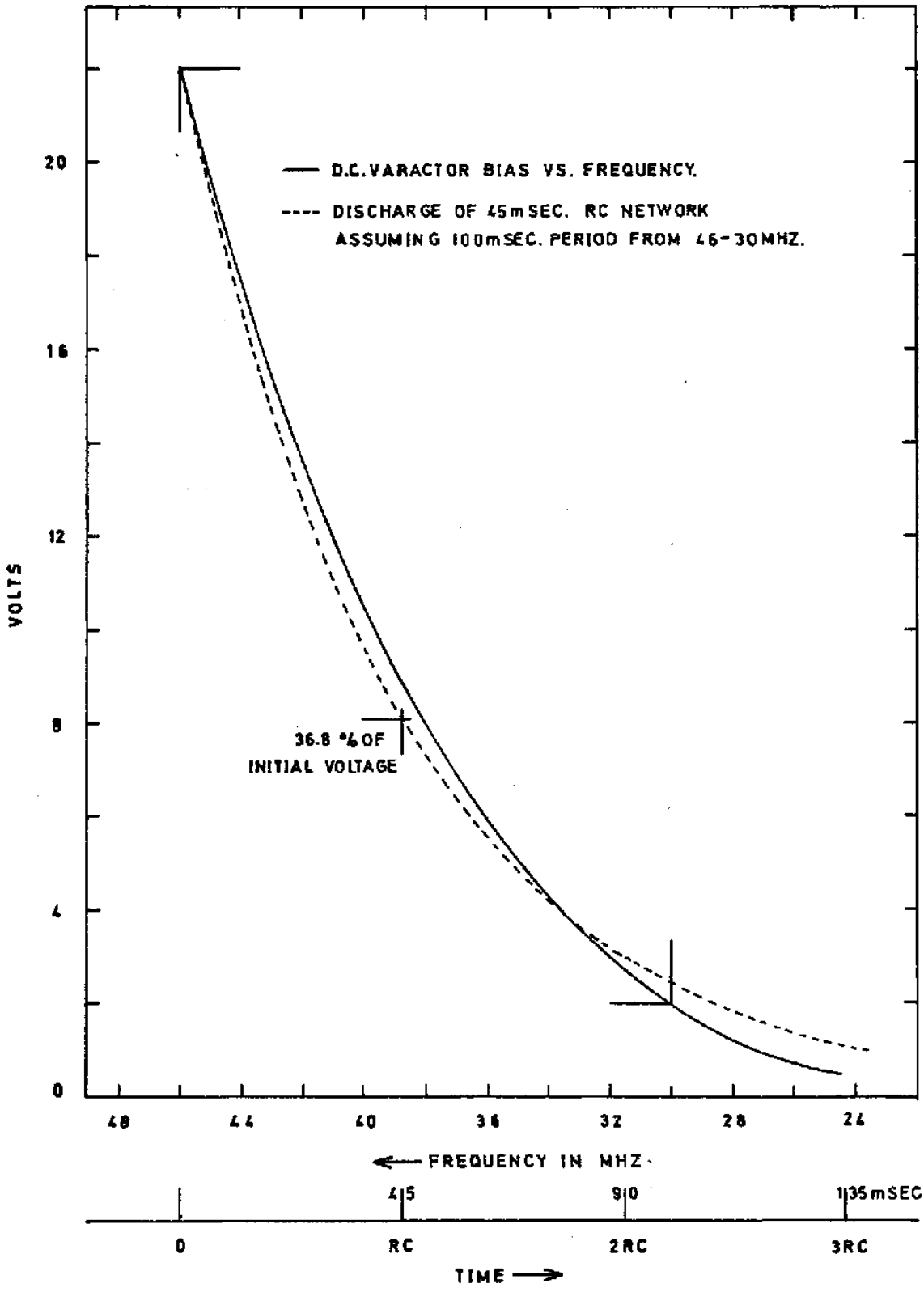

FIG.27. D.C. VARACTOR BIAS VS. RECEIVER RESONANT FREQUENCY AND VOLTAGE VS. TIME FOR RC NETWORK.

milliseconds, assuming a sweep period of 100 milliseconds between 46 and 30 MHz. A comparison of the tuning voltage curves for the LF and HF receivers in figures 26 and 27 shows that the curves are slightly different - they need different starting voltages for the high-frequency ends of the ranges for example. To overcome this difficulty a second sweep generator, identical to the LF sweep generator was built for the HF receiver. This sweep generator is run off a different supply voltage and the zero and linearity controls are used to obtain the best response.

5.43 10 Millisecond-sweep and pulse generator

The 10 millisecond-sweep generator has the same basic circuit as the 100 millisecond-sweep generator and operates in exactly the same way. The only significant differences between the two are the values of the timing components and the linearity potentiometer. The sweep period was set at 10 milliseconds and the off-time was set at 1 millisecond. The circuit diagram is shown in figure 28.

The pulse generator of the 10 millisecond sweep is more complex than that of the 100 millisecond sweep for the following reason. With a sweep repetition period of 11 milliseconds there are about 5,500 sweeps every minute, as compared with about 520 for the 100 millisecond sweep. It would be extremely tedious to pinpoint any particular sweep in time. If every tenth sweep could be missed, identification would be simpler since there would be a blank

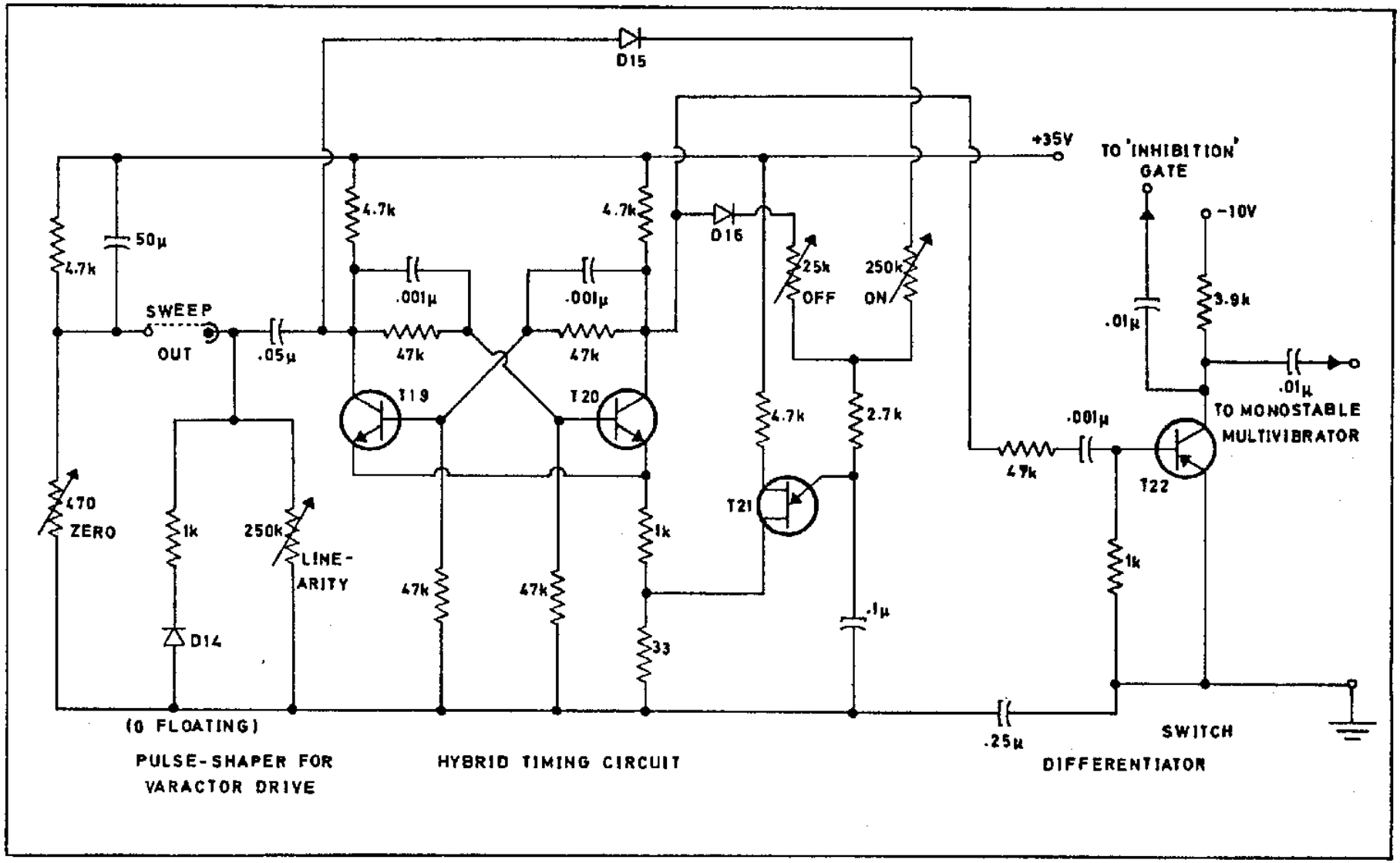

FIG.28. THE 10m SECOND-SWEEP GENERATOR.

trace every 10 traces. Every tenth sweep on the oscilloscope will be missed if every tenth trigger pulse is absent. This is accomplished by the circuitry of figure 29 and the circuitry on the right-hand side of figure 28.

The rectangular wave at the collector of T20 is differentiated to give pulses of about 3 microseconds duration. These pulses are fed to a transistor switch (T22) which gives positive-going pulses at the start of each sweep. The positive-going pulses are fed to an "INHIBITION" gate (T28 and T29) and a monostable multivibrator (T23 and T24). The mark-space ratio of the rectangular wave is set by the 100 k-ohm potentiometer connected to the base of T24. The rectangular wave is fed to a diode-pump decade counter (T26) through an emitter follower (T25). The diode pump gives a positive-going pulse every ten sweeps and this pulse is inverted and fed to the inhibition gate. T29 is usually conducting so that when a positive pulse arrives from the switch it is turned off and gives a negative-going output pulse. Every tenth sweep produces a negative-going pulse at the base of T28 which is then turned on and this inhibits the negative-going pulse which would be produced by T29. Thus every tenth sychronising pulse is missing and every tenth sweep is missed by the oscilloscope.

5.5 DATA DISPLAY SYSTEM

5.51 Data presentation

The data is presented as an intensity-modulated

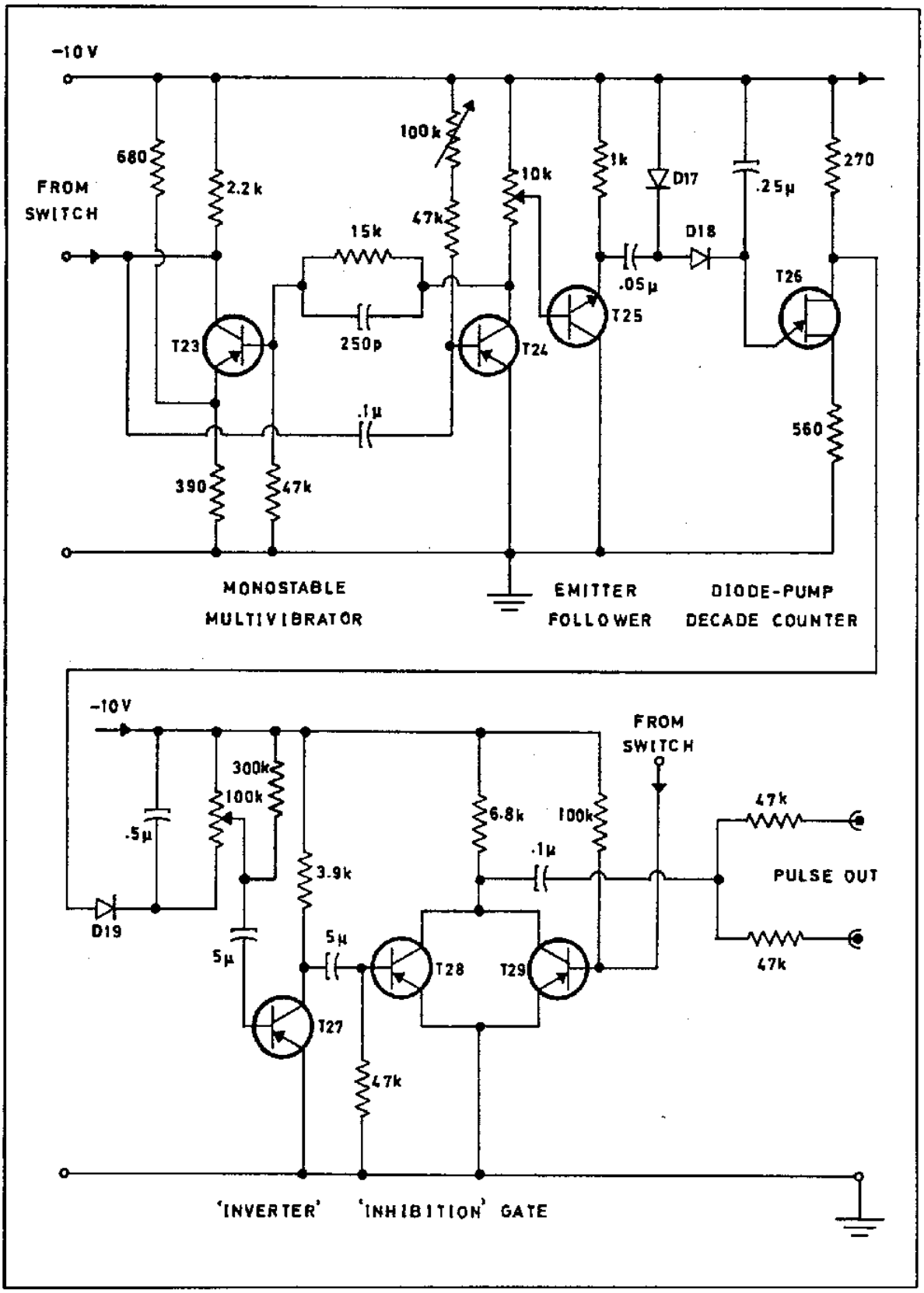

FIG.29. PULSE GENERATOR WITH DECADE COUNTER.
(FOR 10mSECOND SWEEP)

oscilloscope display photographed on 35 mm film. Since there are four receiver output channels, the output signals cannot be processed simultaneously. We decided to record the receiver output signals on a four channel frequency-modulated data recorder (Thermionics Products T3000 Instrumentation recorder) and then to replay the recorded signals when suitable storms had been observed. The two LF receiver outputs were to be displayed side by side and photographed simultaneously . We used a Philips type PM3230 double-beam oscilloscope to obtain two independent traces in the same straight line. This was achieved by switching off the oscilloscope's internal time base and connecting an external time base to the two Y-input sockets of the oscilloscope. The Y-amplifier gain was adjusted by means of the attenuator on the oscilloscope to alter the sweep voltage so as to confine the output signals from either the left- and the right-hand circular channel to half the width of the oscilloscope screen. The external time base was derived from the Tektronix Type 545A oscilloscope synchronised to the receiver sweep by means of the voltage pulse at the start of the sweep. The two traces can thus be photographed simultaneously on a continuously moving film by means of a Philips-Zeiss type PP1021 recording camera. At the observing site the receiver outputs were monitored on a double-beam oscilloscope synchronised to the receiver sweep. The output signals from the left- and right-circular receiver channels were displayed as two traces placed one above the

other and the receiver attenuators could be set to give suitable output signals for the data recorder. The above data display system is depicted by the last four blocks in the centre column of the block diagram of figure 16. The output signals of the HF receivers are displayed in precisely the same way, but there is only one set of photographing equipment. We thus obtain two film strips - one for the LF left- and right-circular channels and one for the HF left- and right-circular channels. These two strips can be aligned to display the total frequency range of the polarimeter.

5.52 Intensity-modulation

The intensity-modulation of the oscilloscope traces presented certain difficulties. The output signals from the receivers are low-frequency waveforms and these are distorted by the 0.01 microfarad internal coupling capacitor in the Z-modulation circuit of the oscilloscope. To overcome this problem a method was used whereby the signal to be applied to the Z-modulation terminal was chopped at a rate of 20 kHz (by this method the trace can be intensity-modulated even by a DC voltage). Figures 30 and 31 show the circuitry used to obtain effective intensity-modulation from the receiver output signals.

The chopper-driving oscillator consists of an emitter-coupled astable multivibrator (T37 and T38) oscillating at

20 kHz. The output from the multivibrator is squared and amplified by T39 and fed to the emitter follower T40. This latter transistor drives T34 which chops the signal at the collector of T33 at 20 kHz. The signal at the collector of T33 is derived from the input signal from the data recorder which is amplified by the DC-amplifier chain T36, T35 and T33. The chopped output signal at the collector of T33 is fed through a 22 k-ohm preset-potentiometer to the Z-modulation driver amplifier. The driver amplifier is capable of delivering a 30V positive swing which is sufficient to intensity-modulate the oscilloscope trace. The 22 k-ohm preset-potentiometer controls the maximum amplitude of the output signals of the driver amplifier. The 150 ohm potentiometer in the base lead of T36 sets the amplitude of the input signal which arrives at the collector of T33. The 220 ohm potentiometer to which the emitter of T33 is attached sets the zero level of the chopped output. Under no input signal conditions the potentiometer is set so that there is no Z-modulation signal at the output of the driver amplifier.

The synchronisation pulse for the Tektronix oscilloscope is derived from the output signals from the data recorder by means of the "AND" gate shown in figure 32. The circuit forms a conventional AND gate, the two arms of the gate consisting of two Darlington pairs of transistors (T41, T42 and T43, T44). Under normal conditions both Darlington pairs

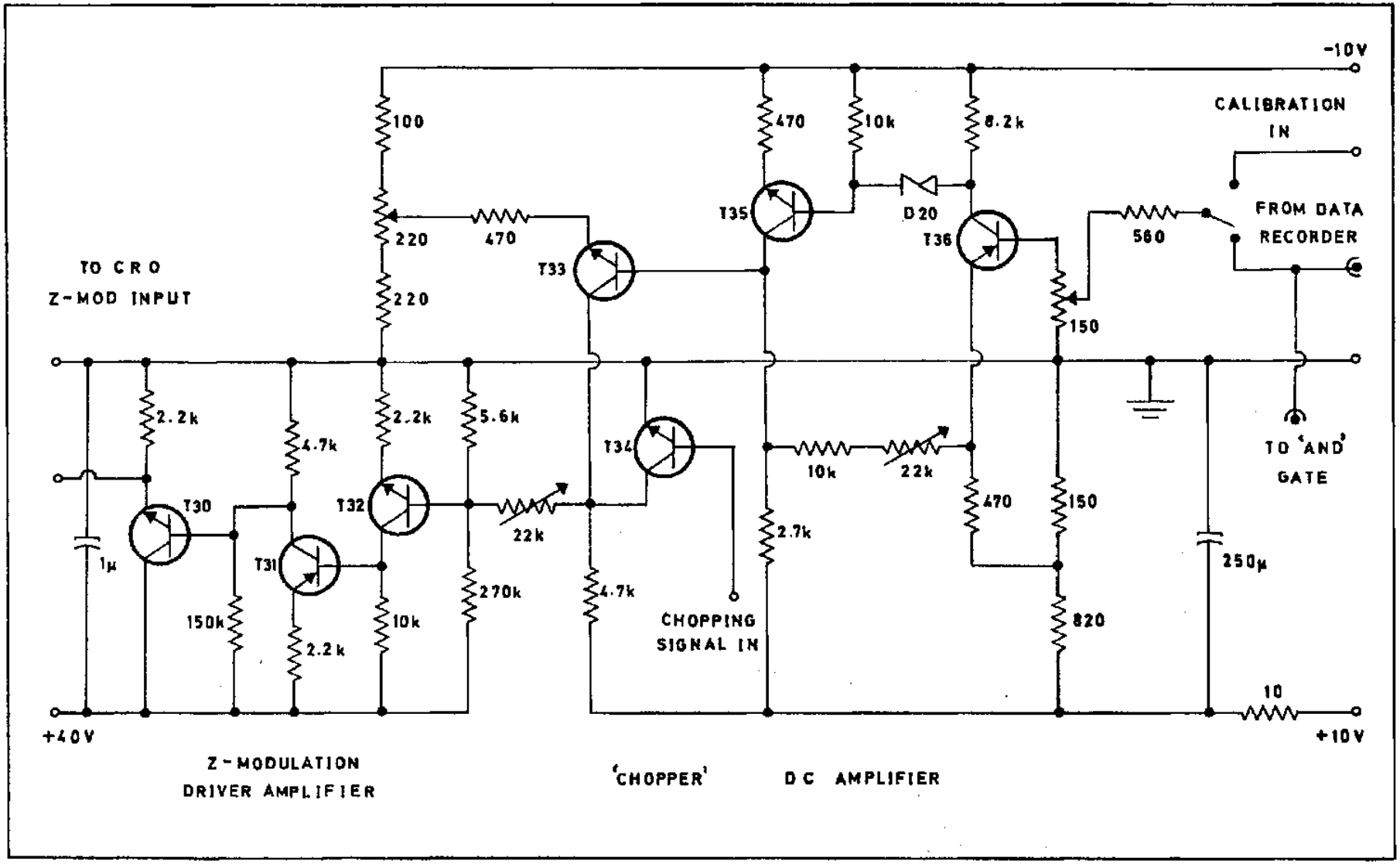

FIG.30. THE Z-MODULATION AND ASSOCIATED CIRCUITRY.

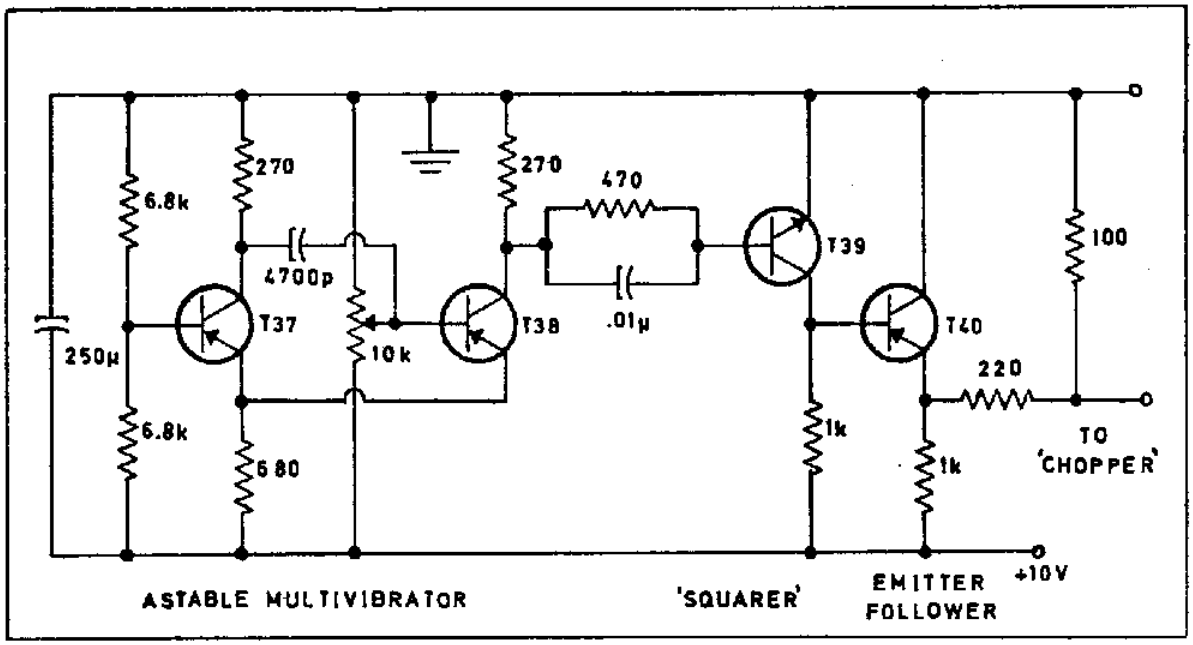

FIG.31. SQUARE WAVE GENERATOR.
(CHOPPING SIGNAL)

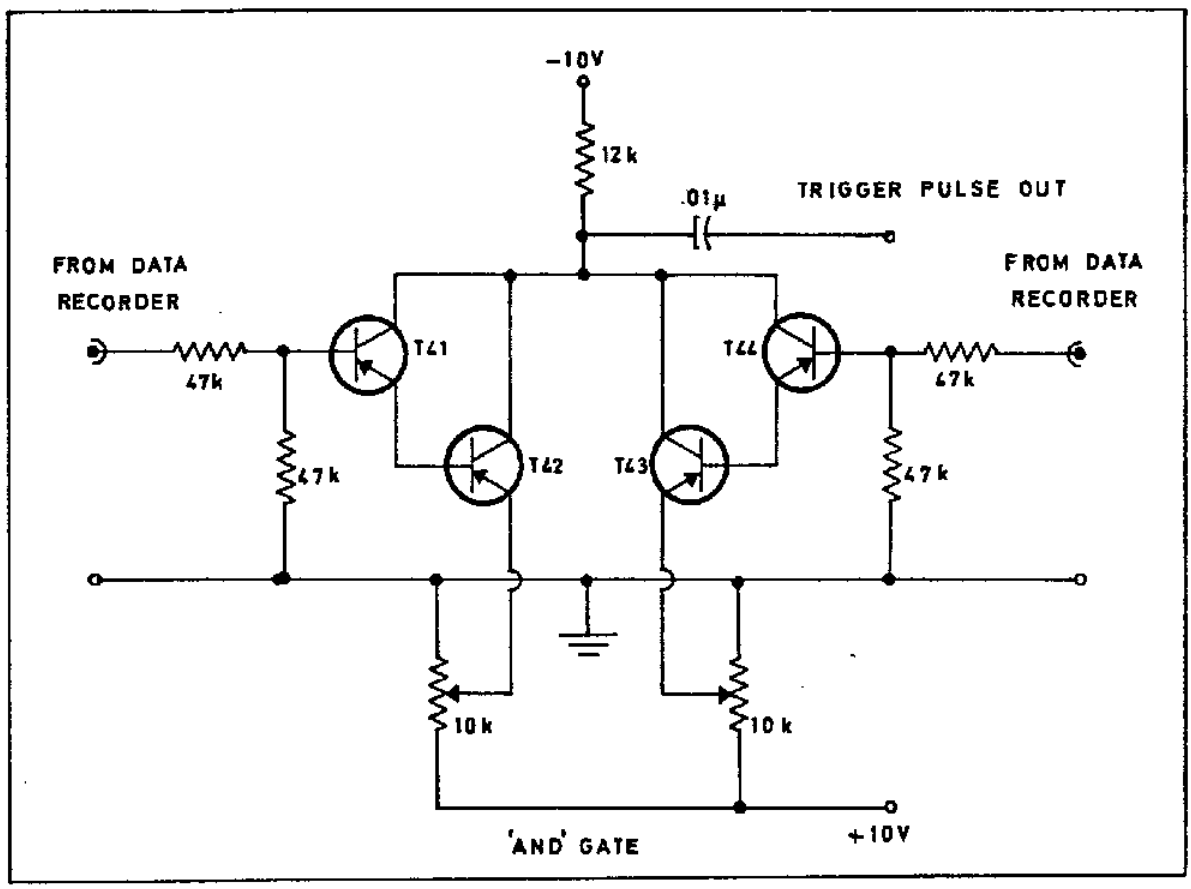

FIG.32. CRO TRIGGER PULSE GENERATOR.

are set in the saturated state by adjusting the 10 k-ohm preset-potentiometers. The Darlington pairs respond only to the positive pulse signal in the data recorder output. If two positive pulses arrive simultaneously at the Darlington pairs, they are both turned off and a negative-going pulse, which can be used to synchronise the oscilloscope, results at the collectors. The arrival of a single positive pulse will not produce an output as one of the pairs will still be in the saturated condition. If only one data recorder output is used (as was usually the case) the one Darlington pair can be turned permanently off by setting its 10 k-Ohm preset-potentiometer to earth. The other Darlington pair then gives an output pulse only for a positive input pulse.

Since two Z-modulation inputs are required to intensity-modulate both the oscilloscope traces, the Z-modulation circuitry has to be duplicated. All the circuitry need not be duplicated, however, only that of figure 30. The new circuit obtains a chopping signal from the squarer in figure 31 through another emitter follower. As the two LF receiver sweeps are made simultaneously at the observing site only one trigger pulse is necessary to synchronise both traces. The Z-modulation apparatus can thus be used to enable the two LF receiver outputs to be filmed simultaneously and then to enable the two HF receiver outputs to be filmed simultaneously. Notice that once the signals from the receiver have been detected

there is no capacitive coupling between any of the stages until the signal enters the Z-modulation circuitry of the oscilloscope. Capacitive coupling is then of no consequence since the signals have been chopped by this stage. The intensity-modulated display should thus give an accurate reproduction of the output signals from the range compressor.

5.53 Staircase calibration

If the amplitudes of the receiver output signals are to be regained from the blackening of the photographic film, the function relating the input amplitude at the Z-modulation terminal and the intensity of the oscilloscope trace must be known. If an input signal with known increments in amplitude (a staircase waveform, for example) is connected to the Z-modulation input terminal of the oscilloscope, we can calibrate the resultant film image densities against the increments of the input waveform. Figure 33 shows the circuit of the staircase calibrator used.

The input pulses to the transistor pump (T46) are supplied by a unijunction-transistor oscillator (T45). The staircase is discharged by the unijunction transistor T47. The staircase output waveform is fed to the input of the Z-modulation DC amplifier through an FET source follower (T48). The 100 k-ohm potentiometer sets the period of the individual steps; the 220 ohm potentiometer sets the amplitudes of the individual steps and the 22 k-ohm potentiometer sets the overall amplitude of the staircase. The functions of

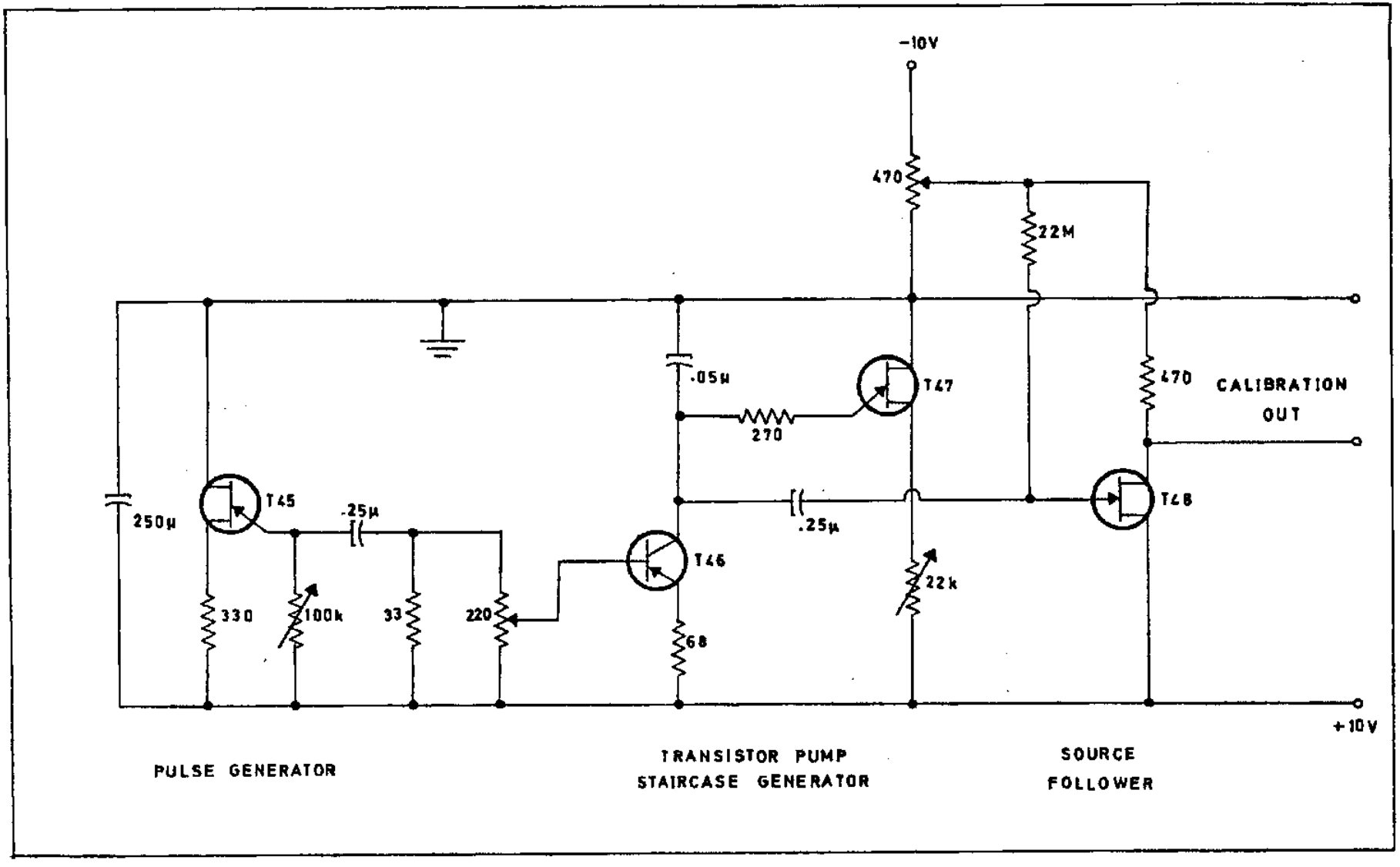

FIG.33. THE STAIRCASE CALIBRATOR FOR THE Z-MODULATION.

the three potentiometers are not independent but by suitable adjustment of all three a staircase waveform with the desired number of steps, period and overall amplitude can be obtained. The DC-zero level at which the negative-going staircase waveform starts is controlled by the 470 ohm potentiometer connected to the negative supply voltage.

The staircase calibration was used to select a photographic film with a dynamic range suitable for recording the intensity-modulated traces. A suitable film is one whose dynamic range is such that the film clearly reproduces the changes in intensity caused by the staircase waveform. The film must just fail to respond to the minimum intensity of the staircase waveform and must just fail to be saturated by the maximum intensity. A large number of commercially available types of film, with speeds varying between 1600 ASA and about 20 ASA, was tested. Kodak Plus-X pan film with a speed of 125 ASA was selected as being the most suitable. Certain waveforms obtained using the staircase calibrator will be displayed at the end of the chapter.

5.6 DEVELOPMENT AND SPECIFICATIONS OF THE SWEPT-FREQUENCY RECEIVERS

Space considerations prohibit a complete description of the development of the swept-frequency receivers and all the problems encountered, hence only the more important stages of the development will be presented. The circuit diagrams which

have already been described are the final circuit diagrams i.e. they are the circuit diagrams of the receivers as they are for the 1969/1970 observing season.

5.61 Development of the receivers

Original low-frequency receiver:

The original swept-frequency receiver for the 15 to 25 MHz frequency range was constructed towards the end of 1967 and was used for Jupiter observations with the horizontally polarized log-periodic dipole antenna during the first half of 1968. This receiver had the following characteristics which were different from those of the receiver which has been described.

1) No high-pass filter was used so that harmonics of strong low-frequency signals caused spurious outputs.

2) The tuning coils had 20 rather than the present 14 turns. The varactor diodes were therefore less effective and a voltage of 55V was needed from the sweep-generator power supply in order to sweep the full frequency range. The voltage across the varactor diodes at the high-frequency end of the range was then 40V and this exceeded the rated maximum reverse bias for the diodes.

3) The harmonics were obtained from an ordinary 1 MHz crystal-controlled oscillator and were fed into the receiver at the radio-frequency pre-amplifier. This meant that the amplitude of the harmonics depended on

the attenuator setting.

4) The receiver used the detector and audio amplifier shown in figure 34. As can be seen from the figure AC coupling is used between the stages. This caused baseline distortion following a large signal and a variation of the overall DC level with the size of the signals being received. These two problems caused difficulties in photographing from an intensity-modulated oscilloscope.

5) The receiver bandwidth was about 400 kHz.

6) The sensitivity was at least three times worse due to the noisiness of the AF 164 transistors which were used for T3 to T6. Also these transistors were not driven hard enough by the base-biasing arrangement.

7) Frequently, when the receiver attenuation was reduced so that small signals could be observed, the data recorder overloaded on the large signals. This led to faulty recording and the loss of records.

Only one spectral record of a Jupiter noise storm was filmed during the first half of 1968. This was due to the insensitivity of the system, terrestrial interference and a malfunction in the data recorder.

Before we proceed to describe how the original LF receiver was improved, we shall give a list of the apparatus developed by other workers. Then we shall list the apparatus constructed by the author in conjunction with other workers

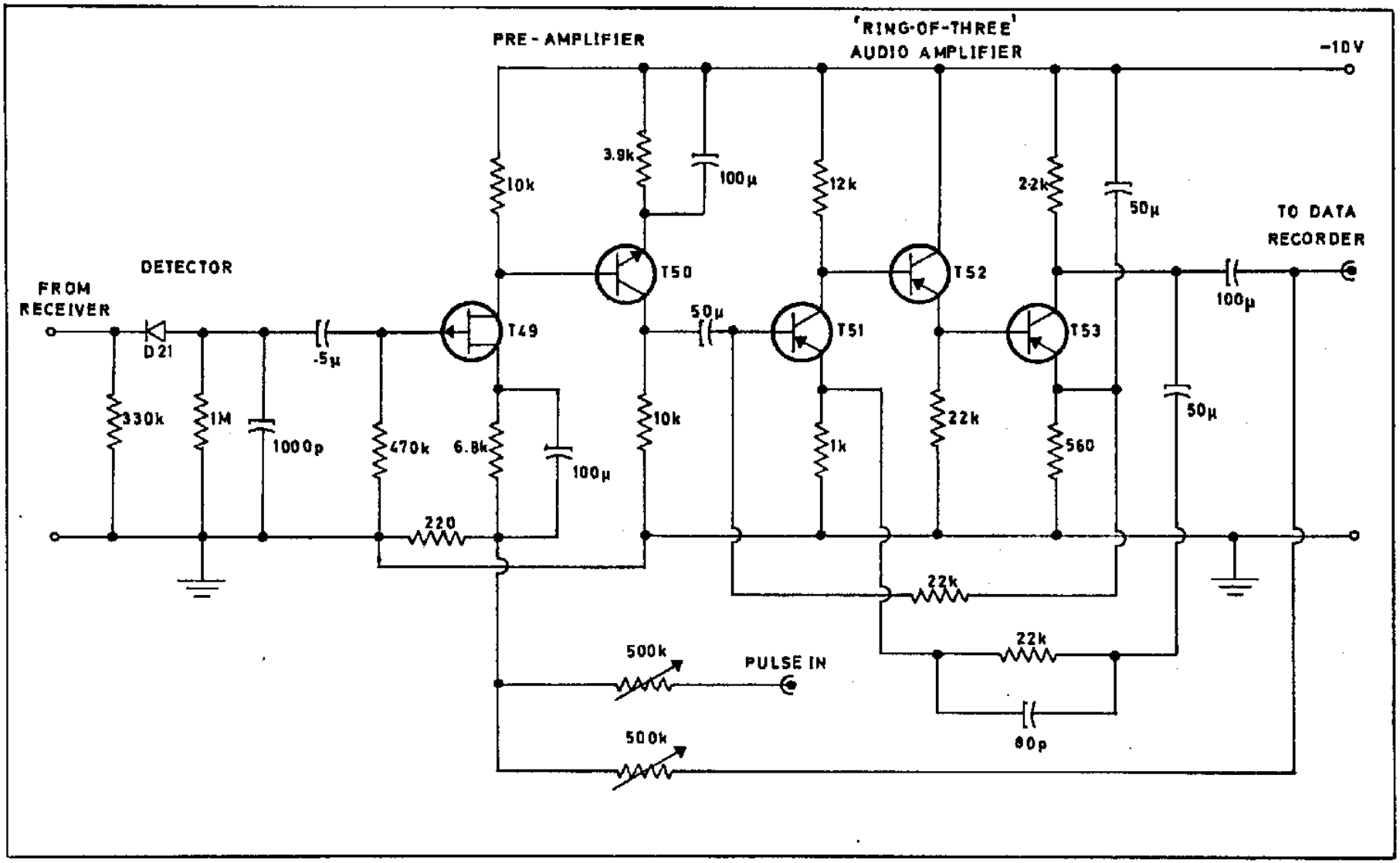

FIG.34. THE ORIGINAL DETECTION AND AUDIO-AMPLIFICATION STAGES.

and finally we list the apparatus designed and constructed solely by the author.

The following apparatus was developed and constructed by other workers:

1) The prototype swept-frequency receiver and the 100 millisecond-sweep generator.
2) The intensity-modulation and film-calibration circuitry.

In conjunction with other workers the author developed:

1) The operational audio amplifier and the range compressor.
2) The 1 MHz harmonic generator.
3) The 10 millisecond-sweep generator and the pulse decade-counter.

All subsequent modifications and the design and construction of the following apparatus were made by the author on his own.

1) The high-pass filters for the 4 receivers.
2) The step-attenuators for the HF receivers.
3) The two HF radio-frequency pre-amplifiers.
4) The 2.42 MHz harmonic generator.
5) The original HF swept-frequency receiver.
6) The final versions of the two LF swept-frequency receivers and the two HF swept-frequency receivers.
7) The additional 100 millisecond-sweep generator for the HF receivers.

An improved low-frequency receiver:

During the middle of 1968, when there were no Jupiter

observations, the LF receiver was modified as follows to overcome most of the problems as numbered previously.

1) A high-pass filter was included to remove spurious outputs.

3) The more refined 1 MHz harmonic generator was devised to give harmonics of almost equal amplitudes which were introduced into the first stage (T3) of the actual receiver, thereby solving the earlier difficulty.

4) The baseline distortion problems were overcome by using the operational audio amplifier which eliminates the coupling capacitors.

5) The receiver was retuned and the bandwidth was reduced to about 300 kHz.

6) The base-biasing resistors of transistors T3 to T6 were changed to drive the transistors harder, thereby giving slightly greater sensitivity.

7) The range compressor was included to reduce the amplitudes of strong signals while leaving the low-level signals unattenuated, thereby solving the data recorder overload problem without losing the low-level signals.

This receiver was used with the log-periodic dipole antenna to observe Jupiter in the 15 to 26 MHz range. Between December 1968 and the end of April 1969 many storms were recorded although some storms were again lost because of a different malfunction in the data recorder.

The first high-frequency receiver:

In November 1968 a HF receiver similar to the newly-modified LF receiver was constructed and operated with the right-handed circularly polarized helical antenna in the 30 to 45 MHz frequency range until April 1969. The receiver had the following characteristics which were different from the final HF receiver.

1) The receiver used a commercial radio-frequency pre-amplifier initially, but it was soon found that the response of the commercial amplifier fell off too rapidly above 30 MHz for it to be suitable. A radio-frequency pre-amplifier was then designed to give a flat overall response in the 30 to 45 MHz range.

2) The receiver used three tuning stages and the response of the output of the receiver fell off at the high frequency end of the range.

3) The receiver used the same sweep-generator voltage as the LF receiver and it was found that the receiver tuned from about 47 MHz to about 28 MHz if the LF receiver tuned its proper range.

4) The bandwidth was about 450 kHz.

5) The receiver was about 4 times less sensitive than the final receiver.

That only very few storms were recorded with this system can be attributed to the reduction in system sensitivity due to antenna mismatching and to high-voltage powerline inter-

ference which was present on the HF receiver for 80% of all observing nights.

5.62 The final receiver system

As soon as the HF helical antennas had proved successful we decided to complete the polarimeter for the 15 to 45 MHz range as quickly as possible. Unfortunately an aluminium shortage delayed the construction of the two helical antennas for the 15 to 26 MHz range until June 1969, near the end of the observing season. Observations were continued with the log-periodic dipole antenna and the HF right-handed helix until the end of April when the receivers were reconstructed and the additional receivers needed to complete the polarimeter were also constructed.

Latest modifications to the LF receiver:

The latest modifications overcame the remaining shortcomings of the original LF swept-frequency receiver as listed.

2) By reducing the number of turns on the coils of the resonant circuits to 14 turns, the upper frequency limit of the receiver can be obtained with a sweep-generator supply voltage of 38.5V. The reverse bias across the varactor diodes is now only 28.5V at 27 MHz which is below the rated maximum reverse bias voltage.

5) Optimum tracking was obtained by selecting the best-matched varactor diodes in the way described in subsection 5.23. This modification narrowed the band-

width to about 200 kHz.

6) The sensitivity was improved by replacing the AF 164 transistors (T3 to T6 in the receiver) with AF 124 transistors since these have lower noise figures, higher current gains and higher cut-off frequencies.

Once this receiver had been tested, a second receiver for the 15 to 26 MHz range was constructed to be as similar to the first as possible. When the receivers were tuned by the same sweep generator, it was found that they tuned over slightly different ranges, the chief difference being at the low-frequency ends. Separate zero controls for the sweeps of the two receivers cannot be used since the sweep terminals attached to the zero controls must all be connected to the 10V negative supply line. The problem was solved by connecting a second pulse-shaping circuit through another 0.25 microfarad capacitor to the collector of T15 in figure 25. By setting the linearities of the two sweeps independently, the 15 MHz low-frequency limit of the receivers can be swept simultaneously. When the low-frequency ends of the receivers are aligned the high-frequency ends differ by less than 200 kHz. The specifications of the two receivers are summarised in table 2.

	Left-hand receiver	Right-hand receiver
sweep period	100 msecs	100 msecs
receiver bandwidth	200 kHz	220 kHz
detection time constant	1 msec	1 msec
voltage sensitivity	0.6 μV	1.0 μV
response across the band	2½ to 1	2½ to 1

Table 2: LF receiver specifications.

The receivers are made more sensitive at their high-frequency ends than at their low-frequency ends to compensate for the smaller sky noise at the higher frequencies. The response is measured for the same input signal at both ends of the band. The voltage sensitivity is the minimum input voltage, at the low-frequency end of the band, which can be detected above the receiver background noise. The left-hand receiver has been made about twice as sensitive as the right-hand receiver since the co-axial cable to its antenna is almost twice as long as that to the antenna of the right-hand receiver.

If we assume that the antennas are perfectly efficient the above voltage sensitivity would give a flux sensitivity at the midband of 2.8×10^{-22} jansky. This is obtained from the formula

$$\text{Minimum flux density} = \frac{4V^2}{R} \frac{1}{A} \frac{1}{B} \text{ in } \frac{\text{watts}}{m^2} \frac{1}{\text{Hz}} \quad (5.1)$$

where V = minimum detectable voltage at 20 MHz,
= 0.5 microvolt

R = input impedance of the receiver;
= 75 ohms

A = maximum effective aperture of the LF helix at 20 MHz as obtained from the last graph in figure 14,
= 240 m^2

B = receiver bandwidth,
= 200 kHz

and the factor of 4 allows for the losses in the matching networks.

This is a conservative estimate of the sensitivity of the system since it makes no allowance for the increase in sensitivity due to sweep repetition. A small signal can be distinguished from noise since it will appear at the same place on successive sweeps. Our system is therefore slightly more sensitive than the Boulder spectrograph (sensitivity between 4 and 5×10^{-22} jansky) and Riihimaa's apparatus (sensitivity

4×10^{-22} jansky), and about 1/10 as sensitive as the Arecibo polarimeter (sensitivity 0.245×10^{-22} jansky). This last comparison is surprising when the size of the Arecibo reflector is considered, but our system has larger bandwidth and integration time constant. Presumably when the 10-millisecond sweep is used with our receiver, the reduction in time constant will yield smaller voltage sensitivity.

Latest modifications to the HF receiver:

The latest modifications to the HF receiver were the inclusion of a specially designed radio-frequency pre-amplifier and four rather than three tuned stages. These two modifications solved the difficulties numbered (1), (2), (4) and (5) for the first high-frequency receiver. The response of the tuning stages of the HF receivers was found to be about 1 to 4 across the band i.e. an output signal at 45 MHz was four times smaller than the output signal at 30 MHz for the same input signal. This problem was overcome by designing radio-frequency pre-amplifiers with a 4 to 1 response across the frequency band (see figure 21). The pre-amplifiers plus tuning stages then have a response of about 1 to 1 across the band. Problem number (3) was overcome by using separate sweep generators for the HF and LF receivers. By using separate linearity controls on the sweep generators of the HF receivers both receivers are made to sweep through the 30 MHz low-frequency limit simultaneously. For this arrangement the upper limits of the receivers are separated by less than 300 kHz.

The specifications of the two receivers are summarised in table 3.

	Left-hand receiver	Right-hand receiver
sweep period	100 msecs	100 msecs
receiver bandwidth	350 kHz	360 kHz
detection time constant	1 msec	1 msec
voltage sensitivity	0.2 μV	0.2 μV
response across the band	1 to 1	1 to 1

Table 3: HF receiver specifications

If we assume that the antennas are perfectly efficient the above voltage sensitivity would give a flux sensitivity at the midband of 0.7×10^{-22} jansky. The values of the quantities in equation (5.1) are as follows :-

V = 0.2 microvolts at 37.5 MHz

R = 75 ohms

A = 88 m^2 as obtained at 37.5 MHz from

the last graph in figure 11

B = 350 kHz

It will be noticed that the HF receiving system is about 4 times more sensitive than the LF system. This is necessary because of the decreasing power of the Jupiter bursts with increasing frequency.

The final Z-modulation circuitry:

The Z-modulation circuitry of figures 30 and 33 was devised in September 1969, to replace the earlier circuitry which also used the chopping principle. The earlier circuitry was less flexible since the input signal attenuators and Z-modulation level controls could not be set independently. The Z-modulation driver amplifier consisted of three 100V transistors in cascade. This system was run off a 300V supply and could give an output swing of 200V which was sufficient to Z-modulate the trace of the Tektronix 545A oscilloscope. The larger voltages required and the distortion introduced by the high amplification made this system undesirable.

5.7 SELECTED WAVEFORMS

In this section we present certain waveforms which illustrate some of the earlier discussions. Time increases from left to right across all the plates and approximate voltages have been indicated on some of the plates. In those plates which display output signals from two receivers, the

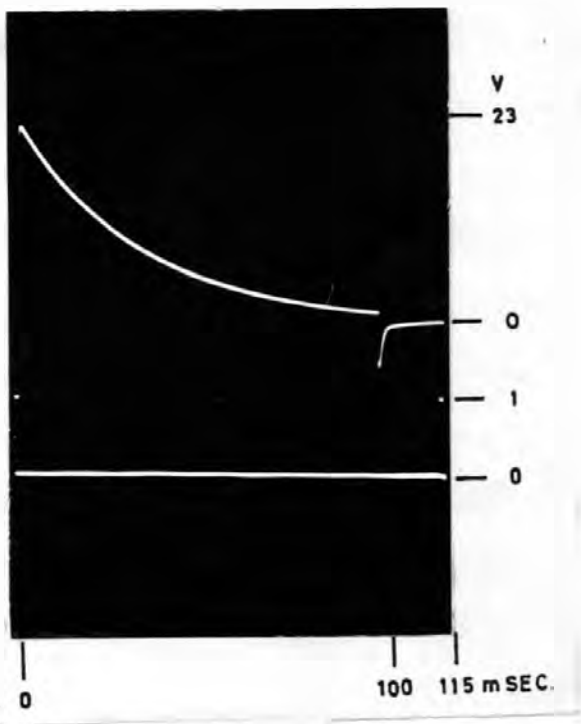

Plate 9.

upper trace is always the output signal from the right-hand receiver channel.

5.71 Receiver waveforms

The upper trace in plate 9 shows the LF sweep-generator output. The 26 MHz end of the sweep is at the left of the plate. The lower trace shows the right-hand receiver output with no input signal. The rise-time of the pulse is too fast to permit the pulse to be displayed but the top of the pulse is visible at the start of the sweep (the amplitude of the pulse is about 1V in all plates). Notice that there is no pulse at the point where the sweep ends and no baseline distortion due to the pulse.

Plate 10 shows the output from the LF receivers when the 1MHz harmonics are injected at the input. The receivers have almost identical frequency axes and the frequency-time linearity is good. The negative-going pulses give rise to intense spots on the intensity-modulated trace and appear as black dots on the film. Plate 11 shows the output of the HF receivers when the 2.42 MHz harmonics are applied at the input.

The effect of the range compressor is illustrated by plates 12 and 13. Plate 12 shows the effect of the range compressor on a signal from a radio-frequency generator. The output signal before the range compressor is shown by the lower trace; the final output signal is attenuated from about 7V to 1.2V. Plate 13 shows the effect of the range compressor on signals from the antenna. The signals are

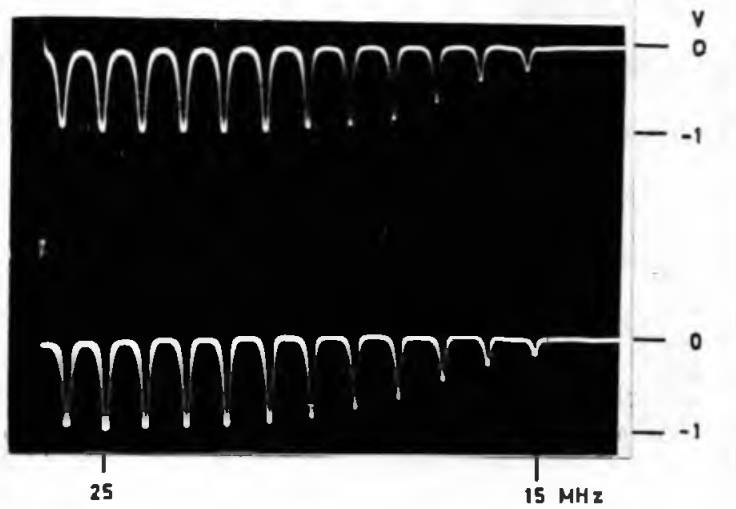

Plate 10.

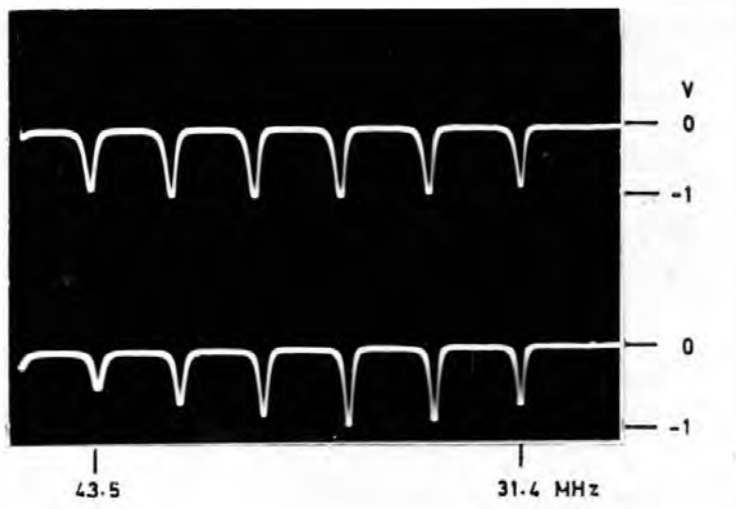

Plate 11.

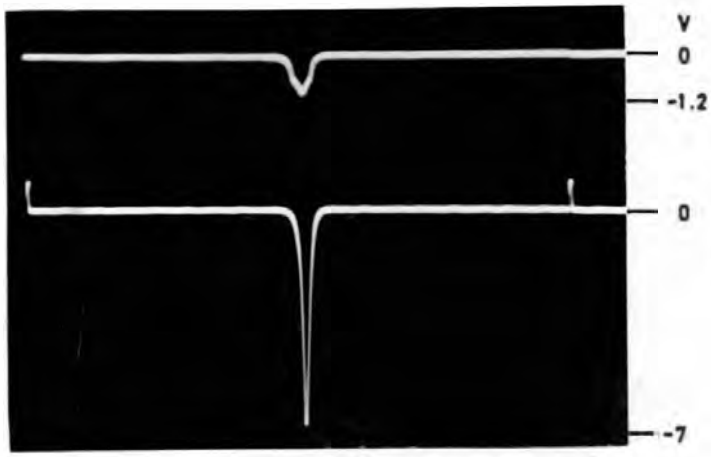

PLATE 12.

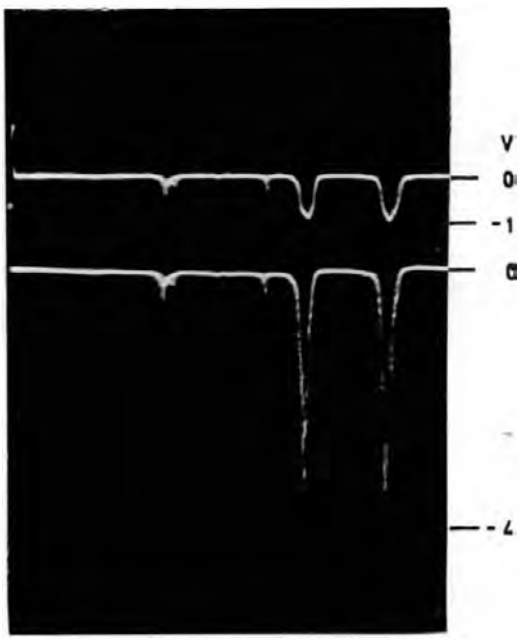

PLATE 13.

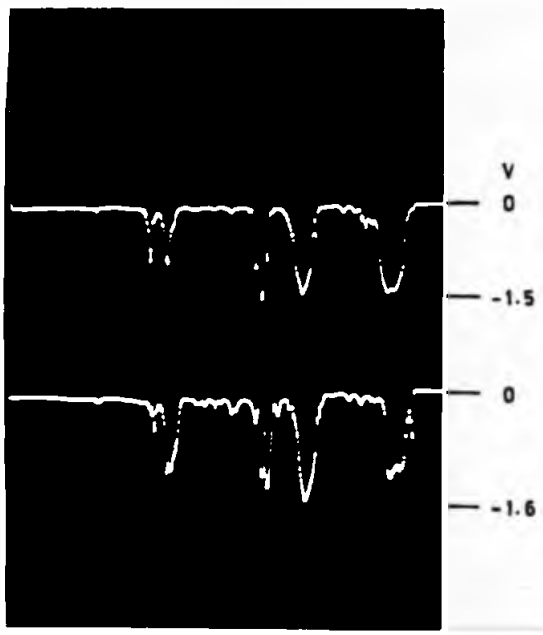

Plate 14.

terrestrial radio stations and fluctuate continuously in amplitude. Notice how the two large signals on the right-hand side of the plate have been reduced from about 4V to 1V while the two low-level signals are almost unaffected.

Finally plate 14 shows the outputs of the left- and right-circular receivers with their attenuators set to the same values. The amplitudes of the signals are fairly well matched although the left-hand receiver channel seems to be slightly more sensitive.

5.72 Intensity calibration

The output from the staircase generator is shown by the upper trace in plate 15. The steps start at -0.5V and climb to 0V. The lower trace shows the output waveform from the Z-modulation driver amplifier; the steps start at +25V and decrease to zero. Note that the output is positive for a negative staircase input signal, thereby brightening the trace for negative input signals. The DC level of the final output step from the Z-modulation amplifier has been adjusted to zero. This step corresponds to no-signal input level and no brightening of the trace occurs. The lower staircase has been chopped at 20 kHz but this is not visible on this time scale. The chopping is shown in plate 16 which has an expanded time scale. Plate 17 is a portion of a calibration film of a trace that has been intensity-modulated by the chopped staircase. There are six scales of brightness corresponding to the six amplitude levels of the staircase. The zero level of the

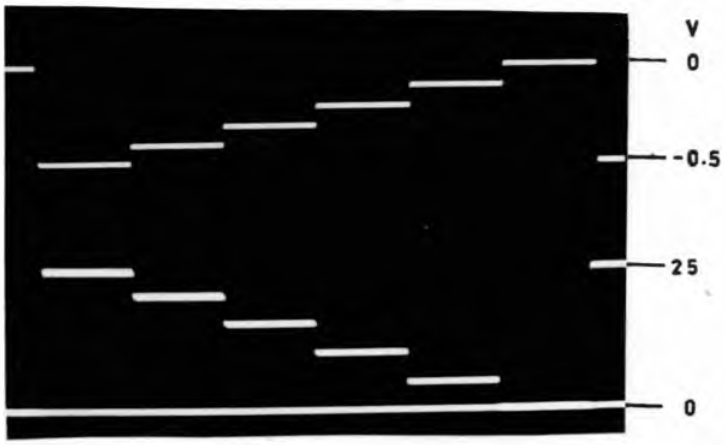

PLATE 15

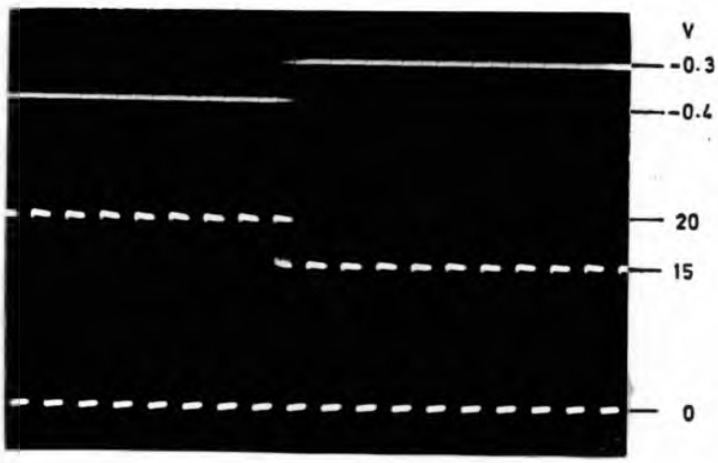

PLATE 16

PLATE 17

staircase has not blackened the film at all and the subsequent levels all give increasing blackening of the film. There is still a detectable difference in the blackness of the last two steps and the film has probably not been saturated by the last step. This film is suitable for recording the data.

Complete list of semiconductor devices and inductances used throughout the circuit diagrams appearing in figures 21 through 34.

Transistors, FET and unijunction transistors:

NO.	TYPE NO.	NO.	TYPE NO.
T1, T2	2N5180	T28,T29	OC70
T3,T4,T5,T6	AF 124	T31	AF118
T7	XK532	T34	2N338
T8,T9,T10, T11,T12	2N916	T35	2N5189
T13,T14,T37 T38,T40	AF164	T36,T46	BFY64
T15,T16,T19, T20,T30,T32, T33	BF114	T41,T42,T43, T44	Unlabelled silicon PNP transistors
T17	2N1671	T48	2N3819
T21,T26,T45, T47	TIS43	T49	2N3820
T18,T22,T23, T24,T27,T52, T53	AC134	T50	2N388
T25,T39	ASY28	T51	OC44

Semiconductor diodes :

NO.	TYPE NO.
D1, D2, D3	BA101
D4, D5, D9, D10	AA123
D6, D7, D8	BY100
D11, D12, D13, D14, D15, D16	OA85
D17, D18, D19, D21	AA121
D20	OAZ208

Inductances:

NO.	SPECIFICATION
L1	2.5 microhenries
L2	16 turns no 24 SWG copper wire on a 0.6 cm former

Low-frequency receiver inductances.

L3 = 30 turns no. 24 SWG copper wire on a 1 cm former

L4 = L6 = L8 = 14 turns no. 24 SWG copper wire on a 1 cm former tapped 4 turns from collector end.

L5 = L7 = 1 turn insulated wire

High-frequency receiver inductances.

L3' = 24 turns no. 24 SWG copper wire on a 1 cm former

L4' = L6' = L8' = L10' = 7 turns no. 20SWG copper wire on a 1 cm former tapped $2\frac{1}{2}$ turns from collector end.

L5' = L7' = L9' = 1 turn insulated wire.

CHAPTER VI

RESULTS AND FURTHER PROPOSALS

The purpose of this project was to construct a swept-frequency polarimeter for the range from 15 to 45 MHz with sufficient sensitivity to detect Jupiter's decametric radiation. The polarimeter is now complete and operating on a routine basis during the apparition of Jupiter starting in December 1969. Unfortunately no records are as yet available from the complete system but many records were obtained using the LF receiver, before its final modification, and the LPD antenna. These records show that the system is sufficiently sensitive to accomplish its object. Examples of these records will be presented but a general analysis of the results will not be attempted as data is still being acquired and such an analysis would go beyond the scope of this project. One storm, however, will be analysed in some detail as it shows an interesting record of Faraday rotation on the bursts from Jupiter.

It is not possible to present original records of the storms; photographic prints have, however, been made of selected portions of some of the records. Storms generally lasted for about one hour and the sections displayed here are all of about 20 minutes duration. The photographic prints are made from intermediate negatives taken of the original records, so that the prints display signals in the same way as the original records. Blackening of the

prints thus corresponds to signals in the output of the receiver. These prints, produced by additional processing from the original records, do not show all the fine details in the original records nor do they have the same range in image contrast.

In all the spectra presented the frequency axis runs across the width of the film, the high frequency end of the range being at the top, and the time axis runs along the length of the film from left to right. The date and the time at which the storm occurred as well as the frequency scale are shown with each portion of record. The central meridian longitude (CML) of Jupiter and Io's departure from superior geocentric conjunction (SGC) as quoted in the text refer to the time in the middle of the displayed portion.

6.1 SELECTED SPECTRA

(1) Plate 18 shows a spectral record of a Jupiter noise storm. Before we describe the spectral features in the record, we will point out some general features. The equally-spaced black dots occurring at 1 MHz intervals along the frequency axis are the 1 MHz harmonics from the harmonic generator. The black lines at 2126 and 2134 U.T. are caused by a negative DC voltage which was applied to the data recorder input at the observing site. This DC voltage was used to mark the record at times which were noted. These DC markers facilitate the locating of a

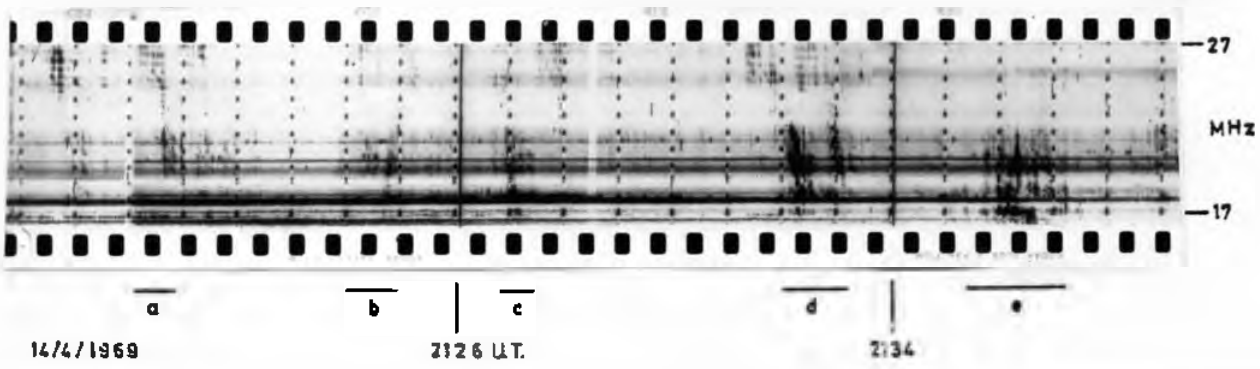

Plate 18. Spectral record of B source emission, 14/4/1969.

particular minute on the photographic records. Terrestrial radio stations appear as black lanes which are constant in frequency along the length of the film (e.g. at 18 MHz). The relative increase in the blackening of the record at 2120 U.T. is caused by a decrease in the attenuation at the input of the receiver brought about by the operator.

This is a record of Io-related emission from the B source region since Jupiter's CML was 154^{o} and Io's departure from SGC was 92^{o} at the time of emission. The portions of the record labelled a,b and c show some Jupiter activity in the range from 18 to 22 MHz while the portions d and e show intense short bursts in the 17 to 23 MHz range. The storm consists of normal bursts accompanied by intense millisecond bursts (these millisecond bursts are often referred to as "spitting"). Although the spitting is not resolved on this record it can be studied by speeding up the camera, as will be shown later. Broadband bursts are present for most of the record between 24 MHz and the upper frequency limit of the receiver. The broadband bursts appear as alternate light and dark bands running parallel to the time axis. The light bands are caused by Faraday rotation on the bursts; we shall return to this point later.

(2) Plate 19 shows a C source storm with very rapid spitting and having slow negative frequency drifts. The drifts appear as a movement to lower frequencies over a period of minutes of the regions of intense activity. Jupiter's CML is 359^{o}

and Io's departure from SGC is 247°. The faint grey bands parallel to the time axis at about 25 MHz and between 19 and 22 MHz are positions at which the receiving system is relatively more sensitive. The grey bands are then a record of the sky background noise. The apparent increase in sensitivity is caused by the fact that the receiver and the antenna are more closely matched in these regions than in adjacent regions. There is almost no terrestrial inter-ference and intense activity (mainly spitting) is present in the portions labelled a,b,c and d. There does not appear to be any marked Faraday rotation on the emission and this means that the bursts are almost circularly polarized. The record does not indicate the sense of polarization. However, fixed-frequency observations made at the same time indicate that the bursts are predominantly right-handed polarized. Plate 20 shows the portion marked XY on an expanded time scale. The black "blobs" in the region XY are resolved into individual short bursts on the negative. The short bursts do, however, still overlap to some extent due to the blooming of the oscilloscope spot. Notice that successive sweeps of the receiver are clearly visible. The frequency marker at 19 MHz appears to be a double marker. The marker at about 19.3 MHz is the 8th harmonic of the 2.42 MHz harmonic generator output and is useful for determining the frequency range of the receiver as this is sometimes altered by means of the "zero" control on the sweep generator to eliminate stations.

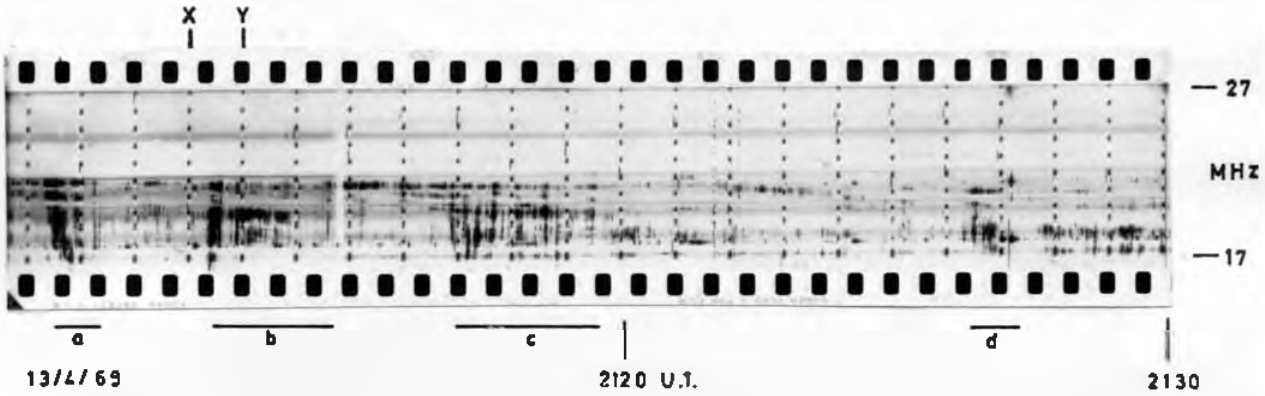

Plate 19. Spectral record of C source emission, 13/4/1969.

Plate 20. Expanded portion of the record of 13/4/1969.

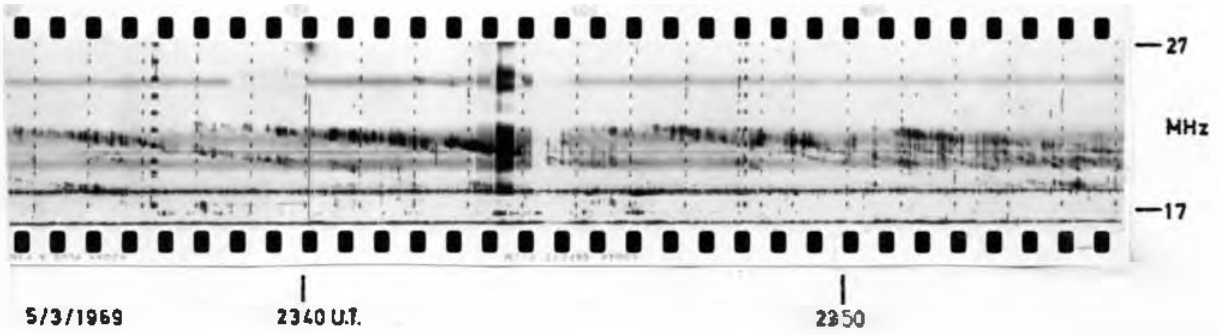

Plate 21. Spectral record of C source emission, 5/3/1969.

(3) Plate 21 shows another C source storm with Jupiter's CML at 332° and Io's departure from SGC at 247°. The vertical black marks between 2343 and 2344 U.T. are caused by a mal-function of the data recorder (a negative shift in the output DC-level of the data recorder brightens the oscilloscope trace). In some parts of the record frequency markers appear in between the normal markers spaced at one minute intervals. These occur when the relay, which switches on the harmonic generator, is closed manually so that the amplitude of the markers can be adjusted. The storm again consists of normal bursts with some spitting. The most interesting feature is the presence of negatively-drifting bands of emission. The emission is about 1 MHz in bandwidth and drifts downwards in frequency at a rate of about 400 kHz/min.

(4) Plate 22 shows one of the few storms observed with the HF receiver, before its final modification, and the right-handed circular helix antenna. This storm was recorded before the helix was matched to the co-axial transmission line. The longitudinal grey streaks correspond to minima in the standing-wave ratio versus frequency curve since the system is relatively more sensitive at these points. The helix has since been matched to the co-axial transmission line and the "bumps" in the sky-noise pattern at the receiver output have been removed. The fact that storms were observed with the less sensitive system indicates that storms should be

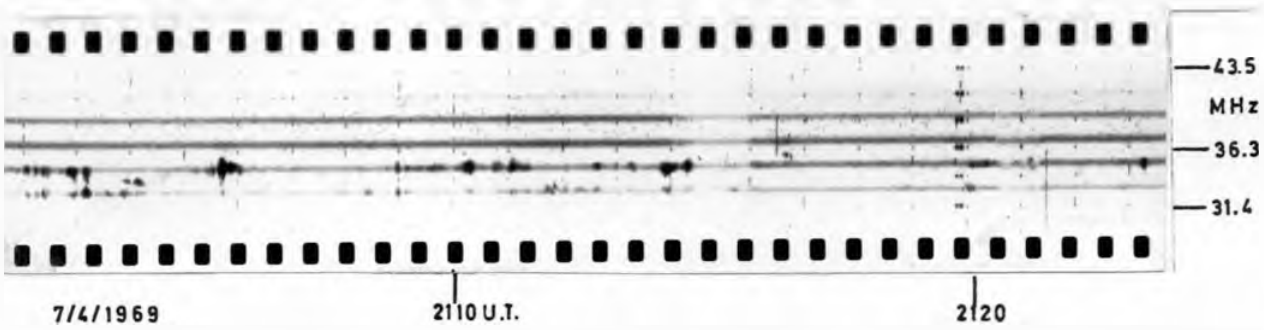

Plate 22. Record of a storm observed on the HF receiving system.

observed with the improved system if conditions are favourable.

This storm is a continuation of a B source storm which is displayed in the next section. Jupiter's CML is 169^{o} and Io's departure from SGC is 104^{o}, indicating that the storm occurred at the end of the B source emission. The bursts drifted up from the low-frequency range (see later) and reached a maximum frequency of about 35.5 MHz. The bursts are clustered mainly at the points where the receiving system is more sensitive although some bursts still survive in the less sensitive regions between the grey lanes.

6.2 FARADAY ROTATION ON JUPITER'S RADIO BURSTS

6.21 Theoretical background

The theory of Faraday rotation in the Earth's ionosphere has been treated by Kelso (1964) and Riihimaa (1966c); we outline the results of their discussions. For the frequencies at which we observe Jupiter's decametric radiation the base modes for propagation in the Earth's ionosphere are circular. Any wave entering the Earth's ionosphere with a polarization other than one of the circular modes will usually split into two waves of opposite circular polarization, the relative amplitudes depending on the polarization of the incoming wave. Both waves then travel with their polarization unchanged, if the parameters of the traversed medium

vary slowly; but the waves have different phase velocities. The polarization ellipse is consequently rotated through an angle depending on the frequency, magnetic field intensity and the distance into the plasma. The resultant Faraday rotation is clockwise (looking along the direction of propagation) when the longitudinal component of the magnetic field along the ray path points in the direction of propagation.

When the two circularly polarized waves travel along the same ray path and the propagation is quasi-longitudinal, then, for frequencies large compared to the plasma frequency and the gyrofrequency,

$$\Psi = \frac{K}{f^2} \int (H \cos \theta) \, N dS \qquad (6.1)$$

where Ψ = total rotation in radians

K = constant

f = wave frequency

H = magnetic field intensity

θ = angle between the direction of propagation and the magnetic field

N = electron density

dS = element of length along the ray path

The integral is taken along the ray path from the source to the point of observation.

If we assume that the Ionosphere does not vary horizontally and that the ray is straight we can write $dS = dh \sec X$, where dh is an element of height and X is

the angle between the ray and the vertical. Then Ψ becomes

$$\Psi = \frac{K}{f^2} \int (H \cos \theta \sec X) \, N dh \qquad (6.2)$$

At any particular time of observation the numerator of the right-hand side of equation (6.2) can be treated as a constant C (Parker, Dulk and Warwick, 1969):

$$C = K \int (H \cos \theta \sec X) \, N dh \qquad (6.3)$$

Hence,

$$\Psi = \frac{C}{f^2} \qquad (6.4)$$

where C is initially unknown. In the next subsection we outline a method of determining C from the Faraday fringes on a spectrographic record.

6.22 The polarization ellipse at Jupiter

Plate 23 shows an original negative of a B source storm. Jupiter's CML is 156° and Io's departure from SGC is 101° at the time of the DC marker at 2047 U.T. This storm is of particular interest since the Faraday fringes are clearly visible throughout most of the record. The fringes are most easily seen by looking along the length of the negative at a grazing angle. The emission as a whole shows a positive drift to the high-frequency limit of the receiver and by 2052 U.T the bursts are no longer present at the high-frequency end of the receiver although isolated

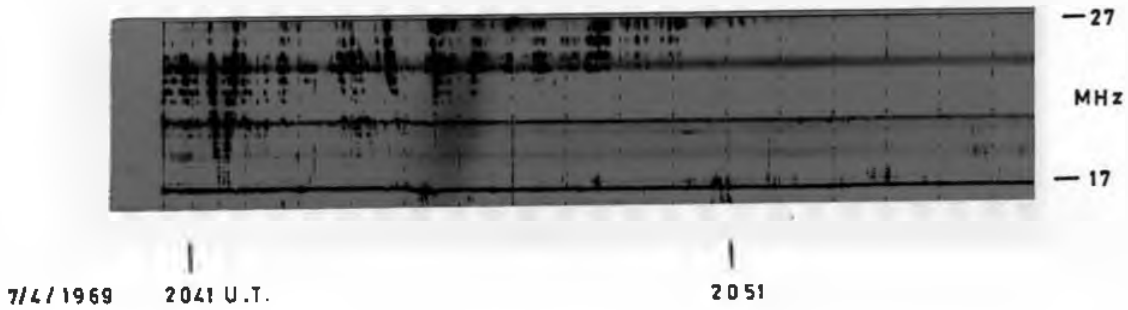

Plate 23. Photographic negative showing Faraday rotation on Jupiter's bursts.

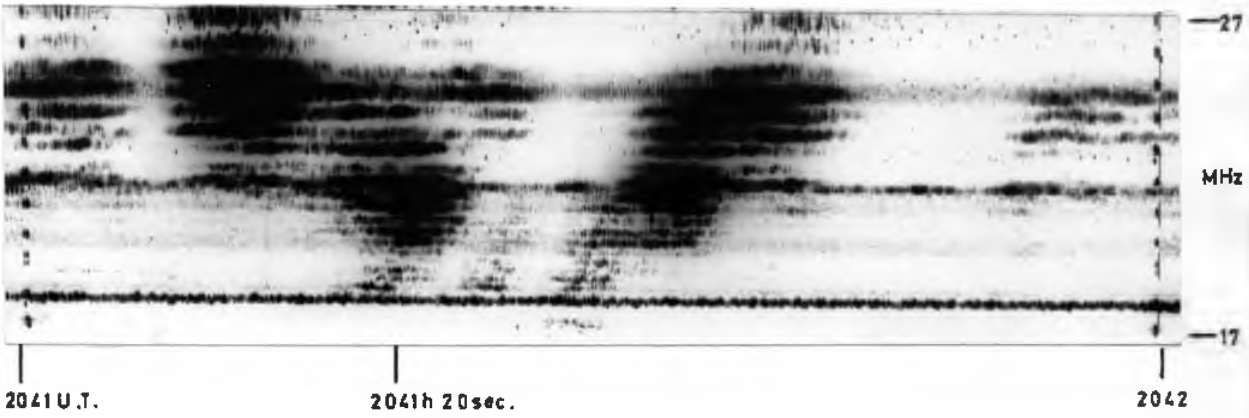

Plate 24. Enlargement of a 1 minute portion of the Faraday rotation record.

bursts are still present around 18 MHz. These positively drifting bursts are the ones referred to in the HF record shown earlier.

Faraday effect criteria:

The following criteria are given by Dulk (1965b) to establish the presence of the Faraday effect on spectral records with certainty. In order to detect Faraday effect it is necessary to have nearly continuous emission over a frequency range of 2 to 3 MHz and lasting for several minutes; to be fully confident that the modulations are due to Faraday effect and not interference or chance enhancements of intensity, the frequency range must be 5 or 6 MHz and the duration of the nearly continuous emission must be about 10 minutes. The fringes must be more closely spaced at lower frequencies and the total Faraday rotation must in fact be inversely proportional to the square of the frequency. The criteria for the bandwidth and duration of the bursts are satisfied by our record and we adopted the following technique to check the inverse square dependence on frequency.

The inverse square dependence:

The largest number of fringes are present in the minute between 2041 and 2042 U.T. and this section was refilmed on an expanded time scale to obtain clearer definition of the fringes. A photographic enlargement from an intermediate negative makes the fringes readily visible. Plate 24 shows an enlargement of the one minute section. An

enlargement about twice the size of the one shown was used for the actual analysis. The minima of the pattern are extremely well defined compared to the broader maxima. For this reason the analysis was done using the minima which occur when the minor axis of the polarization ellipse co-incides with the horizontally polarized LPD antenna. Since the minima are almost zero the bursts must be low-axial ratio bursts. This is confirmed by fixed-frequency observations made at the same time at 20 and 22 MHz. The output signals from the left- and right-circular channels at these frequencies were almost equal.

The frequency markers on the print are fairly broad black spots; the exact frequency of the marker is taken to occur at the middle of the marker along the frequency direction. This is in order since the output signal from the receiver for a particular harmonic is symmetrical (see Plate 10). The centres of the frequency markers on either side of the minute shown are then joined to calibrate the record accurately in frequency. By viewing the record along its length at a grazing angle the centre of a particular minimum is marked at four positions along the record. These four points are joined if they lie on the same straight line, if not an independent estimation of the position of the minimum is repeated at four new positions. Since the minima are very narrow (less than 100 kHz in most cases) the above method enables the position of the minima to be located accurately in frequency. The frequencies at which the minima occur are

then obtained at a particular time (2041 hrs 20 sec in this case) by linear interpolation between the successive frequency markers. The linear interpolation does not introduce serious error since the receiver linearity is good. The author feels that the above procedure enables the frequencies of the minima to be established to better than 2%.

The inverse-square relationship is tested by making a guess at the total rotation (Ψ_o) at the highest frequency (f_o) at which a Faraday fringe is present and, remembering that the Faraday rotation between successive fringes must be π radians, a graph is plotted of the total Faraday rotation in π radians versus the inverse square of the frequency at the particular Faraday minimum. The best straight line through the plotted points is shown in figure 35. The data points almost all lie on the line, thereby establishing the inverse-square relationship.

The polarization ellipse at Jupiter:

Using the method of Warwick and Dulk (1964) we assume that all the rotation occurs in the Earth's ionosphere and that the total rotation and the frequency are related by equation (6.4). We then find the value of C from the data points so that the true total rotations at the frequencies of the minima can be determined. The gyro-frequency f_g is about 1.5 MHz (Riihimaa 1966c) and ionosonde observations at Grahamstown indicate that the plasma frequency f_c never exceeds about 5 MHz at night-time in winter. The lowest frequency f

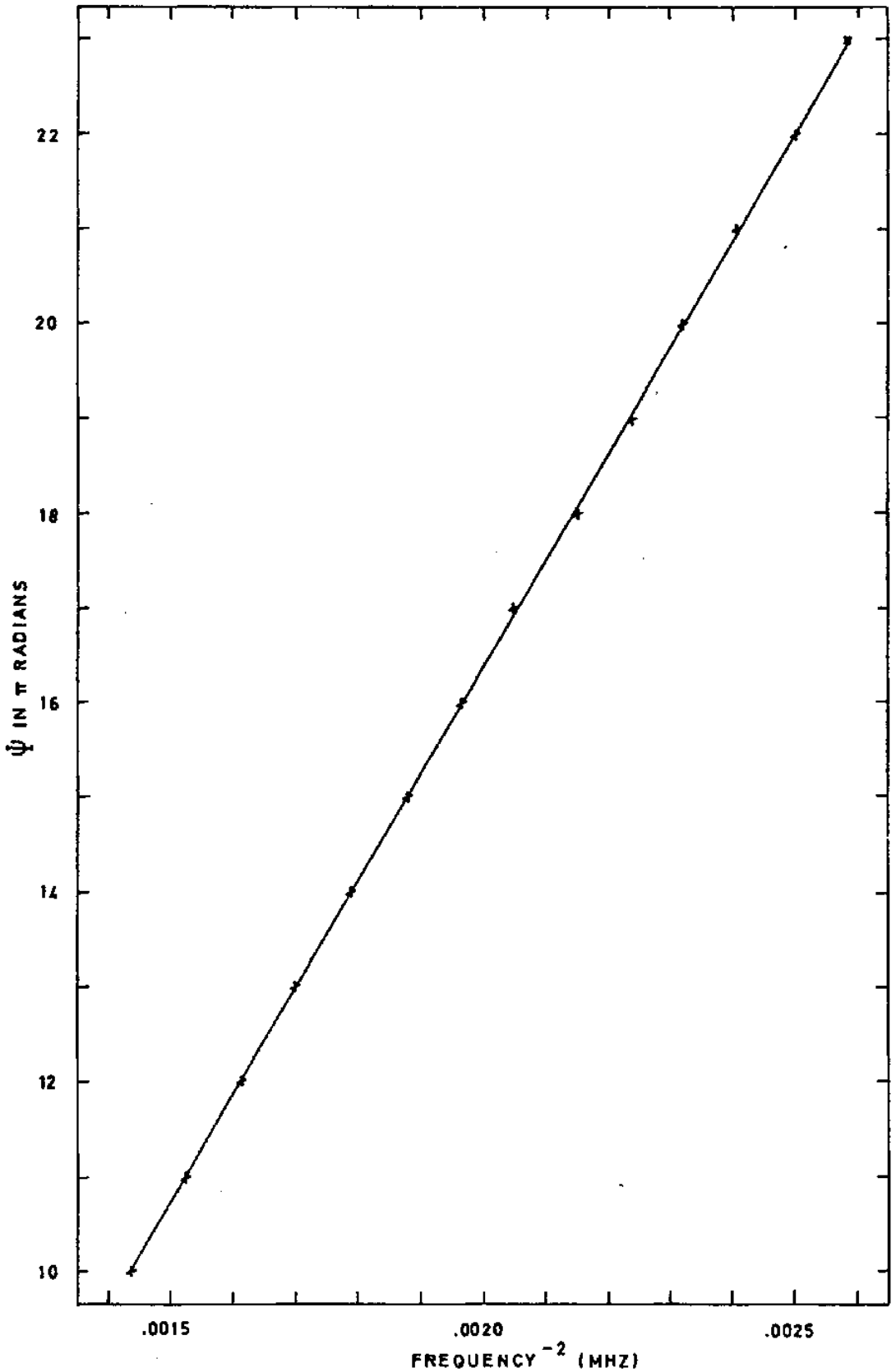

FIG. 35 BEST-FIT CURVE FOR FARADAY ROTATION DATA.

at which we measured a Faraday fringe is about 20 MHz so that $f_g/f \ll 1$ and $(f_c/f)^2 \ll 1$, and the high-frequency approximation in equation (6.4) is valid. We now use a least-squares technique to find the best value of C from the measured fringe frequencies and the known difference in total rotation (π radians) from fringe to fringe. The least squares technique minimises the mean square deviation between the set of data points (Ψ_o, f_o; $\Psi_o + \pi$, f_1; . . . . . $\Psi_o + n\pi$, f_n) and the curve of equation (6.4). We obtain a value of 1.303×10^4 π radians $(MHz)^2$ for C and we use this value to obtain the true total rotation in π radians at each of the Faraday minima. We obtain a value of $16.22\pi \doteq 51.9$ radians for the total rotation at about 25 MHz and this value compares well with some of the values for the total rotation at 30 MHz obtained by Parker, Dulk and Warwick although their observations were made at different times.

The total rotations between the successive fringes are found to be separated very nearly by π radians in each case. The mean and the standard deviation of the mean of the fractional parts of the total rotations are calculated. The fractional parts of the total rotations are the important considerations since each rotation of π re-aligns the minor axis of the ellipse to the antenna.

We obtained a value of 0.23π radians for the mean fractional part of the total rotations in the Earth's ionosphere and a standard deviation of 0.01π radians. These values correspond to rotations of $41^o \pm 2^o$. This value

of the fractional part is now used to project the polarization ellipse from the antenna to the top of the ionosphere. We have to rotate the ellipse anti-clockwise from the antenna to the top of the ionosphere since the Faraday rotation was anti-clockwise (viewed in the direction of propagation) at the time of the storm. Then using standard techniques we find the orientation of Jupiter's rotational axis measured anti-clockwise from the vertex of Jupiter's disc as seen from Grahamstown. We in fact find the projection of the rotational axis on the plane through the centre of Jupiter and normal to the line of sight (the angle between this plane and Jupiter's rotational axis never exceeds $3\frac{1}{2}^{\circ}$). Hence we find the orientation of the polarization ellipse relative to Jupiter's rotational axis.

The major axis of the polarization ellipse at Jupiter is found to be inclined at an angle of 23° to the rotational axis measured from north through west. The geometrical arrangement is shown in figure 36. This result agrees with that of Parker, Dulk and Warwick that the major axis of the ellipse is aligned more closely to Jupiter's magnetic axis and rotational axis than to the equator. It contradicts the result of Bennett et al. (1965), who found that the major axis was very nearly parallel to Jupiter's rotational equator. A more extensive study of all records showing Faraday rotation is in progress.

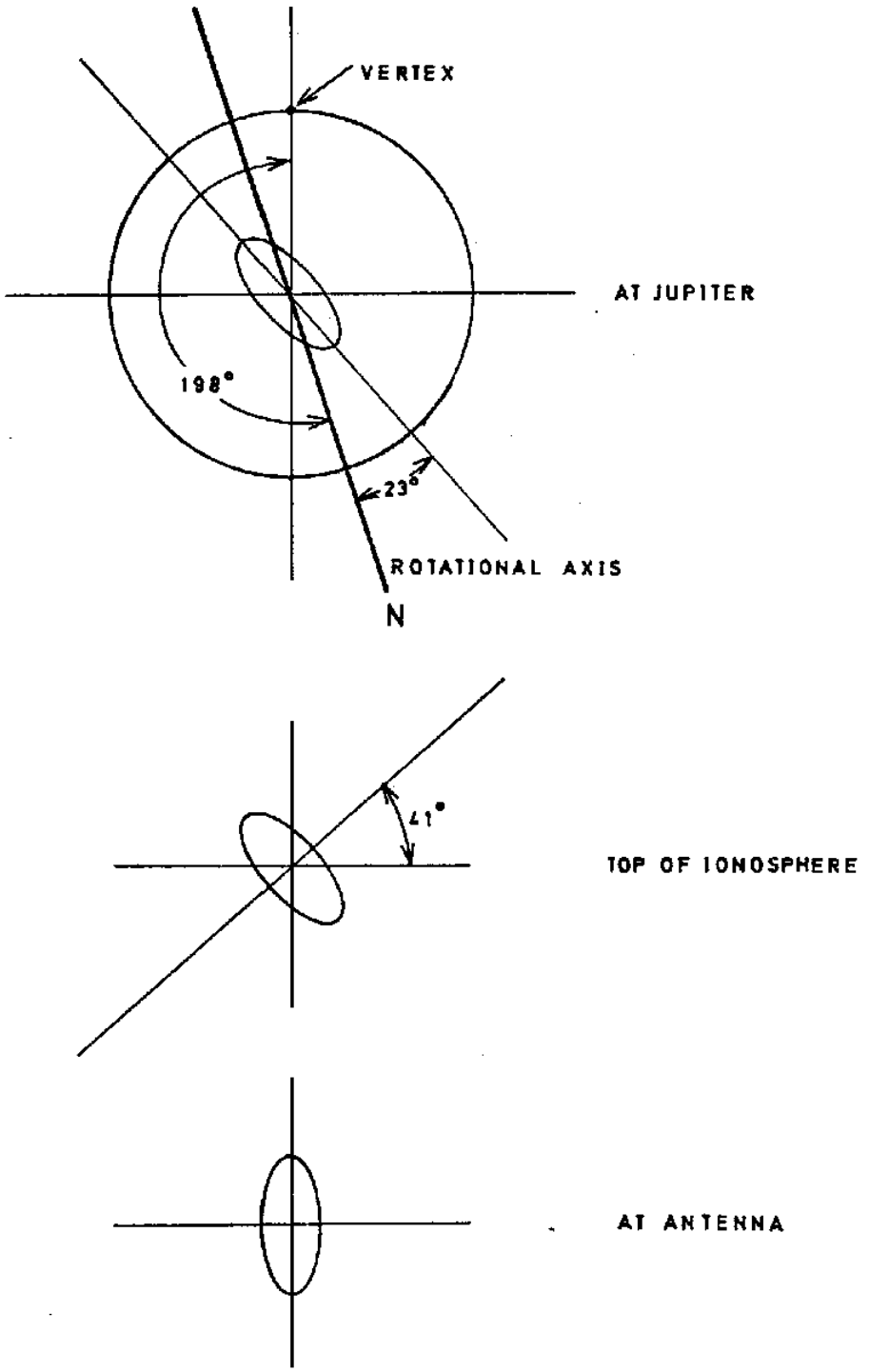

FIG. 35. POLARIZATION ELLIPSE AT JUPITER.

Plate 25. Faraday rotation on Jupiter's bursts near local sunrise.

A further Faraday-rotation record:

Plate 25 shows a record of a B source storm taken near local sunrise. Jupiter's CML is 143° and Io's departure from SGC is 103°. The record is interesting in that the Faraday fringes are not parallel to the time axis but are sloping towards higher frequencies. A given fringe represents a fixed amount of rotation from the source to the receiver i.e. ψ is fixed. The slope towards higher frequencies at sunrise is consistent with equation (6.2) which shows that if a fringe slopes from low to high frequency, the electron content in the ionosphere must be increasing (as is the case at sunrise) to enable ψ to remain constant. Notice that the frequency band below 18 MHz is almost saturated with stations. The zero control of the sweep generator has been used to adjust the frequency range of the receiver to remove strong interfering stations at 15 and 16 MHz.

6.3 PROPOSED MODIFICATIONS AND CONCLUSIONS

The swept-frequency polarimeter for the 15 to 45 MHz range is operating effectively and there are not many improvements to be suggested. Two possible modifications are the following. The high-frequency and low-frequency sweep generators should be synchronised so that the HF and LF records can be exactly aligned thereby facilitating the analysis. One possible way of achieving this would be to trigger the bistable multivibrators, which produce the HF and LF sweep voltages, with pulses from the same unijunction

transistor. That is, we do away with the unijunction transistor and associated timing components for one of the sweep generators and trigger its bistable multivibrator with the pulses from the unijunction transistor of the other sweep generator. Finally, if the problem of interference from the high-voltage powerlines cannot be solved, the receiver sweeps should be synchronised to the mains voltage. The voltage "spikes" caused by the powerline interference will then remain stationary during successive frequency sweeps rather than drifting continuously across the frequency band as is the case at present. In this way records which would otherwise be spoilt could be saved. All that remains is to observe Jupiter's radio storms for one or more apparition and to analyse the results.

APPENDIX I

Shain (1956) introduced a form of analysis in which he plotted the number of bursts in a given longitude interval versus the longitude of the central meridian at the time of observation using System I as well as System II co-ordinates. These two systems of longitude co-ordinates describe the mean rate of rotation of the clouds seen in Jupiter's equatorial and temperate zones.

System I corresponds to a rotation period of $9^h\ 50^m\ 30.^s003$ and refers to the equatorial region. System II corresponds to a rotation period of $9^h\ 55^m\ 40.^s632$ and refers to the rest of the planet (Peek, 1958).

Although there was a definite drift of the radio sources with respect to System I co-ordinates, Shain found little drift when System II co-ordinates were used. Carr et al. (1958) proposed the so-called "System III" which had a period equal to that of the radio sources. Three years later they published a revised equation (Carr et al., 1961). In 1962 System III longitude was defined as follows by the International Astronomical Union (Douglas, 1964):

SYSTEM III (1957.0)

Epoch: 0^h U.T. January 1st, 1957. (Julian Day 2435839.5)

Period: $9^h\ 55^m\ 29.^s37$

Central Meridian Longitude as seen from Earth at epoch:

$108^o.02$

(co-incident with System II)

If any time t is expressed in Julian Days the System III (1957.0) central meridian longitude, λ_{III}, may be calculated from the System II central meridian longitude, λ_{II}, by the equation:

$$\lambda_{III} = \lambda_{II} + 0.2743\ (t - 2435839.5)$$

APPENDIX II

The following nomenclature for source regions on Jupiter was adopted by the Jupiter Observers' Conference at Goddard Space Flight Centre during April 1965.

λ_{III} longitude range in degrees	Region
0 - 70	D
70 - 190	B
190 - 280	A
280 - 360	C

D is the region of low probability in the probability-of-occurrence histograms. B is the broad "source" region sometimes referred to as the "early source" or region 1. A is the "main source" region also called region 2. C is the region on the high longitude side of A sometimes called the "late source" or region 3.

REFERENCES

The abbreviations used throughout the list of references are in accordance with those to be found in the World List of Scientific Periodicals.

Baart, E.E., Barrow, C.H. and Lee, R.T., 1966, "Millisecond Radio Pulses from Jupiter", Nature, 211, 808.

Barrow, C.H., 1962, "Recent Radio Observations of Jupiter at Decameter Wavelengths", Astrophys. J., 135, 847.

Barrow, C.H., 1964a, "Polarization of 16 MHz Radiation from Jupiter", Nature 201, 171.

Barrow, C.H. 1964b, "Polarization Observations of Jupiter at Decameter Wavelengths, Icarus, 3, 66.

Barrow, C.H., 1968, "A Radio Study of the Planet Jupiter", Ph. D. Thesis, University of London.

Barrow, C.H. and Morrow, D.P., 1968, "The Polarization of the Jupiter Radiation at 18 MHz.", Astrophys, J., 152,593.

Bennett, C.L., Bibl, K., Gaunt, D.N. and Reinisch, B.W., 1965, Rept. 65-910, Lowell Tech. Inst. Res. Foundation, Air Force Cambridge Res. Lab.

Bigg, E.K., 1964, "Influence of the Satellite Io on Jupiter's Decametric Emission", Nature 203, 1008.

Branson, N.J.B.A., 1968, "High Resolution Radio Observations of the Planet Jupiter", Mon. Not. R. Astr. Soc.,139,155.

Burke, B.F. and Franklin, K.L., 1955, "Observations of a Variable Radio Source Associated with Jupiter", J. Geophys. Res., 60, 213.

Carr, T.D., Smith, A.G, Pepple, R. and Barrow C.H., 1958, "18 Megacycle Observations of Jupiter in 1957," Astrophys. J., 127, 274.

Carr, T.D., Smith, A.G, Bollhagen, H., Six, N.F. and Chatterton, N., 1961, "Recent Decameter-Wavelength Observations of Jupiter, Saturn and Venus", Astrophys.J. 134, 105.

Carr, T.D., Gulkis,S., Smith, A.G., May, J., Lebo, G.R., Kennedy, D.J., and Bollhagen, H., 1965, "Results of Recent Investigations of Jupiter's Decametric Radiation", Radio Science,69D, 1530.

Carr, T.D. and Gulkis,S., 1969,"The Magnetosphere of Jupiter", Annual Rev. Astr. and Astrophys., 7, 577.

Cohen, M.H., 1958, "Radio Astronomy Polarization Measurements", Proc. Inst. Radio Engrs., 46, 172.

Douglas, J.N., 1964, "Decametric Radiation from Jupiter", Inst. Elec. Eng. Trans. Mil. Electronics, MIL, 8, 173.

Dowden, R.L., 1963, "Polarization Measurements of Jupiter Radio Bursts at 10.1 MHz", Aust. J. Phys., 16, 398.

Dulk, G.A., 1965a, "Io-Related Radio Emission from Jupiter", Science, 148, 1585.

Dulk, G.A., 1965b, "Io-Related Radio Emission from Jupiter", Ph. D. Thesis, University of Colorado.

Duncan, R.A., 1966, "Factors Controlling Jovian Decametric Emission", Planet. Space Sci., 14, 1291.

Ellis, G.R.A., 1962a, "Cyclotron Radiation from Jupiter", Aust. J. Phys., 15, 344.

Ellis, G.R.A., 1962b, "Radiation from Jupiter at 4.8 MHz", Nature, 194, 667.

Ellis, G.R.A., 1963, "The Radio Emissions from Jupiter and the Density of Jovian Exosphere", Aust. J. Phys., 16, 74.

Ellis, G.R.A., 1965, "The Decametric Radio Emissions of Jupiter", Radio Science, 69D, 1513.

Ellis, G.R.A. and McCulloch, P.M., 1963, "The Decametric Radio Emissions of Jupiter", Aust. J. Phys., 16, 380.

Franklin, K.L., 1959, "An account of the Discovery of Jupiter as a Radio Source", Astr. J., 64, 37.

Franklin, K.L. and Burke, B.F., 1958, "Radio Observations of the Planet Jupiter", J. Geophys. Res., 63, 807.

Gallet, R.M., 1961, "Radio Observations of Jupiter. II", in Planets and Satellites, ed. G.P. Kuiper, University of Chicago Press.

Gardner, F.F. and Shain, C.A., 1958, "Further Observations of Radio Emission from the Planet Jupiter", Aust. J. Phys., 11, 55.

Gledhill, J.A., 1967a, "Magnetosphere of Jupiter", Nature, 214, 155.

Gledhill, J.A., 1967b, "The Structure of Jupiter's Magnetosphere and the Effect of Io on its Decametric Radio Emission", Goddard Space Flight Centre Report X615.

Goldreich, P. and Lynden-Bell, D., 1969, "Io, a Jovian Unipolar Inductor", Astrophys. J., 156, 59.

Gordon, M.A. and Warwick, J.W., 1967, "High Time-Resolution Studies of Jupiter's Radio Bursts"., Astrophys, J., 148, 511.

Gruber, G.M., 1966, "An Investigation into the Decametric Radio Emission by the Planet Jupiter", Ph. D. Thesis, Rhodes University.

Gruber, G.M., 1967, "A Further Analysis of the Observations of Jupiter's Decametric Radio Noise for the Apparitions of 1960-1964", Astrophys. J., 148, 541.

Kelso, J.M., 1964, "Radio Ray Propagation in the Ionosphere", McGraw-Hill.

Kraus, J.D., 1947, "Helical Beam Antenna", Electronics, 20, 109.

Kraus, J.D., 1948, "Helical Beam Antennas for Wide-Band Applications", Proc. Inst. Radio Engrs., 36, 1236.

Kraus, J.D. 1949a, "Helical Beam Antenna", Communications, 29, 6.

Kraus, J.D., 1949b, "The Helical Antenna", Proc. Inst. Radio Engrs., 37, 263.

Kraus, J.D., 1950, "Antennas", McGraw-Hill.

Kraus, J.D., 1958, "Planetary and Solar Radio Emission at 11 Meters Wavelength", Proc. Inst. Radio Engrs., 46, 266.

Morris, D. and Berge, G.L., 1962, "Measurements of the Polarization and Angular Extent of the Decimeter Radiation from Jupiter", Astrophys, J. 136, 276.

Parker, G.D., Dulk, G.A. and Warwick, J.W., 1969, "Faraday Effect on Jupiter's Radio Bursts", Astrophys, J., 157, 439.

Peek, B.M., 1958, "The Planet Jupiter", Faber and Faber.

Riihimaa, J.J., 1961, "Voltage-Tuned Swept-Frequency Receiver", Rev. Scient. Instrum., 32, 289.

Riihimaa, J.J., 1964a, "High-resolution Spectral Observations of Jupiter's Decametric Radio Emission", Nature, 202, 476.

Riihimaa, J.J., 1964b, "Observations of Fine Structure in Jupiter's Decametric Radio Emission", Ann. Acad. Sci. Fennicae, 156A, 1.

Riihimaa, J.J., 1966a, "High-resolution Spectra of Decametric Radio Bursts from Jupiter", Nature 209, 387.

Riihimaa, J.J., 1966b, "Spectral Types of Decametric Radiation from Jupiter", Nature, 212, 1338.

Riihimaa, J.J., 1966c, "High-resolution Spectral Observations of Decametric Radio Bursts from Jupiter", Ann. Acad. Sci. Fennicae, 206A, 1.

Riihimaa, J.J., 1968a, "Structured Events in the Dynamic Spectra of Jupiter's Decametric Radio Emission", Astr. J., 73, 265

Riihimaa, J.J., 1968b, "Narrow-Band Decasecond Emissions from Jupiter", Astrophys. Letters, 2, 59.

Riihimaa, J.J., and Warwick, J.W., 1968, "Drift patterns in the Dynamic Spectra of Jupiter's Decametric Radiation", Astrophys. Letters, 2. 185.

Shain, C.A., 1956, "18.3 MHz Radiation from the Planet Jupiter", Aust. J. Phys., 9, 61.

Sherrill, W.M., 1965a, "Polarization Measurements of the Decameter Emission from Jupiter", Astrophys, J. 142, 1171.

Sherrill, W.M., 1965b, "Polarization of Jovian Emission at Decameter Wavelengths", Nature, 205, 270.

Sherrill, W.M. and Castles, M.P., 1963, "Survey of the Polarization of Jovian Radiation as Decameter Wavelengths", Astrophys. J., 138, 587.

Smith, A.G. and Carr, T.D., 1959, "Radio-frequency Observations of the Planets in 1957-1958"., Astrophys. J., 130, 641.

Smith, A.G., Carr, T.D., Bollhagen, H., Chatterton, N. and Six,F., 1960, "Ionospheric Modification of the Radio Emission from Jupiter", Nature, 187, 568.

Smith, C.E. (Editor), 1966, "Log Periodic Antenna Design Handbook", Cleveland Institute of Electronics.

Stratton, J.A., 1941, "Electromagnetic Theory", McGraw-Hill.

Warwick, J.W., 1961, "Theory of Jupiter's Decametric Radio Emission", Ann. N.Y. Acad. Sci., 95, 39.

Warwick, J.W., 1963a, "Dynamic Spectra of Jupiter's Decametric Emission, 1961", Astrophys. J., 137, 41.

Warwick, J.W., 1963b, "Repeatability of Jupiter's Decametric Emission", Science, 140, 814.

Warwick, J.W., 1963c, "Position and Sign of Jupiter's Magnetic Moment", Astrophys. J., 137, 1317.

Warwick, J.W., 1964, "Radio Emission from Jupiter", Annual Rev. Astr. and Astrophys., 2, 1.

Warwick, J.W., 1967, "Radiophysics of Jupiter", Space Science Reviews, 6, 841.

Warwick, J.W. and Dulk, G.A., 1964, "Faraday Rotation on Decametric Radio Emissions from Jupiter", Science, 145, 380.

Warwick, J.W. and Gordon, M.A., 1965, "Frequency and Polarization Structure of Jupiter's Decametric Emission on a 10-Millisecond Scale", Radio Science, 69D, 1537.

Wells, H.W., 1958, "Flux Measurements of Cassiopeia A and Cygnus A, between 18.5 MHz and 107 MHz", Proc. Inst. Radio Engrs., 46, 205.